The Tectono-Sedimentary Development of Smeaheia on the Horda Platform with a Focus on the Cretaceous, and Implications for CO_2 Storage

Sharon Nicole Harris

Master Thesis in Geosciences

60 Credits

Department of Geosciences

Faculty of Mathematics and Natural Sciences

University of Oslo

June 2019

The Tectono-Sedimentary Development of Smeaheia on the Horda Platform with a Focus on the Cretaceous, and Implications for CO_2 Storage

Sharon Nicole Harris

UNIVERSITY OF OSLO
FACULTY OF MATHEMATICS AND NATURAL SCIENCES

Advisors: Ingrid Margareta Anell, Anja Sundal, Alvar Braathen, and Jan Inge Faleide

The Tectono-Sedimentary Development of Smeaheia on the Horda Platform with a Focus on the Cretaceous, and Implications for CO_2 Storage

http://www.duo.uio.no/

Printed: Reprosentralen, Universitetet i Oslo

Abstract

Smeaheia is a proposed site for long-term storage of CO_2. The site is located on the Horda Platform off the western coast of Norway, situated between the Vette and Øygarden Faults. The burial and uplift history of a basin has significant implications for reservoir and overburden properties. The uplift history of Norway is complex and consists of several phases, and the offshore basins have been linked to this development along with undergoing anomalous subsidence.

This study aims to understand the depositional infill of the Smeaheia area with particular emphasis on the Cretaceous development, and how the uplift and subsidence history has affected the deposits with implications for CO_2 storage. The study involves a detailed sedimentary analysis based primarily on seismic data (2D/3D) of the depositional successions on the Horda Platform, with a detailed focus on the Cretaceous sedimentary succession. The site-specific development of the area, based on the variations in sedimentary influx and the tilt and erosion of successions, is used to discuss the overburden properties of the storage site and influence on migration and secondary storage of CO_2.

In this study, Petrel (Schlumberger Ltd.) was used for the seismic interpretation of a 3D seismic cube and three 2D lines. 17 seismic horizons were mapped out, followed by the creation of RMS amplitude and time-thickness maps, which were used to evaluate depositional environments and sediment partitioning within the succession. The study is divided with respect to the Cretaceous, including an analysis of the Pre-Cretaceous, Cretaceous, and Post-Cretaceous development. The primary focus is on the Cretaceous Period, which consists of primarily fine-grained or clay-fraction sediments with some coarse-grained sediments near fault boundaries due to erosion on the edges of rotated fault blocks. The Cretaceous units represent the secondary reservoir of the potential CO_2 storage site, Smeaheia, and are composed of shallow to deep marine mudstones with small amounts of sand. Units above the Alpha Structure of the primary Jurassic reservoir display homogeneity with more lithologic variation between the Vette and Øygarden Faults, while units above the Beta Structure are more varied and display more coarse-grained sediments. The Cretaceous units are in close contact with loosely compacted Quaternary sediments due to erosion along the Base Pleistocene Unconformity, which may be a potential leakage site should CO_2 enter the secondary storage unit.

PREFACE

This thesis is submitted to the Department of Geosciences, University of Oslo (UiO), for the Master of Science in Geosciences, following the Sedimentology program. The thesis is supervised by Ingrid Margareta Anell, Alvar Braathen, Jan Inge Faleide, and Anja Sundal.

The research in this study was conducted throughout the autumn and spring of 2018 and 2019, respectively, as a 60-credit thesis, and is a collaboration and interaction with the NCCS (Norwegian Carbon Capture and Storage) Group.

Sharon Nicole Harris

Oslo, Norway; June 1st, 2019

ACKNOWLEDGEMENTS

I would like to express my gratitude to my supervisors Ingrid Margareta Anell, Professor Alvar Braathen, Professor Jan Inge Faleide, and Anja Sundal for their guidance, constructive discussions and comments, and most of all for their support. I would also like to address a special thanks to Michel Heeremans for preparing the data in the Petrel software.

I want to thank Gassnova, TGS, and NPD for making the seismic and well data available, and Schlumberger for the use of Petrel under academic license.

I also want to express my gratitude to my fellow students and friends at the Geoscience Department at the University of Oslo for influencing my thinking and expanding my knowledge and passion of geology. In addition, I would like to thank my ever-patient partner Lars-Oskar Westavik Gaustad for helping me find joy in my free time, and for his help in proof-reading this thesis.

Finally, I want to thank my father for his long-lasting support. Without you, this dream couldn't have been possible.

Sharon Nicole Harris

Oslo, Norway; June 1st, 2019

Table of Contents

List of Figures

List of Tables

Chapter 1

1 Introduction

The North Sea is being targeted as a site of long-term CO_2 storage. The burial and uplift history of a basin has significant implications for reservoir and overburden properties. The present elevation of the Norwegian mainland is thought to be the result of a series of uplift and erosion events and the offshore basins have undergone rifting, thermal subsidence, tilting, inversion and doming as well as anomalous subsidence.

The study area (Figure 1.1) is located on the Horda Platform, on the eastern flank of the Viking Graben, east of the Troll Field and off the west coast of Norway. The Horda Platform is a north-south trending fault-bounded block of approximately 50 km in length, bound by normal faults (Patruno et al., 2015). It is bordered by the Viking Graben in the west, and the Øygarden Fault complex in the east (Duffy et al., 2015). The proposed CO_2 reservoir extends from 1.2 km to 1.6 km in depth and is composed of three shallow marine, coarse grained siliciclastic wedges from the Middle to Upper Jurassic (Sognefjord, Krossfjord and Fensfjord), and the main injection site is proposed to be within the Jurassic Sognefjord saline aquifer.

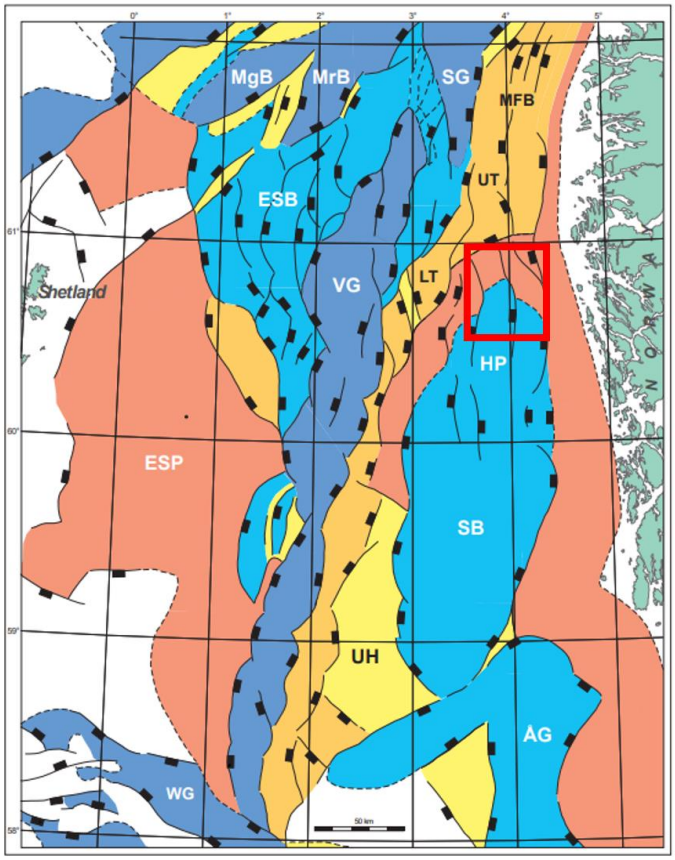

Figure 1.1: Map of the study area including tectonic features. The study area on the Horda Platform is outlined by a red square. Abbreviations: ESB-East Shetland Basin, ESP-East Shetland Plat-form, HP-Horda Platform, LT-Lomre Terrace, UT-Uer Terrace, MGB-Magnus Basin, MrB-MarulkBasin, MFB-Måløy Fault Blocks, SB-Stord Basin, SG-Sogn Graben, TS-Tampen Spur, UH-UtsiraHigh, VG-Viking Graben, WG-Witch Ground Graben. (Faleide et al., 2002)

1.1 Research Objective

The study seeks to examine in detail the development of the study area during the Cretaceous with respect to infill, erosion, uplift and fault activity, along with how a later large-scale Cenozoic uplift of the Norwegian mainland, and tilt, erosion, and truncation has influenced the reservoir successions and overburden properties. Multi-stage rifting up to the early Cenozoic with rotated fault blocks characterize the deeper parts of the study area. The development thereafter indicates multiple stages of Cenozoic uplift and changes in influx, all of which will significantly affect the overburden and influence migration and secondary storage. Detailed seismic analysis of variations in sedimentary influx, seismic attributes, and reflector terminations allows for discussion of sediment composition and partitioning, reworking and tilt and erosion, which may have an impact security of CO_2 storage and migration.

1.2 Technical Background on CO_2 Storage

The capture and storage of carbon dioxide in geological reservoirs is one of many methods of reducing atmospheric greenhouse gas and mitigating climate change. The process involves the capture of CO_2 from industrial sources, transporting it from the source, and then storing it in a geological formation. Once captured, CO_2 can be stored underground in a supercritical phase. The capture of CO_2 involves separating the CO_2 from hydrocarbon gases, then dehydrating and compressing the CO_2 to prepare it for transport (Nguyen, 2003). When the CO_2 is stored, it may be immobilized by structural or stratigraphic traps. With time, it is dissolved in formation water, which causes an increase in acidity of the system and therefore a further dissolution of minerals. The dissolved minerals produce metal cations which bind with the CO_2 and precipitate as carbonate minerals, providing further stability with respect to long-term storage.

The emission of CO_2 in the atmosphere is a challenge faced by the petroleum industry (Nguyen, 2003). To avoid emission into the atmosphere, the CO_2 is captured from industrial sources, transported, and injected into suitable geologic formations. Most of the world's carbon lies in the subsurface, naturally occurring from biologic activity, igneous activity, and chemical reactions that take place in the subsurface (IPCC, 2005). CO_2 will increase in density with depth depending on the geothermal gradient, and at about 800 m or greater, it will have reached a dense supercritical state. Injection in a supercritical phase is desired, as CO_2 will then have the density of a liquid, meaning larger volumes can be stored but act as a gas and fill available storage space rapidly. The geologic storage of CO_2 can occur in a range of geologic formations, including basins, oil fields, depleted gas fields, deep coal seams, and saline formations (Figure 1.2). Utilization of these formations will depend heavily on thorough viability studies to assess capacity and storage potential, possibilities of leakage, short- and long-term storage potential, and cost.

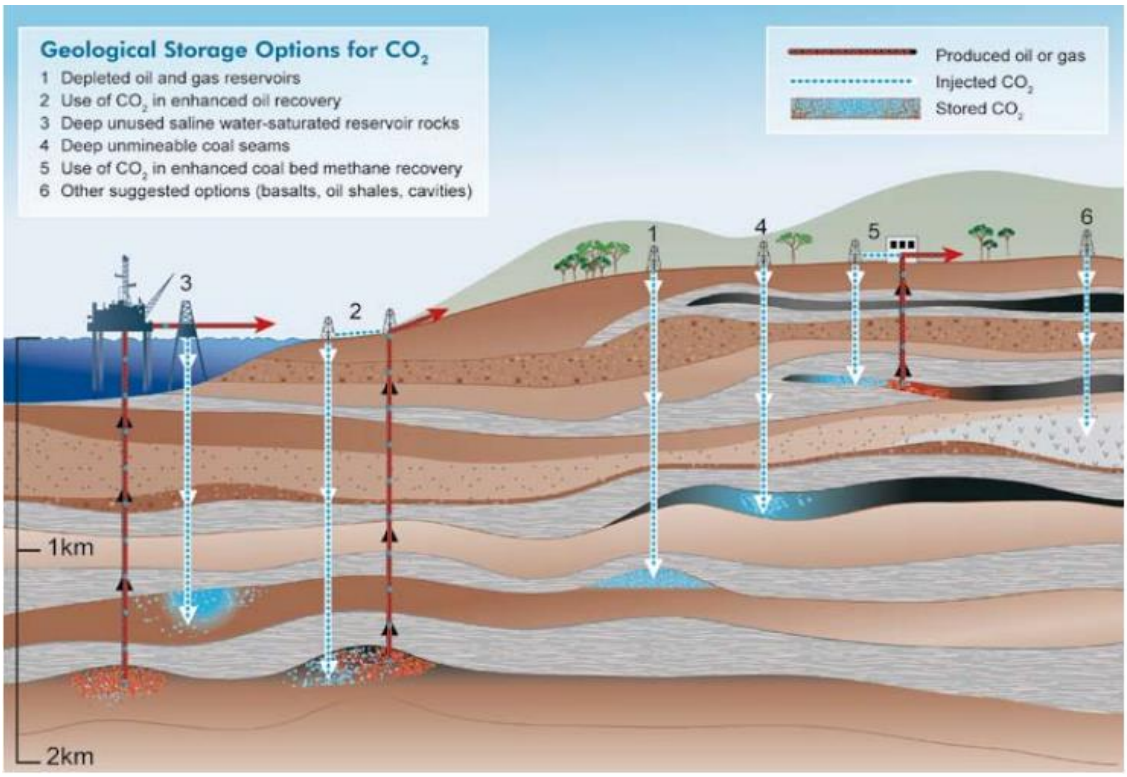

Figure 1.2: Geologic Storage options for CO_2 including basins, oil fields, depleted gas fields, deep coal seams, and saline formations (from IPCC, 2005, after Cook, 1999).

A table displaying major sources of CO_2 along with the number of sources and their emissions in million tons of CO_2 per year ($MtCO_2\ yr^1$) is displayed in Table 1.1. Fossil fuel industries emit higher amounts of CO_2 per year than biomass and have far more sources. Of fossil fuels, the generation of power bears the highest amount of sources, and the greatest amount of emissions of CO_2 per year. Following power is cement production, which is one of the primary CO_2 sources that is aimed to be used for the underground storage of CO_2 in Smeaheia (Gassnova, 2016).

Process	Number of sources	Emissions ($MtCO_2\ yr^{-1}$)
Fossil fuels		
Power	4,942	10,539
Cement production	1,175	932
Refineries	638	798
Iron and steel industry	269	646
Petrochemical industry	470	379
Oil and gas processing	Not available	50
Other sources	90	33
Biomass		
Bioethanol and bioenergy	303	91
Total	**7,887**	**13,466**

Table 1.1: Table of major sources of CO_2 along with emission amounts per year. Power emits the highest amount of $MtCO_2\ yr^1$ per year, followed by cement production, which is a prospective point source to be used for CO_2 capture and storage in Smeaheia. (IPCC, 2005).

The success of CO_2 storage is dependent on a combination of physical and geochemical storage mechanisms, which are commonly divided into four categories: i) hydrodynamic trapping, ii) residual trapping, iii), solubility trapping, and iv) mineral trapping (IPCC, 2005). There is a correlation between storage security and time since injection (Figure 1.3). The orange arrow in the figure represents an increasing storage security over time. Storage is most effective when a geologic trap exists, such as a trap with a thick, low-permeability seal, or when the CO_2 may be converted to solid minerals, or a combination of various trapping mechanisms.

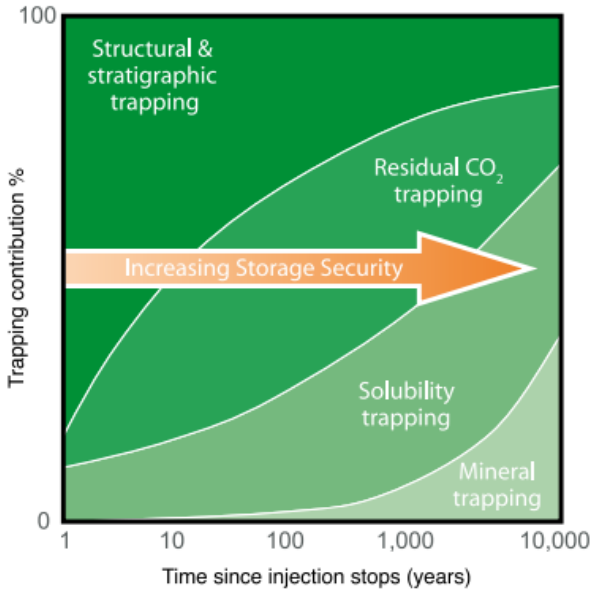

Figure 1.3: Different trapping mechanisms and increasing storage security with time since injection (IPCC, 2005).

Hydrodynamic Trapping

Hydrodynamic trapping concerns CO_2 which is trapped and stored in the supercritical phase under a low permeability caprock (Zhang and Song, 2014). It occurs in saline formations that lack a closed trap, but where fluids migrate very slowly over long distances (IPCC, 2005). Storage capacity in these traps depends the pore space volume, permeability of the reservoir, reservoir connectivity, and the fluid migration path (Zhang and Song, 2014). CO_2 is less dense and therefore more buoyant than formation fluid (usually saline), and will rise until encountering the caprock, where it will continue migrating as a separate phase until it is trapped as residual CO_2 , or until it is captured in structural or stratigraphic traps that have vertical and lateral seals (IPCC, 2005; Zhang and Song, 2014). The latter of these two trapping mechanisms is known as a physical trapping mechanism. Sedimentary basins can contain physically bound traps which are occupied by saline water, oil, or gas, while structural traps consist of folded or fractured rocks (IPCC, 2005).

Residual Trapping

When CO_2 is injected, it initially displaces the brine. Due to differences in density, the brine flows downwards and CO_2 rises. This causes the brine in the wetting phase to enter the pores by the lesser wetting phase, causing the brine to displace the CO_2 and leaving the CO_2 to become trapped in pores in the immobile phase (Zhang and Song, 2014). This is known as residual or capillary trapping.

Solubility Trapping

Following the injection of CO_2, it migrates upwards to the reservoir and caprock boundary, where it spreads under the caprock in a separate phase (Zhang and Song, 2014). This process is known at solubility trapping. The dissolution of CO_2 in the formation fluid occurs until the fluid reaches an equilibrium state. The solubility of CO_2 in water depends on the salinity, pressure,

and temperature of the formation water. As CO_2 dissolves into the formation fluid, the brine density increases, and the heavier brine will flow downwards, causing a convection process which stimulates the mixing of CO_2 and brine, further stimulating the dissolution of CO_2. This dissolution of CO_2 increases the storage capacity (Zhang and Song, 2014). The dissolution of CO_2 in formation water induces the production of a weak carbonic acid, which dissociates into HCO_3^- and CO_3^{2-}, as shown by the following reactions(e.g. Bachu and Adams, 2003).

$$CO_{2(gas)} \leftrightarrow CO_{2(aq)}$$

$$CO_{2(aq)} + H_2O \leftrightarrow H_2CO_{3(aq)}$$

$$H_2CO_3^* \leftrightarrow HCO_3^- + H^+$$

$$HCO_3^- \leftrightarrow CO_3^{2-} + H^+$$

In the above equations, $H_2CO_3^*$ is the sum of $CO_{2\,(aq)}$ and H_2CO_3. The dissolution of CO_2 in formation water is dependent on salinity, pressure, and temperature of the formation fluid (Figure 1.4).

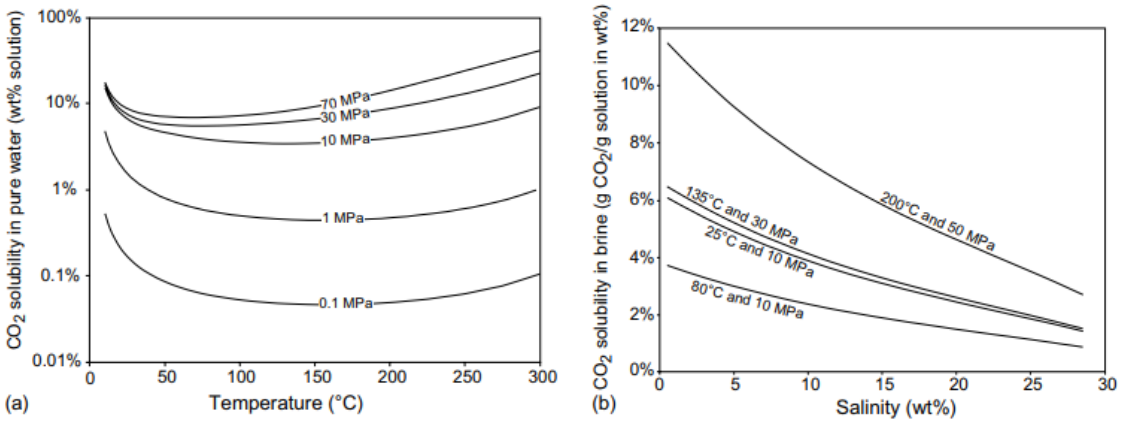

Figure 1.4: CO_2 solubility in fluid with variations in salinity, temperature, and pressure (IPCC, 2005).

Mineral Trapping

CO_2 can be incorporated into a stable mineral phase by reacting with minerals and organic matter within the formation, and CO_2 can be dissolved into formation water which initiates geochemical reactions, therefore increasing storage capacity and effectiveness (Zhang and Song, 2014). This process is known as mineral trapping. The reactions can either form new minerals in conjunction with the CO_2, or aid in the migration of CO_2. The reaction rate of minerals with CO_2 which has been dissolved in formation fluid depends on the temperature, pressure, and pH. Mineral dissolution is a very slow process and the effectiveness is mostly notable on the scale of geologic time.

1.3 The Smeaheia Storage Site

CO_2 capture and storage has become a recognized method for the mitigation of climate change. Large point sources for CO_2 collection include but are not limited to large fossil fuel facilities, natural gas production plants, synthetic fuel or fossil-fuel based hydrogen production plants, and other major CO_2-emitting facilities (IPCC, 2005). Three companies in Norway have researched the potential of CO_2 capture at their industrial facilities; Norcem AS, Yara Norge AS, and the Waste-to-Energy Agency in Oslo municipality (Gassnova, 2016). Norcem AS looks to capture CO_2 from flue gas at their cement factory in Brevik; Yara Norge AS has researched CO_2 capture from their ammonia plant at Herøya in Porsgrunn, at three different emission locations; The Waste-to-Energy Agency overlooks an energy recovery plant at Klemetsrud, which CO_2 can be captured from (Gassnova, 2016). All three emission points have been evaluated to be feasible for CO_2 capture and storage, according to the 2016 feasibility report by Gassnova.

Smeaheia is a prospective storage site located on a large fault block in an unlicensed area east of, and shallower than, the Troll field (Paasch et al., 2017). Its main storage reservoirs are the Jurassic Sognefjord, Fensfjord, and Krossfjord Formations of the Viking Group which range in depth from 1200 m to 1700 m. The area of interest, as shown in Figure 1.5 on the next page, is divided into the Beta and Alpha prospects, with the focus being on the Alpha prospect as the location for CO_2 storage (Lauritsen et al., 2018; Ringrose, 2017). The Alpha prospect contains 200 m thick Sognefjord sandstones with a permeability of 420-1300 mD and a porosity of 30% (Ringrose, 2017). The area of interest contains plugged exploration wells.

The Alpha structure is the primary point of interest for potential storage on Smeaheia. It is bound in the west by the Vette Fault, while the Beta structure is bound in the east by the Øygarden Fault. The top depths of the Alpha and Beta structures are respectively 1200 m TVD and 900 m TVD (true vertical depth) (Lauritsen et al., 2018). However, fault systems in the basement structure on the footwall of the Øygarden Fault Zone may serve as risks for CO_2 leakage, and therefore the Beta Structure is no longer considered for storage (Lauritsen et al., 2018).

The primary seal is made up of the Draupne Formation, which is a mudstone-rich marine deposit (Mondol et al., 2018). It is overlain by the Cromer Knoll and Shetland Groups, which are composed of Cretaceous carbonates and deep-water sediments and act as a secondary reservoir to the prospective storage site.

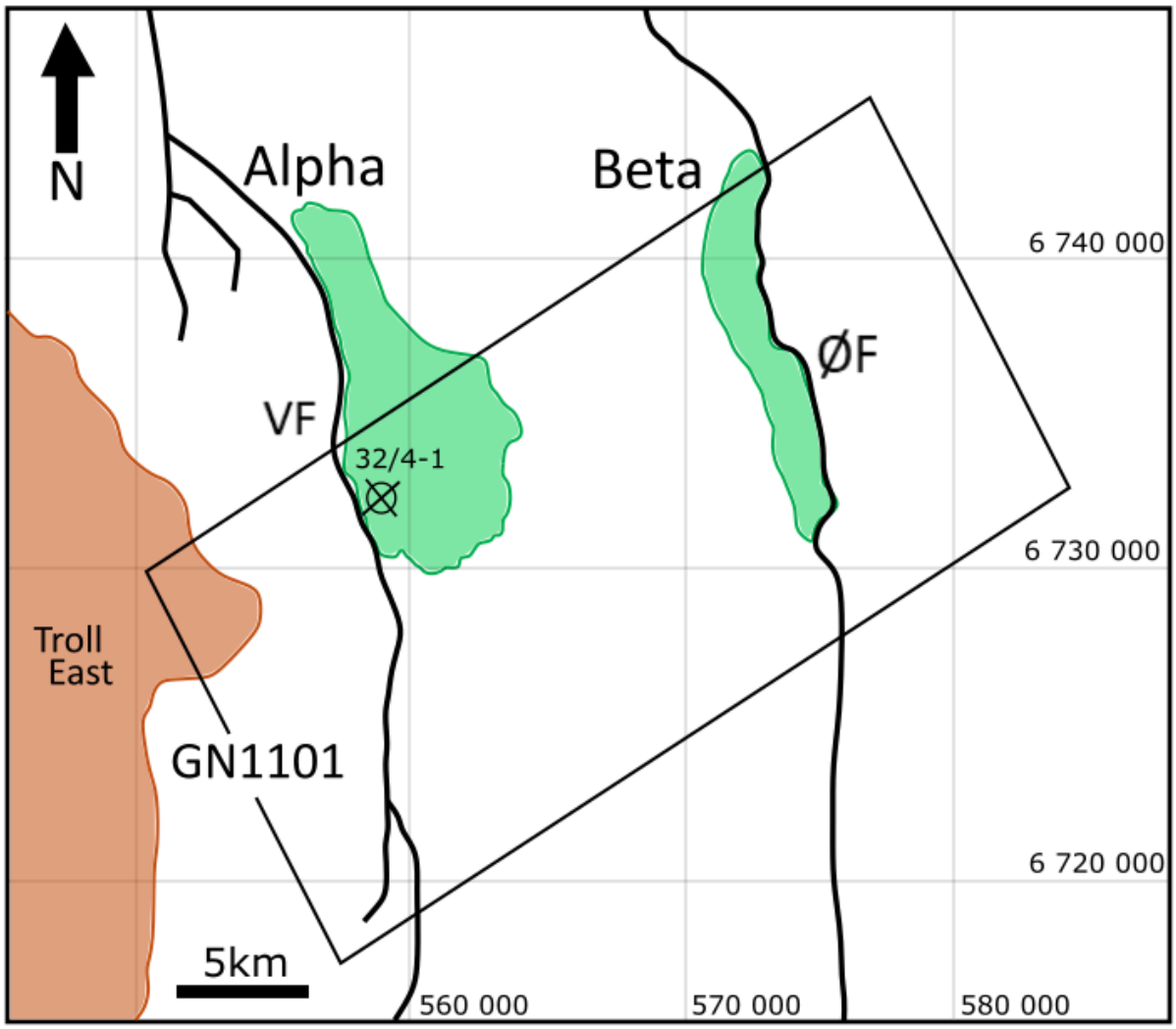

Figure 1.5: Location of the Alpha and Beta structures of the Smeaheia prospect, with the GN1101 3D cube, east of the Troll Field. A well (32/4-1) which is used in this study for well-top correlation is displayed in the Alpha Structure. Øygarden Fault is labelled to the east of the Beta Structure, and the Vette Fault is to the west of the Alpha structure (Modified from Ringrose, 2017).

1.4 Terminology: Uplift and Erosion

Riis and Jensen (1990) distinguished the different terminologies of "uplift" in literature based on definitions and discussions of Brown (1991) and Molnar and England (1990). Confusion often arises due to the term "uplift" being used in different ways, and therefore the following definitions have been presented (Riis and Jensen, 1990).

1. Uplift of rocks (U): This involves the vertical movement of a rock body or specific horizon with respect to a fixed point. Upward movement is referred to as positive, while subsidence is referred to as negative, and a downward movement. Uplift of rocks can be divided into tectonic uplift (Ut; uplift related to tectonic forces or changes in temperature) or isostatic uplift (Ui; uplift related to a change in load on the earth's crust).
2. Surface uplift (R): This involves the vertical movement of the Earth's surface with respect to a fixed point.

The difference between the two terms was defined by Molnar and England (1990) by the two equations:

$$U = Ut + Ui = R + E$$

$$R = Ho - Hi$$

In these equations, E is the change in thickness of overburden at the same location at two points in time, Ho is the present elevation, and Hi is the paleo-elevation (Molnar and England, 1990). To calculate uplift and erosion, physical and chemical changes must be considered.

Norway and the Norwegian Continental Shelf have experienced complex and multiple phases of uplift, which may have influenced rock properties or eroded sediments in the area. Therefore, uplift and burial must be considered for Smeaheia when predicting rock properties and the feasibility of CO_2 storage to prevent leakage (Baig et al., 2019; Hellevang, 2015; Shukla et al., 2010).

Chapter 2

2 Geologic Framework

The following section discusses the regional background as well as the tectono-stratigraphic development of the study area. Lithostratigraphic units in the North Sea are discussed in terms of depositional environment, time of deposition, and development related to tectonic processes.

2.1 Regional Setting

The Smeaheia CO_2 storage site lies on the Horda Platform on the eastern flank of the Viking Graben, east of the Troll Field in the North Sea and approximately 50 km offshore (Figure 2.1). The Horda Platform is a north-south trending fault-bound block approximately 50 km wide (Patruno et al., 2015). It is bordered by the Viking Graben in the west, and by the Øygarden Fault complex in the east (Duffy et al., 2015).

The reservoir extends from 1.2 km to 1.6 km in depth and is composed of three shallow-marine, coarse-grained siliciclastic wedges from the Middle to Upper Jurassic (Sognefjord, Krossfjord and Fensfjord), and the main injection site is proposed to be within the Jurassic Sognefjord saline aquifer. These siliciclastic wedges are interfingered by the Heather Formation, which is a silty-mudstone unit with low permeability and represents transgressive maxima (Patruno et al., 2015). The Sognefjord forms the youngest shallow-marine wedge and contains the main hydrocarbon reservoir for the Troll Field located on the North western part of the Horda Platform. The upper seal is composed of the Draupne Formation, which is a thick Jurassic mudstone-rich marine deposit (Mondol et al., 2018).

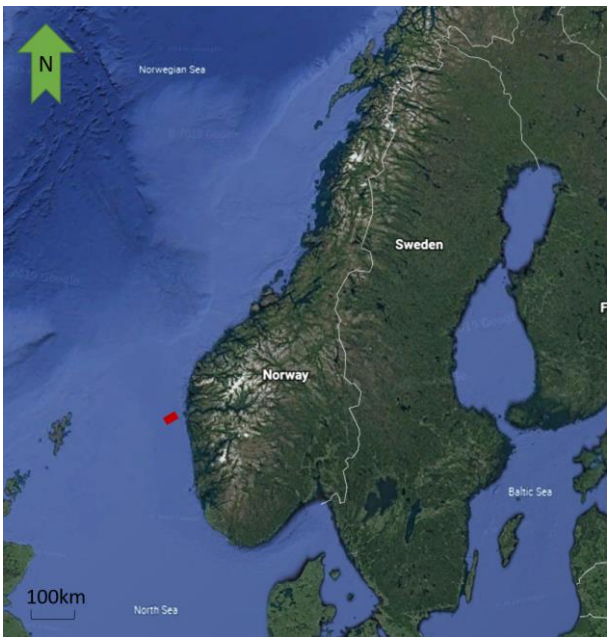

Figure 2.1: Map of the study area. The red square denotes the 3D GN1101 cube which covers Smeaheia (Google Earth).

The North Sea is an intracratonic basin, which is a basin lying upon continental crust (e.g. Faleide et al., 2015; Jordt et al., 1995). It is openly connected to the Norwegian Sea in the north, narrowly connected to the Baltic Sea in the east, and open to the Atlantic Ocean through the English Channel in the southwest. Boundaries include the coastlines of England, Scotland, Norway, Sweden, Denmark, Germany, the Netherlands, Belgium, and France. The catchment area is 850,000 km^2, and the average depth is approximately 90 m, making it a shallow sea (Walday and Kroglund, 2002). The deepest areas of the North Sea are along the Norwegian coastline, in a trench formed by the Norwegian Channel Ice Stream (Sejrup et al., 2000).

2.2 Tectonic Setting

The structure and stratigraphy observed in this study area is attributed to multi-phase rifting, with episodes of extension followed by thermal cooling and subsidence. Three episodes of lithospheric extension occurred in the following periods: the Early Carboniferous to the Middle Triassic, from the Middle Jurassic to the Late Cretaceous, and in the Latest Cretaceous/Early Tertiary (Brekke et al., 2001; Faleide et al., 2015; Nøttvedt, 1995).

The primary structural elements in the northern North Sea and surrounding areas are displayed in Figure 2.2. Characteristic features of the study area are rotated fault blocks with sedimentary basins in asymmetric half-grabens (Figure 2.3, on page 12), which are attributed to a multi-stage rifting process (Faleide et al., 2015). Structures such as the Sogn Graben, the Horda Platform, and the Stord Basin were formed at this time. Rifting phases propagated subsidiary and basement-involved faults, two of which being the N-S striking Vette and Øygarden Faults (Duffy et al., 2015) which bind the study area in the west and east, respectively.

The Caledonian continental collision between Laurentia and Baltica-Avalonia occurred in the Late Silurian to Early Devonian (Andersen et al., 2002). A large basin developed in the North Sea, likely caused by gravitational subsidence of the thickened crust. In the Devonian, a deep pull-apart basin developed with low-angle detachment faults connected by NE trending crustal scale strike-slip faults, which are part of the Møre-Trøndelag/Great-Glen Fault Zone. Baltica and Laurentia were moving laterally to each other at the time. The large faults were reactivated with a reverse movement in the Carboniferous. Carboniferous inversion, volcanism and intrusions occurred, followed by uplift and thermal subsidence (Coward et al., 2003).

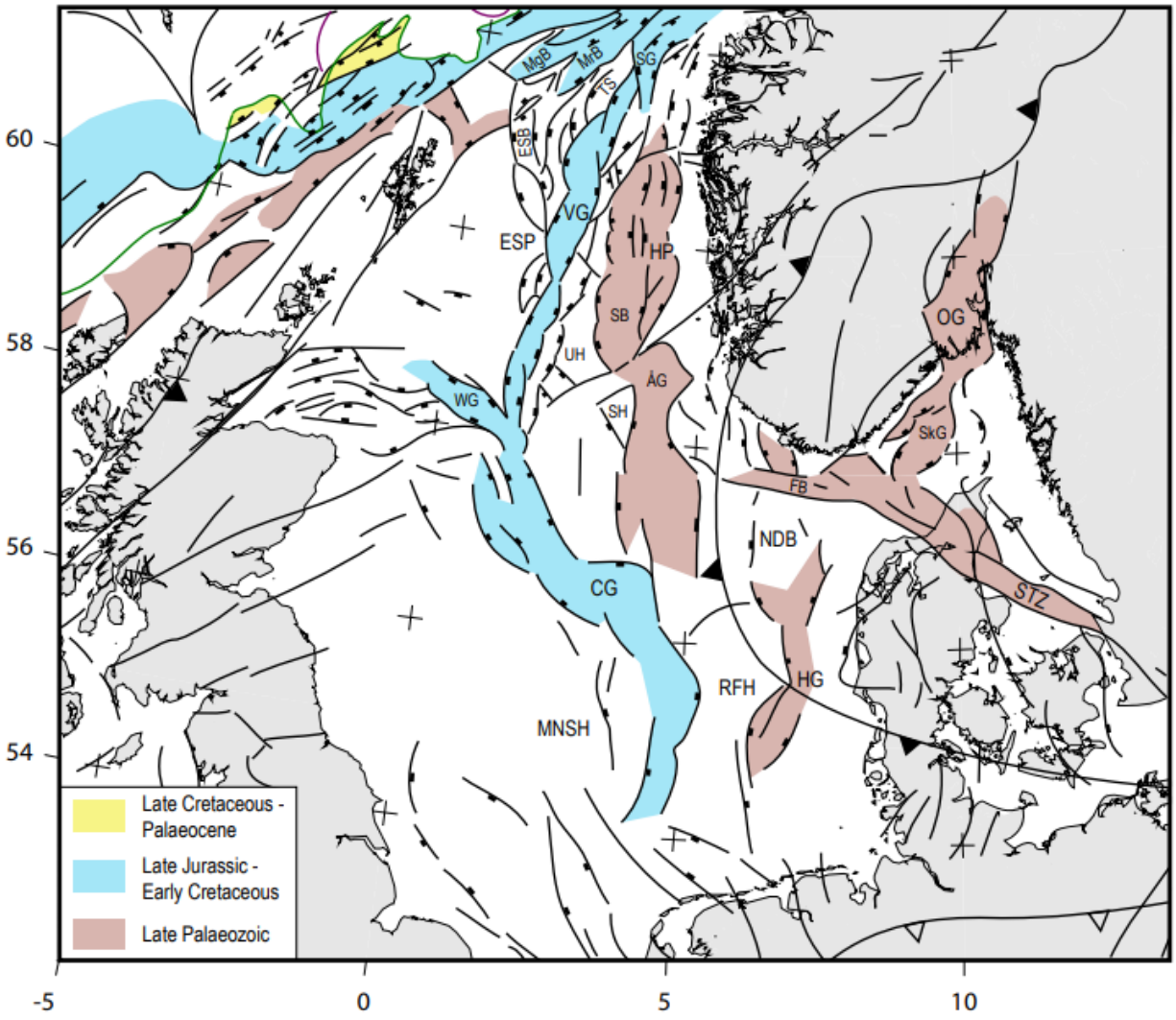

Figure 2.2: Structural elements of the North Sea. CG=Central Graben, ESB = East Shetland Basin, ESP=East Shetland Platform, HG = Horn Graben, HP=Horda Platform, MgB= Magnus Basin, MNSH=Mid North Sea High, MrB= Marulk Basin, NDB =Norwegian-Danish Basin, OG=Oslo Graben, RFH = Ringkøbing-Fyn High, SB=Stord Basin, SG= Sogn Graben, SH=Sele High, SkG=Skagerrak Graben, STZ= Sorgenfrei-Tornquist Zone, TS=Tampen Spur, UH=Utsira High, VG = Viking Graben, WG=Witchground Graben, ÅG= Åsta Graben. (Faleide et al., 2015).

In the Late Toarcian (Early Jurassic), movement of the Brage Horst was triggered by subsidence of the Bergen High in the west, and upheaval of the eastern part of the Horda Platform in the east. The differential movement at the Horda Platform caused the formation of a basin to the west, and an uplifted area in the east (Johnsen et al., 1995).

In the Mid Jurassic, major faults experienced normal faulting leading to minor rotations during the Bajocian to early Bathonian. A major rotation of the Bergen High/Bergen Sub-Basin occurred in the Bathonian and Callovian and was compensated for by normal faulting at the Øygarden Fault Zone, providing accommodation space for the Krossfjord and Fensfjord Formations in the east. During this period, multiple faulted terraces were developed between the Horda Platform and Viking Graben. The rotation of fault blocks led to the reworking of formations from the Brent Group (Ness and Tarbert) on the Horda Platform (Johnsen et al., 1995).

Major rotation of the Bergen High/Bergen Sub-Basin occurred into the Oxfordian and Early Kimmeridgian. In the Kimmeridgian, minor differential subsidence occurred in the Horda Platform area (Johnsen et al., 1995). During the Late Jurassic, a triple junction rift system developed in the North Sea, with the center located where a Middle Jurassic thermal dome preceded. Rifting occurred in multiple phases, with stages of tectonic quiescence in between (Zanella and Coward, 2003). The North Viking Graben trends N-NE, and on the western side of the Viking Graben lies the East Shetland Basin and the elevated East Shetland Platform. East of this area are the Sogn Graben, Horda Platform, Måløy Fault Blocks and the Øygarden Fault Zone. (Fraser et al., 2003).

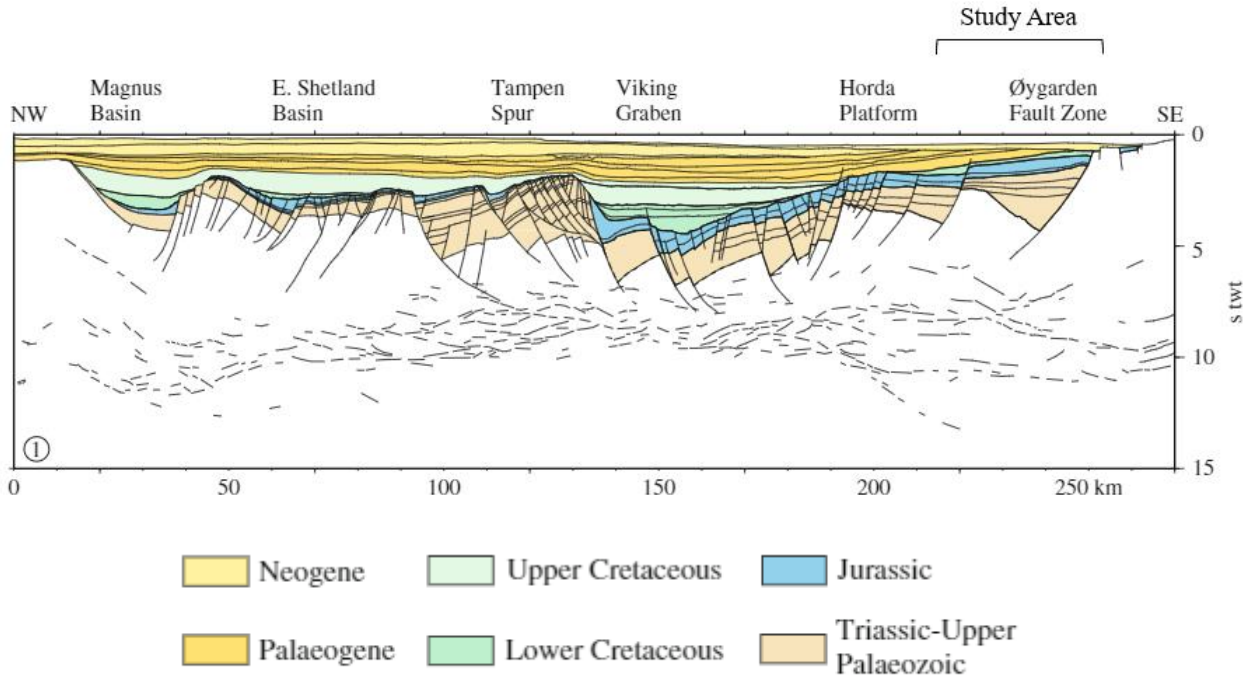

Figure 2.3: Interpreted regional deep seismic line across the North Sea, displaying ages for different sediments. Structures in this area are characterized by rotated fault blocks and sedimentary basins. The area of focus in this study is located on the Horda Platform, west of the Øygarden Fault Zone. Note the difference in thickness of Cretaceous units in the study area in comparison to the Viking Graben (modified from Faleide et al., 2015).

2.3 Regional Development

The spatial and stratigraphic patterns of sedimentary basin infill is predominantly controlled by accommodation space and sediment supply. These factors can be identified in a succession by the changes of grain size, bed thickness, erosional surfaces, and other factors which can be analyzed in outcrops, cores, and subsurface image logs (Folkestad and Steel, 2001).

2.3.1 Devonian

The onshore Devonian sediments from Western Norway are well-recorded (Andersen, 1998; Folkestad and Steel, 2001), and although the rocks from this period are not likely to form reservoir rocks, they are important for implications of offshore development. Devonian sediments in the northern North Sea have been reached in a few wells, but there is reason to believe that the same sediments are regionally present in deeper sections of the pre-Triassic half-grabens beneath the Horda Platform, Viking Graben, and East Shetland Basin (Faleide et al., 2015).

Uplift occurred in the Devonian due to the Caledonian Orogeny, which also led to the formation of a major mountain chain along western Scandinavia and Scotland, East Greenland, and partially in Poland (Faleide et al., 2015). The extensional collapse of the Caledonides is associated with the deposition of thick red continental sediments. In western Norway, Devonian basins such as Hornelen, Håsteinen, Kvanshesten, and Solund, contain thick conglomeratic sediments. Upper Palaeozoic rocks (Devonian and Lower Permian) have been discovered on the East Shetland Platform, and seismic data reveals large sedimentary basins which potentially contain Devonian-Carboniferous rocks beneath the platform (Faleide et al., 2015). In the Late Devonian, the Caledonian plate shifted from subduction to lateral movement between Greenland and Fennoscandia.

2.3.2 Carboniferous

In contrast to the dry climate of the Devonian, the Carboniferous gradually became more humid due to the movement of Northwest Europe away from the southern hemisphere's arid belt and into the humid belt of the equator (Faleide et al., 2015). From the Devonian to Carboniferous, the strike-slip movements along the Greenland/Fennoscandian plate boundary shifted to a zone of divergence and rift formation until the early Eocene, when continental breakup occurred and commenced seafloor spreading. Transgression from the south led to a sequence of shallow marine limestones, clastics, and some evaporites (Anderton et al., 1979). The crustal extension led to the rise of horsts and grabens, leading to topographic differentiation and the distribution of carbonate platforms on highs with clastic turbidites and shalier sediments in the grabens (Grayson and Oldham, 1987).

Tectonic activity in the North Sea ceased in the Middle Carboniferous and subsidence ensued, leading to the drowning of carbonate platforms (Collinson, 1988). The climatic conditions increased in humidity, and the carbonate input was replaced by a more clastic input (Van der Zwaan et al., 1985).The Lower/Upper Carboniferous boundary shows a deposit consisting of cyclic marine carbonates and shales along with fluvial sandstones, which are interpreted as a result of changes in sea level due to southern hemispheric glaciations (Faleide et al., 2015). In

the Middle Carboniferous (Moscovian), the Variscan deformation front advanced towards the north causing uplift and folding. This resulted in unconformities and a widespread deposition of red beds in the North Sea, spreading from both the north and south (Corfield et al., 1996; Dahlgren and Corfu, 2001). In the Oslo Graben, marine fossils from a Moscovian marine limestone can be correlated with Russian marine stages and illustrate that the regional Bashkirian-Moscovian sea-level rise led to a transgression from the north. As a result, a seaway opened at the Baltic Shield from the eastern Barents Sea to the Oslo area (Olaussen et al., 1994).

In the Late Bashkirian, the main depositional environments were shallow-marine deltaic. Cycles of flooding and regression occurred, and during the intermittent regression periods, regional coal beds were deposited (Brekke et al., 2001). Along the subduction zone through Germany and northern France, the Variscan mountain range formed, which was uplifted in the Late Cretaceous. The Variscan foredeep sedimentary successions were deposited, with sediments originating from mountain erosion (Faleide et al., 2015). In the Late Carboniferous to Early Permian times, northern and southern Permian basins were a principal paleogeographic component of the northern and central North Sea areas (Heeremans et al., 2004; Ziegler, 1982, 1987, 1992).

2.3.3 Permian

During the Permian Period, the Variscan Mountain Range continued to be uplifted, leading to the formation of abutting sedimentary basins in the southern North Sea and within subsided areas of the range. Towards the end of the Variscan orogeny, an east-west extension was accompanied by volcanic flare-ups (e.g. Glennie, 1988). The volcanoclastic sediments, mixed with fluvial and lacustrine sediments, are shown by well data to exist in the North Sea (Glennie, 1988).

In the Late Permian, fluvial deposition followed by transgression occurred in the Norwegian Sea, and two Permian basins formed in the North Sea (Brekke et al., 2001). During this time, northwest Europe was shifted out of the humid equatorial belt and northwards into the northern hemispheric arid belt, changing the sedimentary patterns from carbonate to marine clastics (Brekke et al., 2001). Coupled with the high mountain range in the south, the North Sea basin and most of northwest Europe experienced a period of severe aridity (Faleide et al., 2015). A dry environment behind the mountain range let to the formation of a marine evaporite basin, potentially with a passage through the Viking Graben to a seaway between Norway and Greenland, along with a connection though Poland in the east (Faleide et al., 2015). In the Late Tatarian, the North Sea Permian basins became flooded allowing for the deposition of the Zechstein Evaporites (Brekke et al., 2001). The latest Carboniferous-Permian rifting phase was associated with widespread igneous activity, which can be seen from the presence of extrusives and intrusives in the subsurface offshore (Faleide et al., 2015).

2.3.4 Triassic

Rifting in the Early Triassic continued until the Middle Jurassic, leading to patterns of outbuilding clastic wedges deposited within the Viking Graben and Horda Platform (Gabrielsen et al., 1990). Aside from this event, the Triassic was a period of thermal relaxation (Doré et al., 1999; Glennie and Underhill, 1998; Jarsve et al., 2014; Johansen et al., 1993; Roberts et al.,

1999; Surlyk, 1990). Sediment was still being supplied from the Variscan mountain range in the south, and uplift of Scandinavia supposedly occurred at this time as well (Faleide et al., 2015). The Øygarden Fault Zone formed the eastern margin of the Permo-Triassic basin and was active throughout most of the Triassic (Rohrman, 1995). The sedimentation rate was primarily high enough to balance with the subsidence rate, leading to flat topography with gently flowing rivers rather than a marine landscape (Faleide et al., 2015). Triassic sediments in the middle North Sea display a thickness of 5 km or more (Færseth, 1996). Underlying Permian salt layers begin to form diapirs, and Triassic sediments were either eroded or not deposited at the top of structures (Faleide et al., 2015).

Carbonates and salt deposits are found in the Upper Triassic area in the southern part of the North Sea. Continental clastic sediments exist in the central and northern areas, and deposition of these continued until the end of the Triassic. Sabkha environments with evaporite basins are also present. The climate towards the end of the Triassic became less arid, shifting towards fluvial and eventually marine deposition (Faleide et al., 2015).

2.3.5 Jurassic

The shift from continental to shallow marine depositional environments is marked by the Triassic-Jurassic boundary. This shift towards shallow marine deposition is associated with a more humid climate due to the movement of northwest Europe northwards and out of the arid belt (Faleide et al., 2015). The shallow marine sediments from the Early Jurassic are reflected by the Dunlin Group (Martinsen and Dreyer, 2001), followed by the Brent Group sandstone. The Brent Group sandstone represents a prograding delta in the northern North Sea which was deposited in a delta that drained the central part of the North Sea southwards towards a marine embayment between the Shetland and Horda Platforms (Faleide et al., 2015).

An erosional hiatus exists in the Lower Jurassic, which is potentially related to thermal updoming in late-Early Jurassic times (Leeder, 1983; Underhill and Partington, 1993; Whiteman et al., 1975). As a result of the domal uplift, an increase in erosion occurred (Underhill and Partington, 1993). The Brent Delta prograded northwards in the Middle Jurassic as a result of the erosion and the uplift of the Shetland area (Doré et al., 1999) and Norway (Van der Beek, 1994). The Brent Delta was gradually submerged as basin subsidence outpaced sediment supply from the south (Faleide et al., 2015). In the Middle Jurassic, a phase of extension that caused the Central Atlantic breakup commenced in the North Sea and Norwegian-Greenland Sea (Blystad et al., 1995; Færseth, 1996).

In the Late Jurassic, subsidence occurred due to the deflation of the North Sea dome (Brekke, 2000; Underhill, 1998). Basement blocks and overlying sediments were rotated due to normal faulting along the Viking Graben, exposing the shoulders to erosion and causing the Lower-Middle Jurassic and some Upper Triassic strata to be removed (Faleide et al., 2015). During this time, a major sea level rise flooded the topography and led to a period dominated by clayey sediments such as those of the Heather Formation (Brekke, 2001). Following this was a regional sea level fall (Doré, 1992). These cycles in sea level led to the widespread deposition of black shales (Brekke, 2001).

The shift from margin-fed shallow marine environments to an axial system which prograded and retrograded in north-south directions is marked by the deposition of the Brent Group (Martinsen and Dreyer, 2001). Sediments of the Upper Jurassic consisted of syn-rift clastic wedges and shallow marine sands that are associated with deltas and coastal plains, likely derived from the crest of the fault block (Brekke, 2001). High-energy shallow-marine sheet sands such as those of the Sognefjord Formation are believed to be derived from the clastic shorelines of delta or coastal plains (Brekke, 2001). The Draupne Formation was deposited in the Late Jurassic as a thick rich source rock due to a high sedimentation rate and poor bottom water circulation in over deepened basins which formed according to rift topography (Bugge, 2001). These organic-rich sediments continued to be deposited through the Early Cretaceous in some areas (Faleide et al., 2015).

2.3.6 Cretaceous

A change from shallow-marine sedimentation to deep-water sedimentation is associated with tectonism and rifting in the Late Jurassic to Early Cretaceous (Martinsen and Dreyer, 2001). The isolated basins that led to the deposition of the Draupne Formation became more oxygenated (Hesjedal and Hamar, 1983), reflecting the occurrence of the Base Cretaceous Unconformity. It is absent in deeper parts of the rift basins where continuous sedimentation may have occurred but is well marked on most seismic sections. In the Early Cretaceous, subsidence occurred due to crustal cooling after the Jurassic rifting period leading to the development of deep basinal areas along the rift axis of the North Sea (Brekke, 2001; Faleide et al., 2015). In the North Sea, uplifted structures were subaerially exposed and were bordered by transgressive shallow marine sands (Brekke, 2001, 1999; Garbielsen et al., 2001; Oakman and Parington, 1998).

The Cromer Knoll Group is deposited in the Early Cretaceous and consists of shallow to deep marine mudstones with little sand (Isaksen and Tonstad, 1989). At the end of the Early Cretaceous, the lowlands had been flooded and clastic input was cut off from the area, leading to the deposition of pelagic chalk sediments (Oakman and Parington, 1998). A transgressive maximum was reached in the Late Cretaceous (Campanian times), and parts of Scandinavia were most likely covered by sea (Brekke, 2001). Towards the end of the Cretaceous, the Alpine Orogeny in the south influenced compression accommodated along diagonal fault zones. Parts of the North Sea and the Polish Basin were uplifted and eroded (Faleide et al., 2015).

Faleide et al. (2015) identified three stages of the post-rift Cretaceous development in the northern North Sea. The first phase is the *incipient post-rift stage*, which occurred from the Ryazanian to latest Albian. Different degrees of subsidence occur, and sediment distribution is heavily influenced by the major structural features from the syn-rift development. The second phase is the *middle phase*, which occurs from the Cenomanian to Late Turonian. In this phase, sediment supply outpaces subsidence and the internal basin relief is flooded by sediments. Therefore, the syn-rift basin topography was less significant than the subsidence pattern. The subsidence pattern is dependent on the crustal thinning profile, which relies on thermal contraction and isostatic response to sediment loading. The third stage is the *mature post-rift stage* and occurred from early Coniacian to the early Palaeocene. The basin developed a wide,

saucer-shape and syn-rift features were removed. Subsidence stopped due to a thermal equilibrium (Faleide et al., 2015).

2.3.7 Cenozoic

The sedimentary architecture of the Cenozoic northern North Sea basin is widely affected by uplift of surrounding clastic sources and tectonic subsidence. (Faleide et al., 2002). Uplift and various vertical changes have been indicated by changes in depocenters, outbuilding locations, and composition of sediments (Faleide et al., 2002). In the early Cenozoic, rifting, break-up and onset of seafloor spreading occurred, causing vertical movements and uplift of surrounding clastic source areas which had a heavy influence on the sedimentary architecture of the North Sea. The carbonate depositional environments were replaced by clastic input derived from the uplifted Shetland Platform (Brekke, 2001). In the Palaeogene, sedimentary environments shifted from continental rift settings to drift and passive continental margin settings (Brekke, 2001).In the Palaeocene to early Eocene, progradational sedimentary wedges formed in the basin from platforms on both sides in the North Sea (Brekke et al., 1999; Martinsen et al., 1999) At the end of the Palaeocene, a basin-wide anoxic state occurred due to the North Sea basin being cut off from oceanic circulation (Brekke, 2001). Prior to continental breakup, subsidence occurred in the North Sea area, followed by the deposition of deep-water sandy turbidites in the Eocene as a result of relative sea-level fluctuations (Brekke, 2001).

The opening of the North Atlantic is associated with extensive volcanism and the expulsion of basaltic lavas (Brekke, 2001). During the Eocene, a major depocenter existed in the Viking Graben, sourced by progradation from the East Shetland Platform. Palaeocene and Eocene submarine fans of turbidites extend into the central North Sea (Faleide et al., 2015).

Uplift of southern Norway occurred at the transition between the Eocene and Oligocene, which, along with progradation from the east and west created a shallower northern North Sea and separated the deeper water in the south and north (Jordt et al., 1995). This uplift episode also led to the out-building of coarse-grained sediments towards the west and south. At the Norwegian continental margin during the Oligocene and Miocene, sedimentation reflects a marine environment associated with a subsiding passive margin related to phases of tectonic activity (Brekke, 2001). Uplift and shallowing continued into the Miocene when an extensive hiatus was formed in the northern North Sea. A change from progradation to aggradation in the Mid-Oligocene is attributed to a regional rise in sea level and a reduction in sediment supply to the basin center (Jordt, 1995). In the Late Oligocene, sand-rich sediments from the East Shetland Platform were deposited in the basin due to uplift in the northwest. In the mid-Miocene, a subsidence episode occurred with the uplift of southern Norway, as shown by a basin-wide downlap surface. The Miocene also correlates with the last outbuilding event from the west, and the sediment source instead is primarily from the east (Jordt et al., 1995). During the Pliocene, as the uplifted land increased in elevation and the climate in the North Sea became more humid, snowfall and glacial activity occurred, causing sediments to be transported towards the coast. Sediment distributions at this time also indicate that the North Sea Basin had evolved as a narrow sea (Jordt et al., 1995). The current Cenozoic sequence geometry can most probably be attributed to tectonic uplift from the Oligocene to Pliocene, and glacial erosion-related uplift and isostatic rebound in the Pliocene-Pleistocene (Jordt et al., 1995).

2.4 Lithostratigraphy

The following section will describe in detail some of the formations involved in the study area, based on groups. Some of the formations described are observed in adjacent areas but are not seen in the specific study area. In 1977, a lithostratigraphic nomenclature for the Central and Northern North Sea areas was published by Deegan and Scull (1977), which was later revised by Vollset and Doré (1984). The lithostratigraphic formations and their correlating groups are displayed in the chronolithostratigraphic table in Figure 2.4, with the stage and period which they were deposited in.

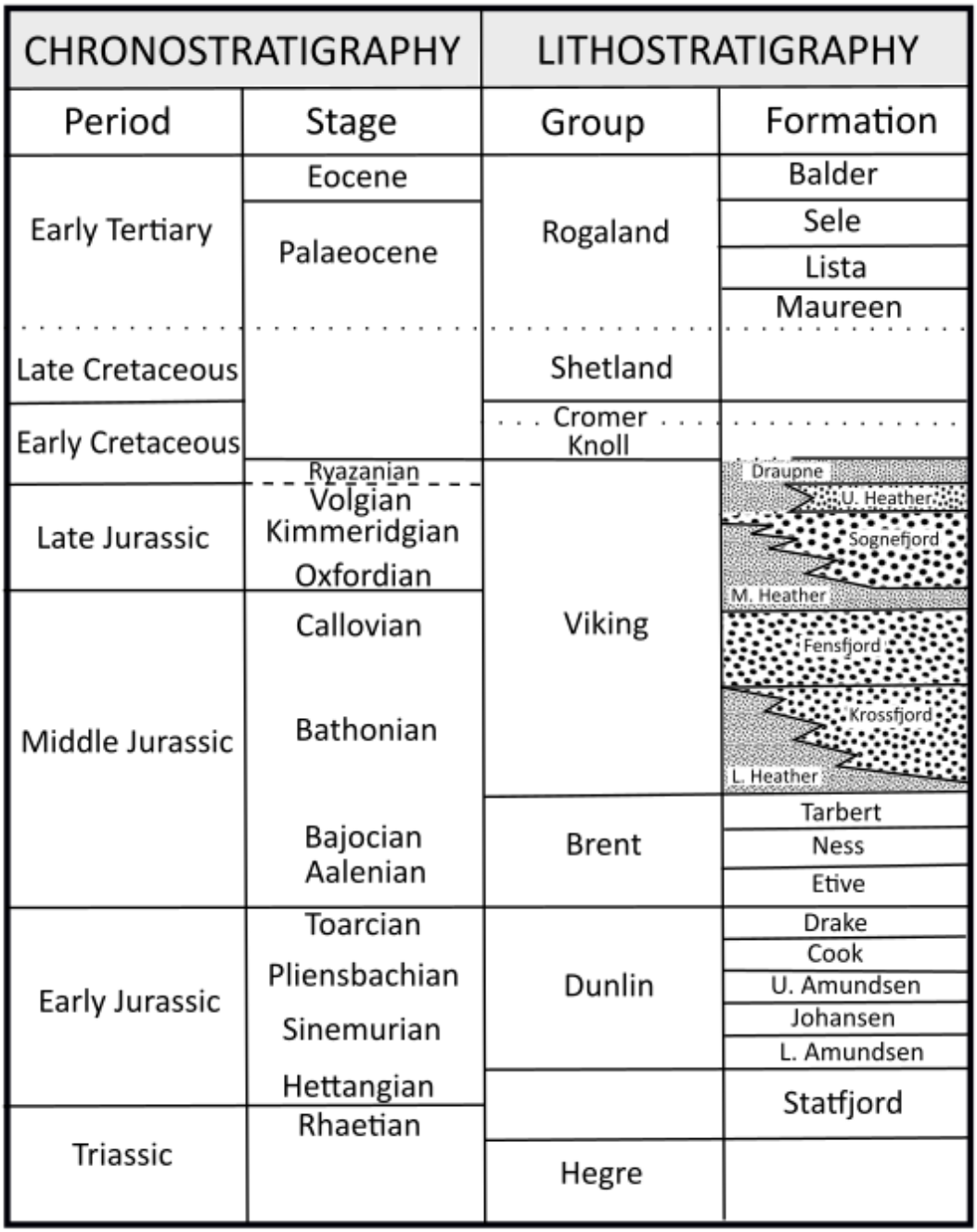

Figure 2.4: Chrono and lithostratigraphy of the northern North Sea, from the Triassic period to the Early Tertiary. Only the Brent sandstone formations (Etive, Ness, and Tarbert) are included in the figure (Redrawn after Bolle, 1992).

2.4.1 Brent Group

The Brent Group is divided into five subunits: the Broom (base), Rannoch, Etive, Ness, and Tarbert Formations. The thickness of the group varies considerably but was found to be between 78 m and 159 m on and around the Horda Platform according to well data (Vollset and Doré, 1984). The group primarily consists of grey to brown sandstones (Figure 2.4), siltstones, and shales. However, only the sandstones of the Etive, Ness, and Tarbert Formations are displayed in Figure 2.4. The following descriptions of the five subunits are originally cited from Deegan and Scull (1977) and revised by Vollset and Doré (1984).

The Broom subunit corresponds to the base of the Brent Group, and is comprised of pale grey to brown, poorly sorted coarse-grained conglomeratic sandstones with shale clasts. The age is likely Late Toarcian to Early Bajocian. The depositional environment is shallow marine (Vollset and Doré, 1984).

The Rannoch Formation consists of light brown, well-sorted and fine-grained micaceous sandstones, also displaying micaceous siltstones and thin shales in the lower part of the unit in the Brent Field area. The formation can be locally divided into two members based on grain size and sorting, according to Hodson (1975). The high mica content helps to distinguish the unit from the under and overlying units. The Rannoch Formation, similarly, to the Broom Formation, is likely Early Bajocian. The depositional environment is likely delta front sheet sands, or sands of a progradational shoreface (Vollset and Doré, 1984).

The Etive Formation consists of brown to grey massive fine to medium grained clean sandstones, lacking in mica and displaying crossbedding. This formation is likely Bajocian, and the depositional environment is upper shoreface, barrier bar, mouth bar, and distributary channel deposits (Vollset and Doré, 1984).

The Ness Formation displays carbonaceous interbedded sandstones and shales with some siltstones and coal. The sandstones in this formation are grey to brown, clean, fine to medium grained, and fairly well-sorted. The shale is dark grey, silty, and contains pyrite or mica. The formation thins and becomes more shale-rich towards Norway. The Ness Formation is Bajocian in age, and the depositional environment is potentially a delta or coastal plain deposit (Vollset and Doré, 1984).

The Tarbert Formation consists of grey to brown, massive fine to medium grained sandstones with some thin beds of siltstone, shale, coal, and calcareous beds. It thickens and shows a higher frequency of coal beds towards Norway. The age of this formation is likely Bajocian to Bathonian, and the depositional environment was marginal marine (Vollset and Doré, 1984).

2.4.2 Viking Group

The Viking Group was deposited onto tilted fault blocks related to tectonic activity, thus giving the group considerable variations in thickness, from just a few meters up to 1039 meters (Vollset and Doré, 1984). The group is subdivided into five different formations: the Heather, Draupne, Krossfjord, Fensfjord and the Sognefjord Formations. The Heather and Draupne Formations are regionally defined, while the Krossfjord, Fensfjord, and Sognefjord Formations are primarily located on the Horda Platform and more northwards. (Vollset and Doré, 1984)

The Heather Formation is primarily composed of grey silty claystones with streaks of limestone. In the Viking Graben area, two subdivisions of the formation are recognized. The upper division is a dark grey silty claystone consisting of carbonaceous sediments and some limestones, and the lower division is a light to dark grey hard silty claystone which is micaceous and calcareous. The silty claystones of this formation were deposited in an open marine environment. The age ranges from Bathonian to Upper Kimmeridgian (Vollset and Doré, 1984).

The Sognefjord Formation consists primarily of grey-brown medium-coarse grained, well-sorted and unconsolidated sandstones and sands. The depositional environment of this formation was likely a coastal-shallow marine environment. The lower boundary is gradational due to the interfingering of the Heather Formation, and the upper boundary is defined by the contact with the Draupne Formation claystones and shales. The age ranges from Oxfordian to Kimmeridgian/Volgian (Vollset and Doré, 1984).

The Draupne Formation (Oxfordian to Ryazanian) contains black mudstones with high organic content, resulting in high gamma ray values, and also making it a hydrocarbon source in the North Sea. Deegan and Scull (1977) named it the “Kimmeridge Clay Formation” but the name was changed to “Draupne” by Vollset and Doré (1984). The depositional environment is marine, likely in anaerobic conditions. Sandstones may exist throughout the formation as turbidites. It overlies the Heather Formation at some locations, but on the northern part of the Horda Platform it overlies the Sognefjord Formation sandstones. (Vollset and Doré, 1984).

The Krossfjord Formation is of Upper Middle Jurassic to Bathonian age, the Fensfjord Formation is of Upper Middle Jurassic to Callovian age, and the Sognefjord Formation is of Upper Jurassic, Oxford to Kimmeridgian age. They are three sandy wedges which interfinger with the Heather Formation on the northern part of the Horda Platform (NPD).

2.4.3 Cromer Knoll Group

The Cromer Knoll Group (Figure 2.5) was defined by Deegan and Scull (1977) with the conclusion that all Lower Cretaceous sediments below the Rødby Formation in the Norwegian sector could be grouped into one formation, called the Valhall Formation (Isaksen and Tonstad, 1989). New data and analyses have allowed for the separation of the Valhall Formation into several units. Formations were named by Hesjedal and Hamar (1983), Jensen et al. (1986), and Isaksen and Tonstad (1989), the last of which will be used in the following sections. The Cromer Knoll Group can be defined by the following five formations beneath the Rødby Formation: the Åsgard, Tuxen, Sola, Mime, and Agat Formations (Isaksen and Tonstad, 1989). However, due to the nature of the rift basin which the Cromer Knoll Group lies in, mainly lower Cretaceous deposits are found on the Horda Platform (Figure 2.3).

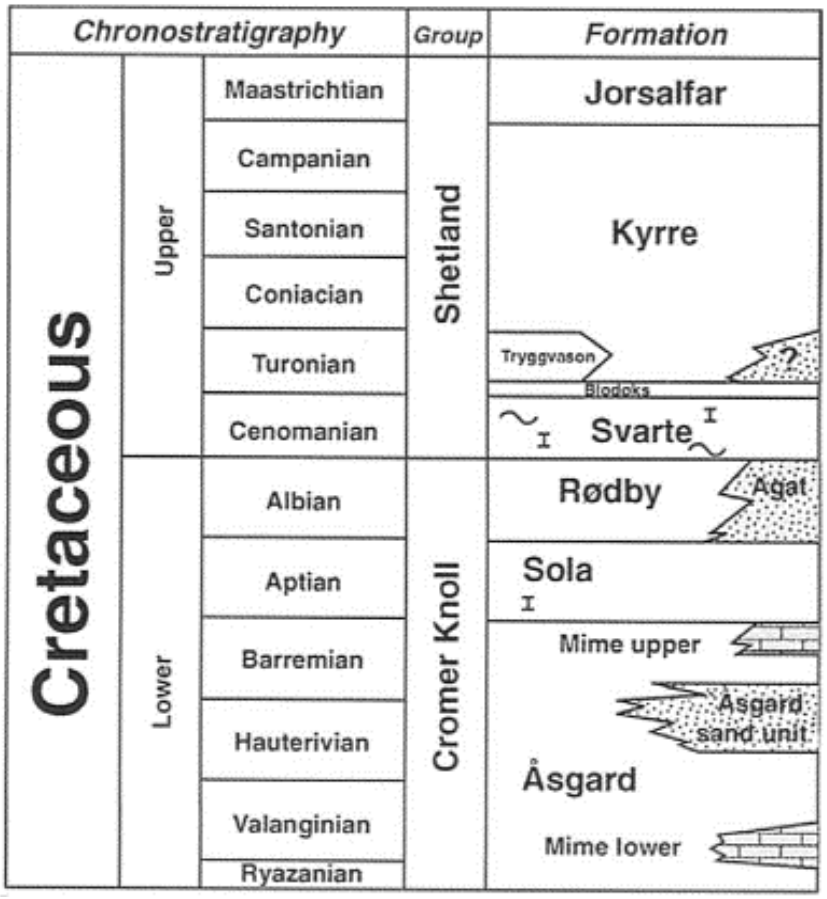

Figure 2.5: A schematic representation of deposits of the Cromer Knoll and Shetland Groups during the Cretaceous. Although listed together under the formation column, it is rare to find all deposits of the Cromer Knoll Group together (Skibeli et al., 1995).

Thickness of Cromer Knoll Group deposits varies considerably due to deposition in response to a Late Jurassic tectonic phase (Isaksen and Tonstad, 1989). In the Viking Graben area, the thickness can be found to be 600 m, and thins towards basin margins. In the Sogn Graben, seismic data indicates thicknesses reaching 1400 m. The Cromer Knoll Group consists primarily of fine-grained, argillaceous marine-sediments with varying amounts of calcareous material. The top of the Draupne Formation defines the base of the Cromer Knoll Group (Isaksen and Tonstad, 1989).

The Cromer Knoll Group was divided into supersequences by Skibeli et al. (1995), giving them the informal names of K1-1 and K1-2. Supersequence K1-1 ranges in age from the Ryazanian to Late Barremanian, while supersequence K1-2 ranges from the late Aptian to Albian. Biofacies analysis from wells suggest that K1-1 was deposited in a shelf environment with highstand and transgressive systems tracts, while K1-2 was probably deposited in a bathyal environment, displaying lowstand systems tracts. Skibeli et al. (1995) attempted a correlation to units from the Lower Cretaceous deposits and prospected them to be the Åsgard unit which ranges from the Hauterivian to Barremanian and consists primarily of highstand systems tracts, and the Agat unit which is of Albian age and consists of lowstand systems tracts. An unconformity exists in most wells between the two units, which is potentially due to a drop in sea level, which was claimed to be a global occurrence in the early Aptian by Haq et al. (1987).

2.4.4 Shetland Group

The Shetland Group (Figure 2.5) was defined by Deegan and Scull (1977) and includes the Upper Cretaceous siliciclastic sediments from the North Sea. Deegan and Scull (1977) also defined a Chalk Group, which has now been integrated into the Shetland Group (Isaksen and Tonstad, 1989). The group is divided into multiple formations separated into chalk facies (defined by Deegan and Scull, 1977) and siliciclastic facies. The chalk facies include the Hidra, Hod, Tor, and Ekofisk Formations, while the siliciclastic facies include the Svarte, Blodøks, Tryggvason, Kyrre, Jorsalfare, and Hardråde Formations (Isaksen and Tonstad, 1989). The Shetland Group was deposited in an open marine environment during a general rise in sea level, and the chalk facies was deposited as coccolith matter and other carbonate grains.

In the graben areas, seismic data indicates that the group ranges in thickness from 1000 m to 2000 m, with thinning towards and on the platform areas. The siliciclastic facies of the Shetland Group consist of mudstones and shales with interbedded limestones, while the chalk facies consist of chalky limestones, marls, and calcareous shales and mudstones. In the Maastrichtian part of the group, the amount of limestone is considerably higher on the Horda Platform than in the Viking Graben (Isaksen and Tonstad, 1989). The lower boundary is usually the contact against the Cromer Knoll Group, while at the upper boundary, Palaeocene marls, mudstones, or sandstones of the Rogaland Group are overlain. The siliciclastic facies are strictly in the Late Cretaceous, but due to the integration of the Chalk Group, the Shetland Group ranges in age from the Cenomanian to Danian (Isaksen and Tonstad, 1989).

2.4.5 Rogaland Group

The Rogaland Group (Palaeocene to Early Eocene) consists of marine sediments, primarily being shales with interbedded sandstones (Isaksen and Tonstad, 1989). The group according to Deegan and Scull (1977) contains four formations, including the Lista, Fiskebank, Sele, and Balder Formations. However, Isaksen and Tonstad (1989) combined Deegan and Scull's Montrose Group with the Rogaland Group, creating a total of 12 formations, few of which are found on the Horda Platform. These will be defined in the following descriptions.

Dominant lithologies of the Rogaland Group vary with location. In the west, sandstones interbedded with shales tend to dominate, while towards the east, the sandstones form lobes which interfinger with shales. The main depositional environment of this group is distal marine

(Isaksen and Tonstad, 1989). The Lista Formation is Late Palaeocene in age and consists primarily of non-tuffaceous and non-laminated shales with minor interbeds of sand. The depositional environment is relatively deep water with low energy. The Sele Formation is Late Palaeocene to early Eocene in age and consists primarily of medium to dark grey or green-grey shales and siltstones, with minor interbeds of glauconitic sandstones. The depositional environment is in a deep marine setting. The Balder Formation is Palaeocene to early Eocene in age, consisting of laminated shales with interbeds of grey, green, or buff sandy tuffs. The formation depositional environment is deep marine, primarily as hemipelagic sediments. The sands in this formation are locally developed, potentially as turbidites (Isaksen and Tonstad, 1989).

2.4.6 Hordaland Group

The Hordaland Group ranges from Eocene to Early Miocene, and primarily consists of light grey to brown marine shales with limestone streaks. Localized sand groups may also occur, consisting of fine to medium grained sands with shale streaks. In the Hordaland Group, Deegan and Scull (1977) only identified one formation: the Frigg Formation. However, Isaksen and Tonstad (1989) identified and described three additional formations: the Grid, Skade, and Vade Formations. The average thickness of the Hordaland Group in the central and southern parts of the Viking Graben is between 1100 m and 1200 m (Isaksen and Tonstad, 1989). The depositional environment is open marine.

The Frigg Formation is of Eocene age, and is composed of massive, poorly consolidated, light brown to buff, micaceous and carbonaceous sandstones (Deegan and Scull, 1977). The formation was deposited as submarine fans by gravity flows, sourced by the East Shetland Platform in the west (Isaksen and Tonstad, 1989). The Grid Formation is of Middle to Late Eocene age, composed primarily of sandstones with interbedded claystone and siltstone. A higher clay content is noted in distal areas, and the depositional environment is likely open marine during a regression. The Skade Formation is of Late Eocene age and is composed of marine sandstones interbedded with thin claystones. Fossils and shell fragments are found in this formation, and the depositional environment was potentially open marine after a fall in sea level. The Vade Formation is of Late Oligocene age, and is composed of thinly interbedded, light green to grey, very fine-grained sandstones and siltstones with the presence of fossils. The depositional environment was likely shallow marine, either as a response to eustatic sea level fall or tectonic uplift. The sediment source area was in the east or northeast (Isaksen and Tonstad, 1989).

2.4.7 Nordland Group

The Nordland Group ages from Middle Miocene to recent and is composed primarily of grey to grey-brown, slightly micaceous, and silty marine shales and clays. Sands were also deposited during regressions in this period, leading to the deposition of the only formation outlined by Deegan and Scull (1977): the Utsira Formation. The upper part of the group consists of uncompacted muds which are typically overlain by glacial deposits (Deegan and Scull, 1977), but the depositional environment for the group is open marine (Isaksen and Tonstad, 1989). The upper boundary of the Nordland Group is the seabed.

The Utsira Formation ranges from the Middle to Late Miocene and consists primarily of light green to grey marine sands and shales with plentiful deposits of macrofossil fragments (Deegan and Scull, 1977). The depositional environment is likely shallow marine shelf sandstones (Isaksen and Tonstad, 1989).

2.5 Evolution of Ideas Regarding Cenozoic Uplift

The evolution of topography during the Cenozoic in the North Sea is subject to debate, and uncertainty exists of the impact glaciations have had on the morphology. Several compilations of literature exist which indicate evidence for widespread regional uplift during the Cenozoic (e.g. Anell et al., 2009; Japsen and Chalmers, 2000; Stuevold and Eldholm, 1996) as well as compilations of literature to explain the uplift features with climatic change effects, thus implying that uplift is not evident (Molnar and England, 1990). The development and evolution of sedimentary basins has been modelled by McKenzie (1978), giving foundation to the standard tectonic evolution model which explains subsidence rates in rifted settings. The theory explains a multi-event process as a simple model for sedimentary basin evolution and development. The first event in this process involves rapid stretching of the lithosphere, which leads to crustal thinning and hot upwelling, associated with fault blocks and subsidence. Heat conduction causes thickening of the lithosphere, followed by slow subsidence, both of which are dependent on the amount of stretching.

Early studies of uplift were based on geomorphic analysis, and advanced techniques such as reflection seismic studies, apatite fission track analysis, maximum burial studies, sediment supply studies, mass balance studies, and onshore extrapolation were later applied. Each technique has limitations and uncertainties, leading to current methods which consist of the utilization of multiple techniques in a study (Anell et al., 2009). Molnar and England (1990) suggested that features of uplift may be explained by climatic changes such as glaciation or eustatic sea-level fall which affect the rate of erosion, making tectonic uplift irrelevant. Lidmar-Bergström et al. (2000) argued that the Norwegian margin displayed geomorphologic similarities to unglaciated margins in Australia, Africa, and India. A combination of both glacio-isostatic rebound, and a tectonic component was presented by Mörner (1977). Regional geologic data has been compiled by Anell et al. (2009) to review current understandings of Cenozoic topographic evolution of the North Atlantic Margin, specifically focusing on uplift and subsidence.

Regional uplift occurred in the Palaeocene to Eocene period, followed by subsidence in the Eocene. The regional uplift is believed to have occurred on the border of the North Atlantic break-up, possibly related to mantle processes. It has been suggested that the uplift was related to the Iceland plume, and/or a Palaeogene rifting phase (e.g. Faleide et al., 2002; Jordt et al., 1995; Skogseid et al., 1992; Stuevold et al., 1992). Multiple phases of uplift occurred moving progressively northwards, the first being near the northern British Isles, the second being at the Norwegian western margin, and the last being in the far north region of Norway during the Eocene. This last phase was potentially caused by the northward propagation of rifting between Norway and Greenland during the Eocene. Aside from this phase and anomalous subsidence, which is noted in the same time period, the Eocene was noted mostly as a period of tectonic quiescence.

A relative change in the spreading between Norway and Greenland is theorized to have caused compressive stresses during the Oligocene, and local uplift occurred in the North Sea region and some surrounding areas. Uplift of the Fennoscandian mainland is noted by an offshore

influx of coarse-grained sediments from Norway (Danielsen et al., 1998) along with progradational wedges offshore of South Norway (e.g. Ghazi, 1992; Jordt et al., 1995; Martinsen et al., 1999). The timing of such uplift events, however, is under debate and multiple uplift events are recorded in literature: one event being in the Late Eocene-Early Oligocene in West Greenland (Bonow et al., 2006; Japsen et al., 2005, 2006), and another in the Oligocene in the eastern North Sea (Clausen et al., 2000; Wien and Kjennerud, 2005).

Uplift of the Norwegian mainland was suggested to have occurred in the Neogene (e.g. Faleide et al., 2002; Jensen and Schmidt, 1992, 1993; Riis, 1996). During the Miocene, local uplift occurred on the SW and NE coasts of Greenland (Hamann et al., 2005), and in the North Sea region, particularly at the shelf area of Norway (Henriksen et al., 2005). Uplift during this period in the western European region includes Scotland, the northern North Sea, the mid-Norwegian margin, the Norwegian mainland, and the eastern North Sea and Denmark.

Regionally extensive uplift occurred during the Plio-Pleistocene period, affecting most regions around the North Atlantic, possibly related to glacial erosion and isostatic rebound. Tectonic relevance is currently unknown. This is determined by the presence of late Neogene sedimentary wedges, which are products of erosion (Ryseth et al., 2003; Sættem et al., 1994; Vorren et al., 1991). A cooling phase was identified on Svalbard to suggest an erosional response from glaciation (Blythe and Kleinspehn, 1998), but it is under debate whether such a response can account for the uplift observed (Eidvin et al., 1993).

Chapter 3

3 Data and Methodology

The following sections explain the software and data set used in this study, as well as interpretation techniques and specific attributes which were used to attain the results. The focus is on the study area, covered by both 3D and 2D seismic data.

3.1 Software

Petrel (2018 version), and Inkscape have been used for this thesis. Petrel is a Schlumberger program which can be used for interpretation of seismic data, well correlation, volume calculations, map generation, etc. (developer: Schlumberger Limited, http://www.software.slb.com). Unless stated otherwise, all interpreted horizons and cross-sections are displayed in two-way time (TWT). 2D lines were selected to give a regional understanding of sediment distribution over a wider area, and each is in proximity of the 3D cube to ensure better correlation to horizon tops (Figure 3.1). Inkscape is a vector graphics software program which was used to create the figures in this study.

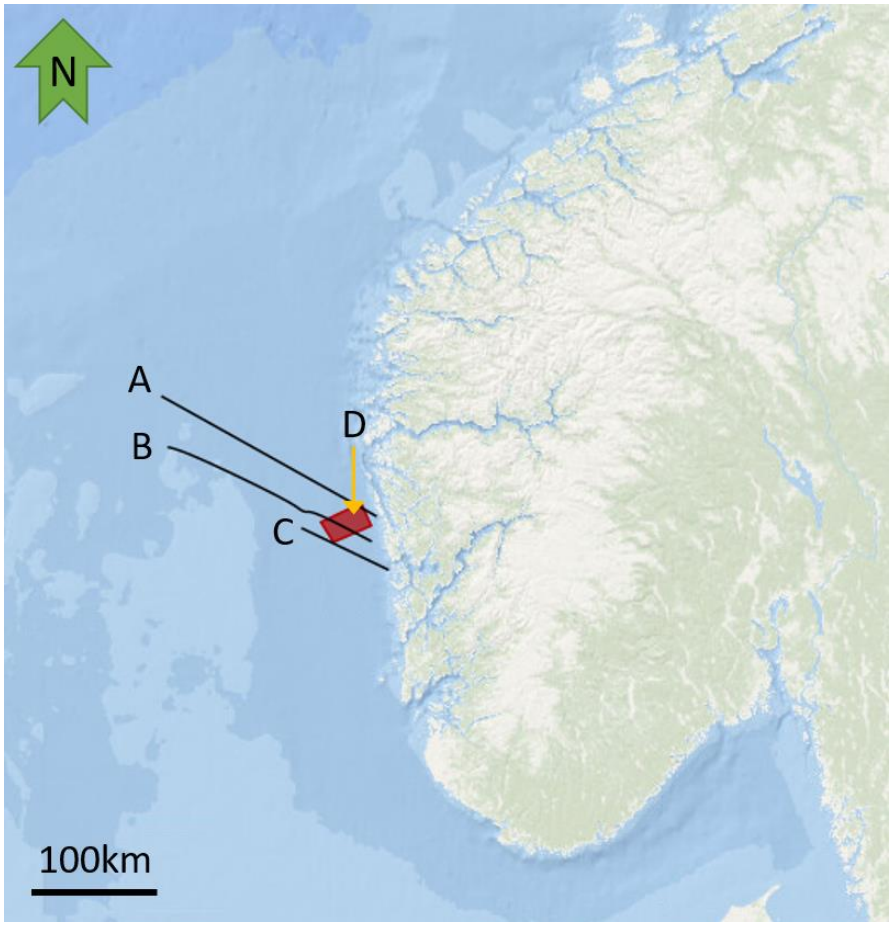

Figure 3.1: Regional setting including tectonic elements for the 3D and 2D seismic surveys. A: SG8043-404A; B: SG8043-402A; C: SG8043-401A; D: GN1101.

3.2 Data Set

The data implemented in this study comes from the 3D seismic survey GN1101 and the SG8043 2D seismic survey (Table 3.1). Additionally, eight wells were utilized for seismo-stratigraphic control (Table 3.3, on page 36). The primary well used for seismic survey GN1101 was 32/4-1, although there are two wells in the vicinity of the cube. Seismic-to-well ties serve as points of certainty, which decrease with radius from the well.

3D Seismic	Year of Survey	Company	TWT-axis	Line orientation
GN1101	2011	GASSNOVA SF	5000 ms	ILN = WSW-ENE (25.00 meters) XLN = NNW-SSE (12.50 meters)

2D Seismic	Year of Survey	Company	TWT-axis	Lines used in this study
SG-8043	1991	-	7000 ms	401A, 402A, 403A

Table 3.1: 3D and 2D seismic survey information.

3.2.1 Seismic Survey GN1101

The main seismic survey used in this study is a three-dimensional cube, called GN1101. It was originally acquired by Gassnova SF in 2011. The inline orientation is WSW-ENE, and the x-line orientation is NNW-SSE. Two wells are in the vicinity of this seismic survey (32/4-1 and 31/6-6), and well 32/4-1 is the one used in this study.

3.2.2 Seismic Survey SG8043

Three 2D lines are used from seismic survey SG8043, including SG8043-401A, SG8043-402A, and SG8043-404A. The lines are oriented NW-SE and were acquired in 1991. The TWT axis is 7000 ms, and each line has some wells in their vicinity. SG8043-401A is associated with wells 31/6-2R and 31/6-1; SG8043-402A is associated with wells 31/3-1 and 31/2-4R; SG8043-404A is associated with wells 31/2-8 and 31/2-3.

3.3 Seismic Data

Seismic data provides a way to view the subsurface structure by giving a “time picture” which is acquired offshore using a marine vessel which emits acoustic energy. The seismic waves produced by the source propagate through the subsurface and the refracted or reflected waves return to the surface to be collected by hydrophones. The sound wave stimulates an electric signal proportional to the wave’s amplitude to be generated and registered by the hydrophone. The raw data is processed and displayed for seismic interpretation (Keary and Brooks, 1991; Landrø, 2010).

In the interpretation process, horizons for strong or notable reflectors were interpreted and named from A to P in addition to the seabed, with A correlating to the Top Brent surface, and P correlating to the Base Pleistocene Unconformity. The packages beneath each horizon were given correlating unit names accordingly (e.g. Seismic Horizon A is the top of Unit A, Seismic Horizon B is the top of Unit B, and so on). Onlaps, toplaps, and downlaps were noted throughout

the section. Time-thickness maps, seismic attribute maps, and surface maps were made and are displayed in the following sections.

Time-thickness maps are displayed in a 2D window, and are scaled from 0 ms to 500 ms, with increments of 25. Smoothing operations with increments of 2 were used to highlight most important data contrasts. Z-values less than zero were removed from the data, as they represent misinterpretations. For time-thickness maps with eroded sections, the base surface is transparently shown and covered in grey lines to display that sediments were deposited there but have been eroded.

Surfaces are displayed in a 2D window and are all scaled from -400 ms to -2000 ms, with increments of 100. A smoothing operation with increments of two was used to highlight larger contrasts in the data. Flattened surfaces are displayed on inline 1291 (Figure 3.2).

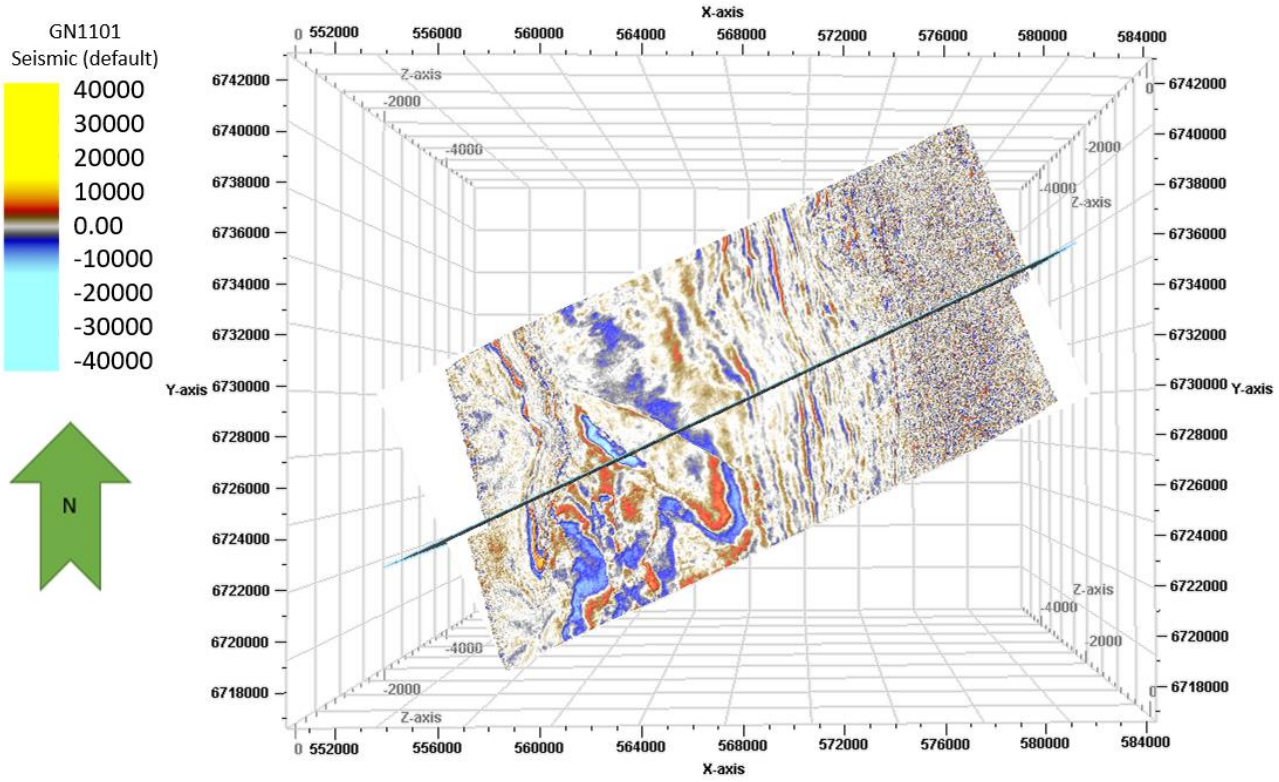

Figure 3.2: Inline 1291 placement on the GN1101 3D cube. Inline 1291 is the NE-SW trending line, while the flat time-slice is the NE-SW trending rectangle.

3.3.1 Phase and Polarity

Prior to interpretation, it is important to understand the phase and polarity of the data, particularly when looking at direct hydrocarbon indicators (DHIs). The Society of Exploration Geophysicists (SEG) has defined the current convention of red color as positive (peaks) and blue as a negative reflection coefficient (troughs), respectively, in normal polarity and vice versa in reversed polarity (Brown, 2001). The polarity can render a seismic reflection from two endmembers: minimum phase (asymmetric-design) or zero-phase (symmetric-design), (Brown, 1999).

3.4 Seismic Interpretation

Seismic stratigraphy is defined by Mitchum et al. (1977) as the use of seismic data to study stratigraphy and depositional facies. Sequence analysis is undertaken by dividing seismic sections into packages based on reflection behavior, followed by separation into depositional sequences bounded by unconformities or correlative conformities (Mitchum et al., 1977). Prior to interpretation, seismic data was displayed and viewed, and the polarity and phase wavelet were established. Stratigraphic horizons and reflection signatures were tied and evaluated for the possibility of horizon-mapping. Various parameters such as stratigraphic position and age, seismic reflection amplitude and continuity, and seismic to well correlation were considered upon choosing appropriate reflections. The designated seismic horizons and their expressions in the data are shown in Table 3.2, on page 33.

Seismic sequences can be defined as depositional sequences identified on seismic sections. The sequences can be divided by discontinuous surfaces which are defined by reflection terminations. Reflection terminations can include erosional truncation, toplaps, onlaps, and downlaps (Figure 3.3). Erosional truncation implies that deposition and removal of those deposited sediments occurred on an unconformable surface. Toplaps are reflection terminations against overlying surfaces as a result of sedimentary bypass, or nondeposition. Onlaps imply that initially horizontal strata terminate against an initially inclined surface, or that initially inclined strata terminated against a surface of greater inclination. Downlaps can be interpreted as initially inclined strata terminating downdip onto an inclined or horizontal surface. It may be difficult to distinguish between downlaps and onlaps due to deformation, so the term “baselap” may be used instead (Mitchum et al., 1977).

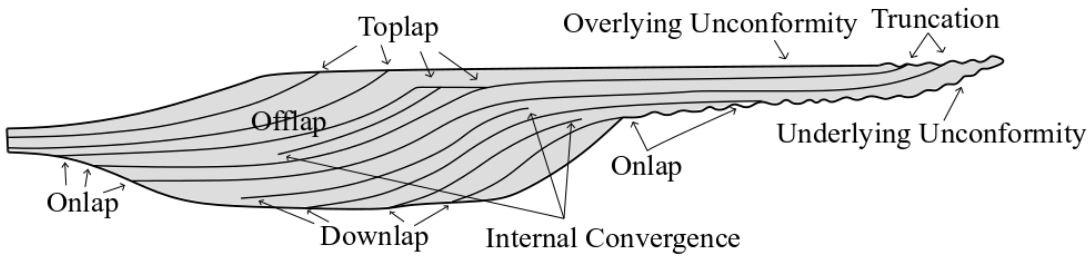

Figure 3.3: Reflection terminations of an idealized seismic section (redrawn after Mitchum et al., 1977).

Seismic facies can be grouped based on the reflection characteristics such as configuration, amplitude, continuity, frequency, and velocity. Reflection configurations can be described as parallel, subparallel, divergent, prograding, chaotic, or reflection-free (Figure 3.4). Parallel and subparallel configurations suggest uniform deposition rates on a subsiding shelf, or a stable basin plain setting. Divergent configurations can occur due to a progressive stratal thinning, and lateral variations in deposition rates, or tilting of the depositional surface (Mitchum et al., 1977). An approach to seismic stratigraphy was described by Mitchum et al. (1977), and includes two main steps: 1) analysis of seismic sequences, which includes dividing packages based on discontinuous surfaces and interpreting them as separate depositional sequences, and 2) analysis of seismic facies, which includes analysis of the configuration, continuity, amplitude, frequency, and velocity of reflection patterns to be interpreted for depositional environments and lithological analysis. Reflection configurations may reveal stratification patterns, which can be interpreted to understand depositional processes, erosion, or paleotopography. Reflection continuity can be associated with strata continuity, because continuous reflections suggest uniform and widespread distribution of sediments. Reflection amplitude can give information on the lateral distribution and changes of bedding, and occurrences of hydrocarbons. Frequency is related to reflector spacing or lateral changes in internal velocity, such as in the case of a gas occurrence.

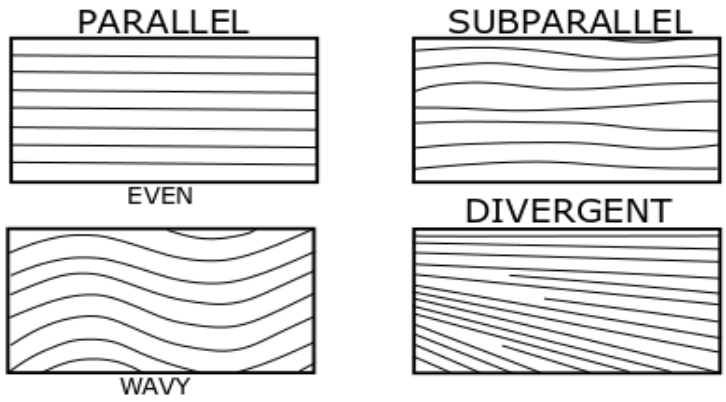

Figure 3.4: Schematic illustration of parallel (even, wavy), subparallel, and divergent reflection configurations (Redrawn after Mitchum et al., 1977).

After relevant reflections were established, horizon interpretation commenced. Seismic horizons are chosen from reflectors which are strong, or display surfaces of discontinuity. Reflectors surrounded by terminations such as onlaps, downlaps, or toplaps were preferentially chosen. Seismic horizon interpretation is conducted using four basic methods:

1. Manual interpretation: Points can be manually decided upon between the points which Petrel interpolates linearly.
2. Guided Auto tracking: Starting and ending points of a reflector are picked manually, and the interpretation will follow between the two points.
3. Seeded 2D Auto tracking: Picked points are tracked along a reflection until a discontinuity is reached.
4. Seeded 3D Auto tracking: Points are tracked outwards in all directions until discontinuities are reached.

To maintain quality of interpretation, a combination of the four methods was often utilized. The most commonly used method was guided auto tracking, which could be used on reflections of good quality. In areas of poor seismic reflection quality, manual interpretation was used, while areas of very good and extensive reflector quality allowed for the use of seeded 2D auto tracking. 3D auto tracking was only used once inlines and x-lines were fully interpreted to complete the surface and prepare it for the creation of amplitude and time-thickness maps. A total of 17 key horizons were interpreted based on the seismic data and named Seismic Horizons A-P, in addition to the Seabed surface (Figure 3.5). The interpreted reflections, except the seabed, were tied to all available well tops that included the respective horizons, shown in Table 3.2. Interpretation of the horizons was performed on inlines with increments of 10 for the GN1101 cube, and crosslines were used in greater increments for conditioning purposes. However, the density of the grid fluctuates with horizon complexity and reflection energy strength, and crosslines would often be interpreted to assist with inline interpretation. 3D auto track with >80% confidence was applied to each horizon.

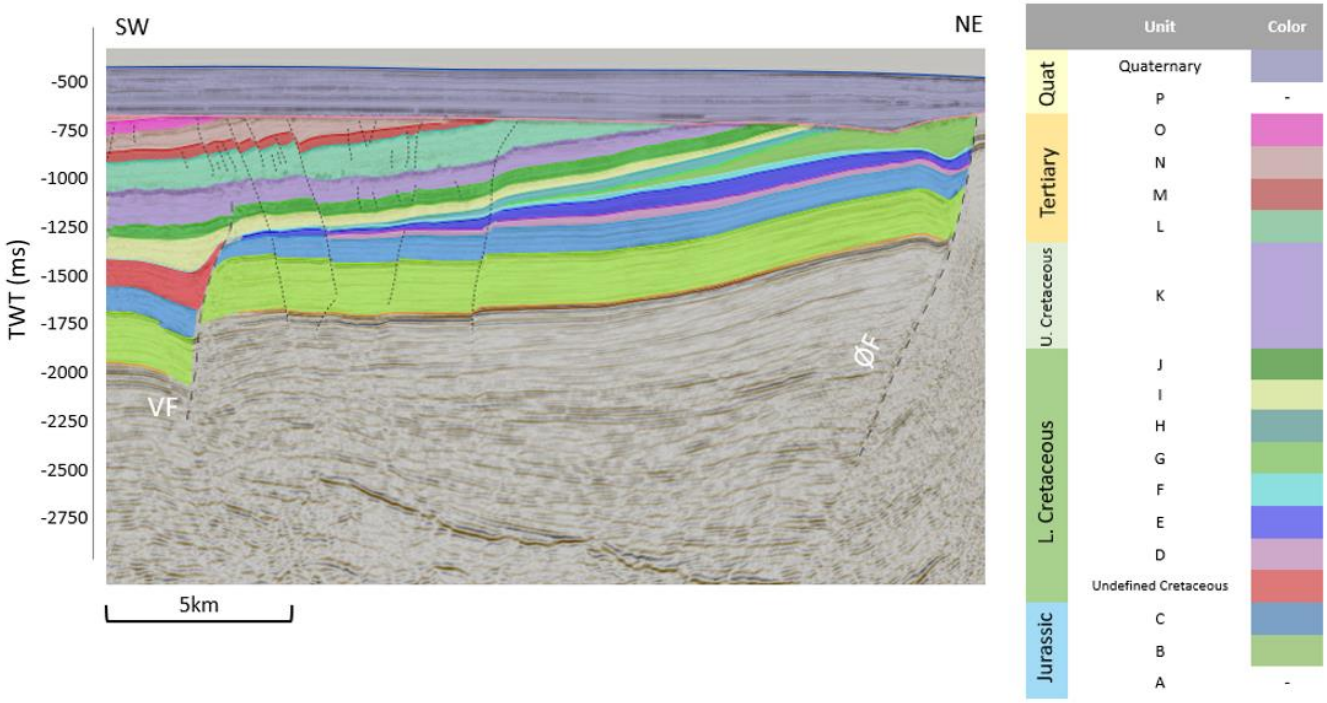

Figure 3.5*:* GN1101 cube oriented SW-NE with seismic horizons (SH) correlated to geologic time. The red package above Unit C represents undifferentiated Lower Cretaceous Units. VF: Vette Fault; ØF: Øygarden Fault.

Seismic Horizon (SH)	Stratigraphic Correlation	Normal Polarity	Reflection Quality	Age	Literature Correlation
Seabed		Trough	Very good, continuous	Recent	-
P	Base Pleistocene Unconformity	Peak	Strong, continuous	Base Pleistocene	NEO-4 (Anell et al., 2010), CSS-9 (Jordt et al., 1995)
O	-	Trough	Strong	Tertiary	?
N	Top Sele	Peak	Intermediate, disrupted	Late Palaeocene	CSS-1.2 (Jordt et al, 1995)
M	-	Trough	Weak, disrupted	Palaeogene	?
L	Top Lista	Peak	Strong, disrupted	Palaeogene	CSS-1.1 (Jordt et al., 1995)
K	Top Shetland	Peak	Strong, disrupted	Base Palaeocene	K6 (Kjennerud et al., 2001)
J	Top Cromer Knoll	Trough	Strong	Top Lower Cretaceous	?
I	Cromer Knoll	Trough	Intermediate	Intra-Lower Cretaceous	?
H	Cromer Knoll	Peak	Weak, truncated	Intra-Lower Cretaceous	?
G	Cromer Knoll	Trough	Weak, truncated	Intra-Lower Cretaceous	?
F	Cromer Knoll, Erosional Surface	Peak	Intermediate	Intra-Lower Cretaceous	?
E	Cromer Knoll	Trough	Intermediate, truncated	Intra-Lower Cretaceous	?
D	Cromer Knoll	Trough	Intermediate	Intra-Lower Cretaceous	?
C	Top Draupne	Trough	Intermediate	Base Cretaceous Unconformity	?
B	Top Sognefjord	Peak	Strong, continuous	Late Jurassic	?
A	Top Brent	Trough	Strong, continuous	Early Jurassic	?

Table 3.2*:* Display of each individual seismic horizon, their stratigraphic correlation, polarity, reflector quality, age, and correlations to literature.

3.4.1 Surface Operations and Attribute Maps

Seismic attributes are becoming more frequently used in petroleum exploration and production. They have been developed since the 1990's and have developed into multiple variations of structural and stratigraphic attributes. They assist in revealing characteristics of the seismic data which are not so easily viewed by amplitude itself and may increase the interpretability of geologic formations (Koson et al., 2014).

Surfaces may be displayed in a 2D or 3D format, and colors can be scaled to highlight geological features in the data. Surfaces in this dataset have been scaled form -400 ms to -2000 ms with increments of 100, and time-thickness maps have been scaled to 0 ms to 500 ms with increments of 25 to assist in consistent analysis. Seismic attributes may be displayed on various products, such as surfaces and time-slices. The primary attributes used in this study include RMS amplitude and variance. A smoothing operation was used on each surface and time-thickness map to condition the data and reduce noise.

Smoothing Operation

The smoothing operation works by applying filters at grid nodes. The filter may function by deleting a certain node value and calculating a new node value from a circular range of values around the centered node. To increase the smoothing factor, the circular range can be increased, and values are taken farther from the center for the calculation of the new node value. The smoothing operation is controlled by *number of iterations* and *filter width* (SCM, 2011).

The smoothing operation used by Petrel is Gaussian, and can be expressed mathematically by the following equation (Daber et al., 2008):

$$hG(\mathrm{k}) = \frac{1}{\sqrt{2\Pi\sigma}}\, exp\ (-\frac{1}{2}\ \frac{k^2}{\sigma^2}\ )$$

Root Mean Square (RMS) Amplitude

RMS amplitude gives a scaled estimate of the trace envelope and smooths the reflection strength, revealing bright spots and amplitude anomalies to highlight hydrocarbon indicators and to display details about the geologic formation. It can highlight coarser-grained sediments, unconformities, and effects of compaction (Koson et al., 2014). Higher RMS values can indicate the presence of coarse clastics, differential compaction, and evidence of an unconformity. RMS amplitude can be expressed mathematically by the following equation, with the variable k representing the number of samples:

$$\sqrt{\frac{1}{N}\sum_{n-1}^{N} w_n\ x_n^2}$$

Variance

The variance method is used to image discontinuities in the horizontal continuity of amplitudes in the data. It is commonly used for delineation faults but is also used to highlight stratigraphic features such as channel edges. It is effective for displaying major fault zones, fractures, unconformities, and major sequence boundaries (Koson et al., 2014).

3.5 Well Data

The following section describes the well data that was involved in the process of this thesis. During the interpretation process, well tops were displayed over the 3D cube and 2D lines in Petrel. The well top depths are based on data by the Norwegian Petroleum Directorate (NPD). In the GN1101 3D cube, only one well is in close enough vicinity to be of use (Figure 3.6), and several other wells are close enough to the 2D data to be used, as displayed in Table 3.3. Wells containing well top depths and stratigraphic information were used during the interpretation, although some ambiguous reflectors can be problematic to follow, and stratigraphic information from previous data was also used to ensure improved quality control. Geophysical well data is also implemented in this thesis for interpretation of lithology.

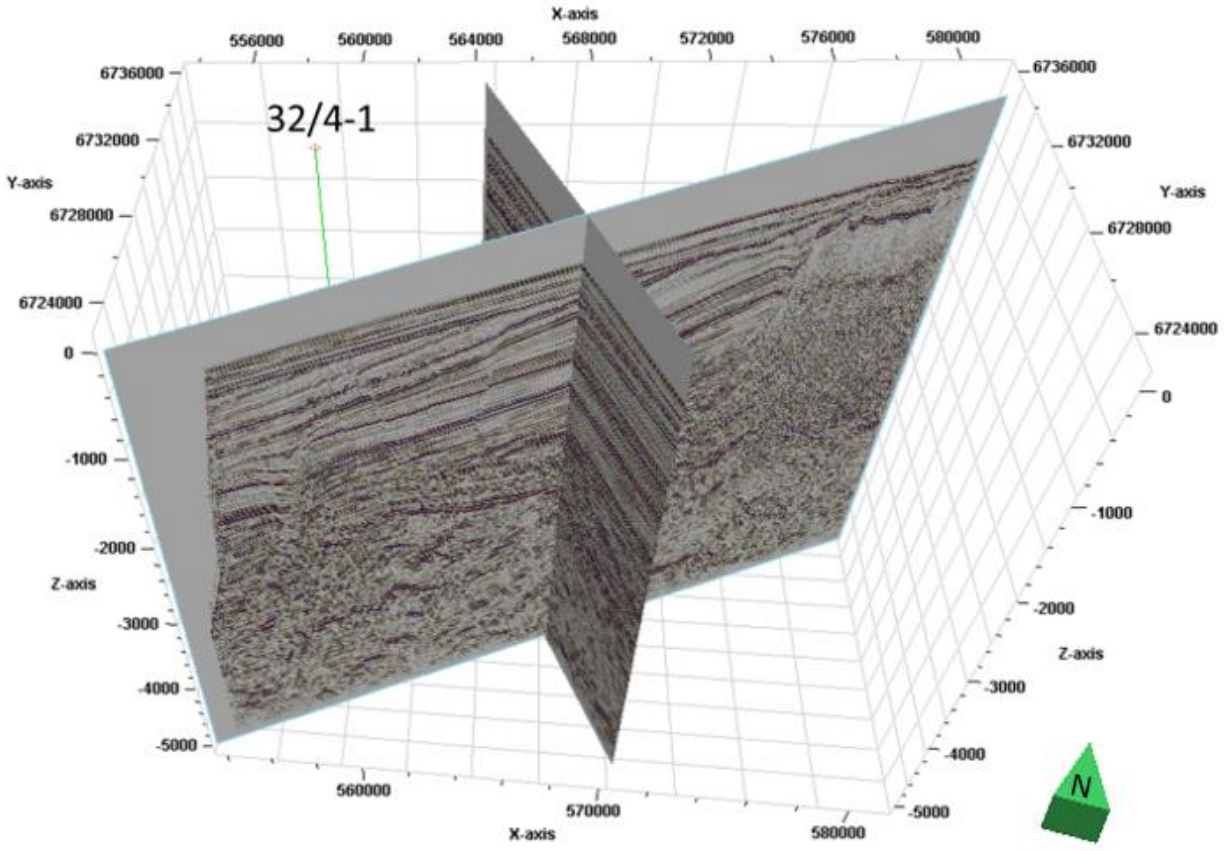

Figure 3.6: Map displaying well 32/4-1, which was the primary well used for seismic-to-well ties in the 3D GN1101 cube.

	Wellbore Name	32/4-1	31/6-6	31/6-2R	31/6-1	31/3-1	31/2-4R	31/3-3
	Drilling Company and Year	Philips Petroleum Company Norway, 1996	Den norske stats oljeselskap AS, 1984	Den norske stats oljeselskap AS, 1984	Norsk Hydro Produksjon AS, 1983	Norsk Hydro Produksjon AS, 1983	A/S Norske Shell, 1980	Saga Petroleum, 1984
Time	Seismic to well tie	GN1101	GN1101	SG8043-401A	SG8043-401A	SG8043-402A	SG8043-402A	Proximity of SG8043-404A
Miocene	Nordland Gp	336	336	326	327	357	361	358
Eocene	Hordaland	-	531	505	531	531	724	540
	Rogaland	535	650	626	972	932	1203	826
	Balder	-	650	626	972	931	1203	826
Palaeocene	Sele Fm	535	798	-	1084	1038	1234	914
	Lista Fm	652	949	776	1194	1136	1256	1085
	Våle Fm	837	-	885	-	1225	1357	-
L. Cretaceous	Shetland Gp	846	1018	968	1232	1235	-	1230
	Jorsalfare Fm	846	-	-	-	-	-	-
	Kyrre Fm	849	-	-	-	-	-	-
	Tryggvason Fm	894	-	-	-	-	-	-
	Blodøks Fm	940	-	-	-	-	-	-
	Svarte Fm	956	-	-	-	-	-	-
E. Cretaceous	Cromer Knoll Gp	1081	1204	1128	1304	1273	-	1378
	Rødby Fm	1081	1204	1128	-	1273	-	-
	Åsgard Fm	1106	1340	1223	-	-	-	-
L. Jurassic	Viking Gp	1109	1392	1322	1313	1320	1365	1633
	Draupne Fm	1109	1392	1322	1313	1320	-	1633
	Heather Fm	1216, 1306, 1595	1515, 1706, 1976	1435, 1625, 1910	1335, 1488, 1776	1497, 1779	1460, 1710	1747, 1905, 2134
	Sognefjord Fm	1238	1561	1460	1352	1352	1365	1753
	Fensfjord Fm	1366	1719	1642	1518	1516	1520	1931
	Krossfjord Fm	1598	1947	1875	1720	1668	1625	2077
M. Jurassic	Brent Gp	1650	2008	1931	1805	1796	1784	2163
E. Jurassic	Dunlin Gp	1680	2045	1975	1835	1844	1902	2209
	Drake Fm	1680	2045	1975	1835	1844	1902	2209
	Cook Fm	1733	-	-	1962	1945	2008	-
	Burton Fm	1783	-	-	-	-	-	-
	Johansen Fm	1785	2122	2055	1981	2001	2126	2306
	Amundsen Fm	1791	-	2138	2083	1992, 2088	2107, 2241	2293
L. Triassic	Statfjord Gp	1816	2225	2164	2111	2105	2256	2432
	Hegre Gp	1832	2277	2198	2156	2160	2422	-
Permio-Triassic	Basement	3132	-	-	4014	-	-	-

Table 3.3: Wells in the vicinity of the 3D cube and 2D lines. Well tops and their correlating stratigraphies are listed next to well top depths (well tops from NPD).

The primary well used in correlation with the seismic data for the 3D GN1101 cube was well 32/4-1 which was drilled by Philips Petroleum Company, Norway, in 1996. This wildcat well is located on the Horda Platform. The main objective of drilling this well was to determine commercial reserves for the Upper Jurassic Sognefjord sandstone reservoir, as the Alpha prospect was believed to contain oil spilled from the nearby Troll Field. Two cores were taken from the silt and sandstones of the Heather Formation, and two others were taken from the Sognefjord Formation, which is interfingered by the Heather. The well was considered to be a dry well and was subsequently plugged and abandoned Well top depths and correlating formations or groups are displayed in Table 3.4.

Stratigraphic Unit	Top depth (m)	Thickness (m)	Age
Sele Formation	535	115.5	Late Palaeocene
Shetland Group	846	234.5	Late Albian - Maastrichtian (Late Cretaceous)
Cromer Knoll Group	1080	28.5	Late Albian - Cenomanian (Mid Cretaceous)
Draupne Formation	1109	106.5	Mid Volgian - Early Barremanian (Late Jurassic - Early Cretaceous)
Sognefjord Formation	1238	68	Early to Middle Oxfordian (Late Jurassic)
Brent Group	1649.5	30.5	Aalenian to Early Bajocian (Middle Jurassic)

Table 3.4: Stratigraphic units and their top depths, ages, and thicknesses according to well data from well 32/4-1, which is in the vicinity of the GN1101 3D cube (NPD).

Chapter 4

4 Results

The following chapter outlines the results attained in this study, beginning with 2D seismic interpretation and followed by 3D seismic interpretation. Analysis of the depositional history emphasizes the units that lie within the Cretaceous succession, particularly Seismic Horizons C through K (Units C-K). Seismic Horizon C represents the top of the Draupne Formation, and correlates to the Base Cretaceous Unconformity (e.g. Jackson et al., 2008). Seismic Horizon J represents the top of the Cromer Knoll Group, which represents the latest Lower Cretaceous, and Seismic Horizon K represents the end of the Cretaceous succession, and the top of the Shetland Group (Figure 4.1).

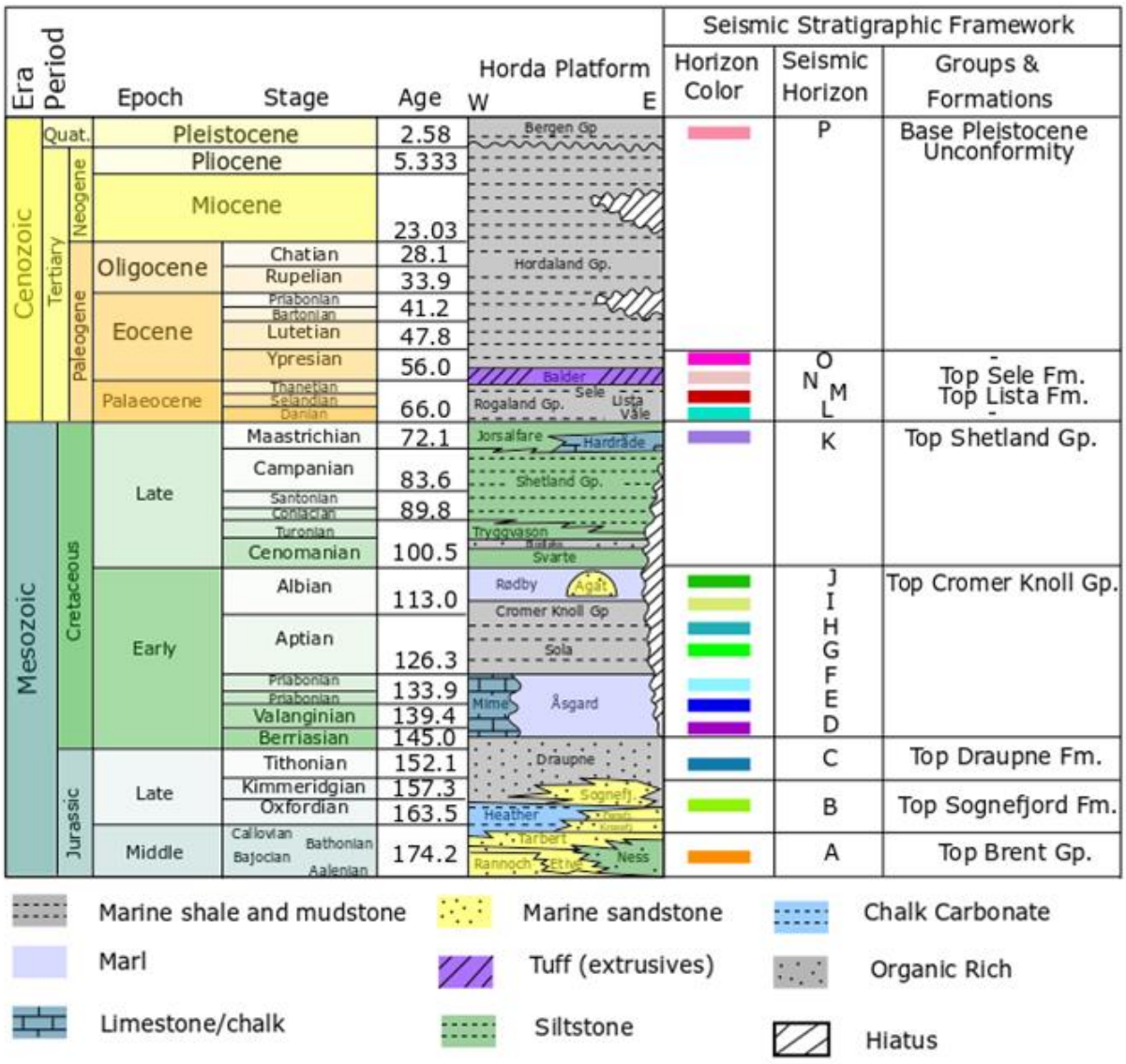

Figure 4.1: Selected horizons with a lithostratigraphic column and correlating colors for interpreted groups and formations (Redrawn after Jonassen, 2015).

4.1 2D Interpretation

This section includes the interpretation of 2D lines according to their correlating place in geologic time. The packages are separated into basement, Pre-Jurassic (Triassic and Upper Palaeozoic), Jurassic, Cretaceous, Tertiary, and Quaternary. A major unconformity lies between the Jurassic and Cretaceous packages, called the Base Cretaceous Unconformity. This represents a shift from syn-rift to post-rift, which is reflected by a change in sediment geometries and distribution. Another unconformity exists at the Base Pleistocene, which affects and erodes sediments from the Tertiary, Cretaceous, and Jurassic packages. Locations of the 2D lines relative to the 3D cube have been displayed previously in Figure 3.1, on page 27.

4.1.1 SG8043-404A (Line A)

The first 2D line interpreted was SG8043-404A (Figure 4.2), which is oriented NW-SE and cuts across the NE-most corner of the GN1101 cube. The seismic data is poor and difficult to interpret in some places, so an interpretation according to geologic time was made rather than according to the seismic horizons which correlate to the GN1101 3D cube. Only the right side of the 2D line, which intersects with the 3D cube, was used in this section. This 2D line displays similar geometries as the two previous 2D lines. The Jurassic sequence displays a uniform thickness in the southeast with slight thickening towards the faults, which is typical of syn-rift deposits. However, towards the northwest, the Jurassic sequence becomes very thin and the Cretaceous sequences dominate instead. The Cretaceous sequence in the southeast is thin, but towards the northwest, the package becomes relatively thick in comparison, and the geometry becomes more wedge shaped. To the west of the Vette Fault, sediment infill shows a clear wedge-shape geometry as the sediments infill the underlying rifted topography in the northwest-most part of the 2D line, the Cretaceous sequence develops a half saucer-shape.

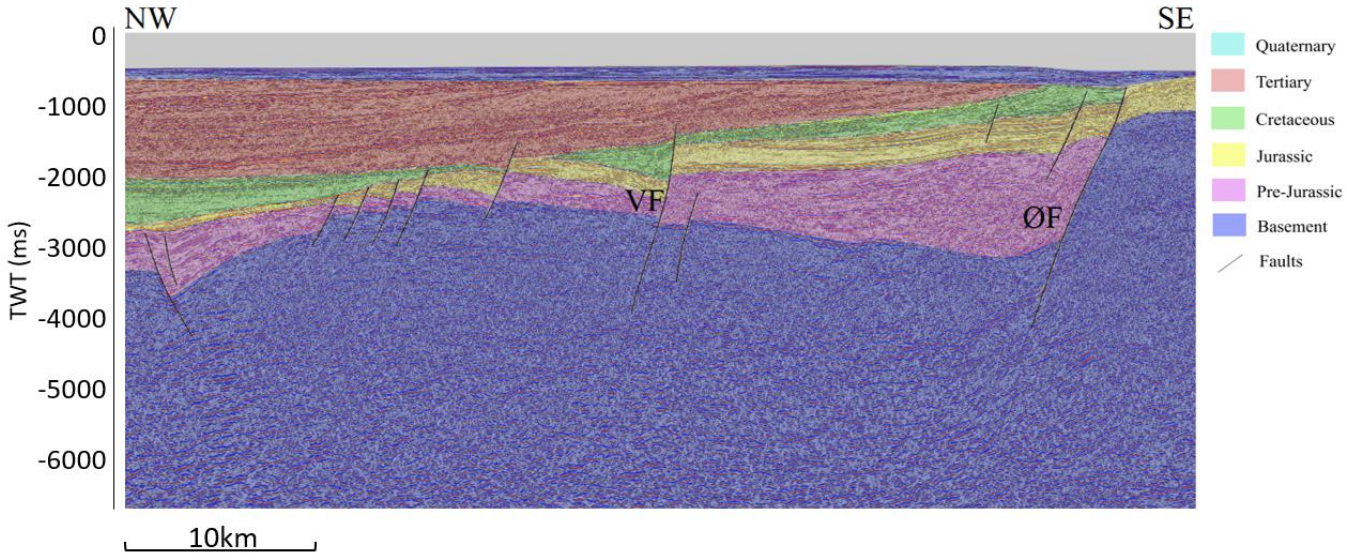

Figure 4.2: Eastern segment of SG8043-404A. Units are colored based on time period. Note the change in thickness of the Cretaceous Unit from the southeast to the northwest. VF: Vette Fault; ØF: Øygarden Fault.

4.1.2 SG8043-402A (Line B)

The second interpreted 2D line (Figure 4.3) was also from the SG8043 data set and lies slightly more south than SG8043-404A. This 2D line cuts through the GN1101 3D cube, and interpretations from the 3D cube were used to correlate horizons onto this 2D line, as there were few well tops to be observed in this area.

The eastern segment of SG8043-402A displays a similar geometry at SG8043-401A in that the Jurassic sequences are uniform in geometry towards the southeast. Towards the northwest, they become more irregular and thinner. The Cretaceous sequence also displays the wedge-shape geometry seen in SG8043-401A, and slight thickening towards the faults. On the northwest side of the 2D line, the Cretaceous sequence becomes very thick in comparison to the sequences in the southeast. Erosion from Tertiary, Cretaceous, and Jurassic units also occurs along the Base Pleistocene Unconformity.

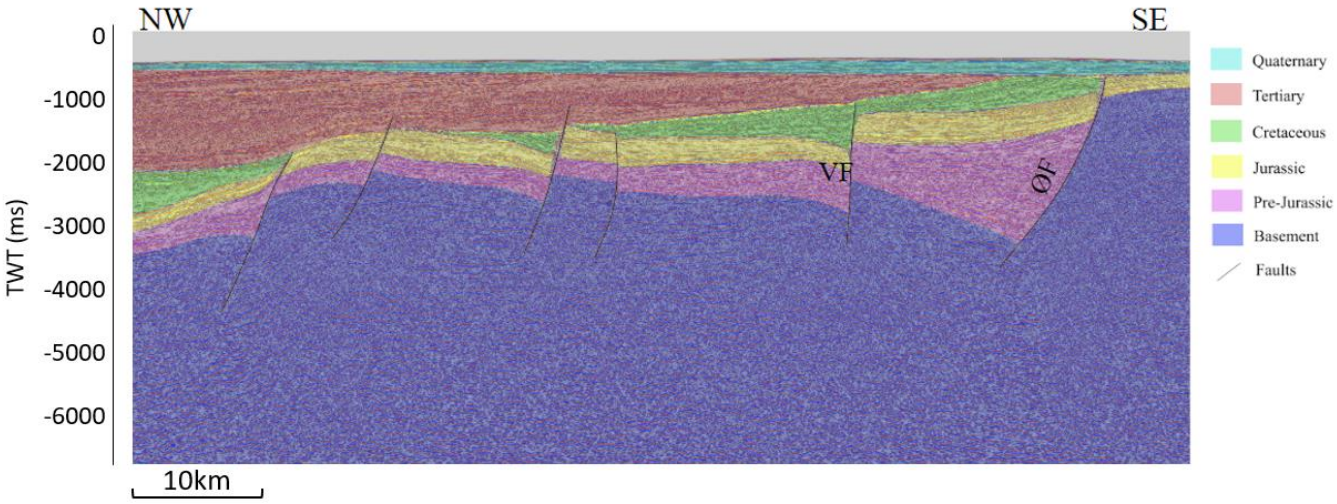

Figure 4.3: SG8043-402A Eastern segment. Note the wedge-shape geometry of the Cretaceous unit. VF: Vette Fault; ØF: Øygarden Fault.

4.1.3 SG8043-401A (Line C)

The third interpreted 2D line was SG8043-401A (Figure 4.4), which is oriented NW-SE. The Jurassic sequence displays a relatively uniform thickness and geometry. In the northeast to the east of the major fault, the Jurassic sequence dominates the package between the basement and the Base Pleistocene Unconformity. The Cretaceous sequence displays a wedge shape geometry and is eroded in the northeast by the Base Pleistocene Unconformity. The Tertiary sequence continues out of the section and is also eroded by the Base Pleistocene Unconformity.

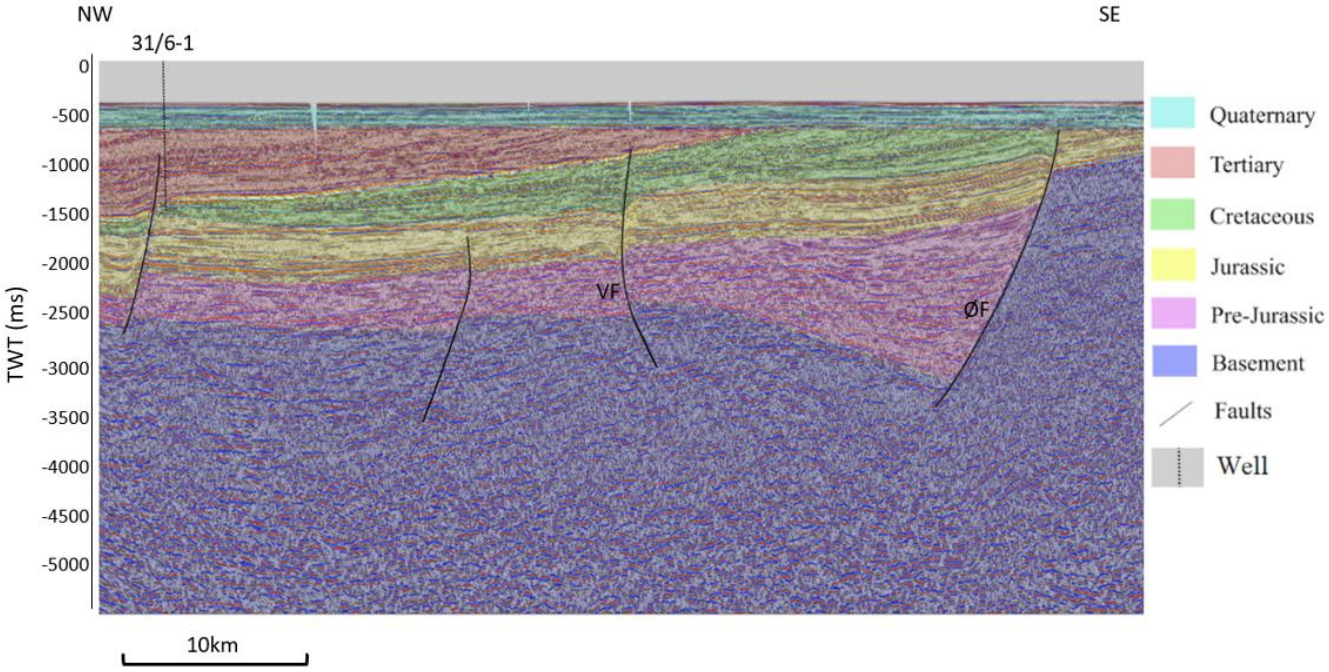

Figure 4.4: 2D line SG8043-401A with chronologic interpretations, major fault zones, and well 31/6-1. VF: Vette Fault; ØF: Øygarden Fault.

4.2 3D Interpretation

The following section outlines the results from the 3D seismic interpretation part of this study. The Pre-Jurassic sequence displays a prominent wedge-shaped geometry and thins to the west of the Vette Fault. The Jurassic sequence maintains relatively uniform thickness between the Vette and Øygarden Faults but becomes thicker to the west of the Vette Fault, and thinner to the east of the Øygarden Fault. Only Jurassic reflectors are found to the east of the Øygarden fault beneath Quaternary fill, as shown in Figure 4.5. Major faults exist in this sequence, including the Vette and Øygarden Faults, along with a few minor faults. Faulting is most prominent in the Pre-Jurassic to Jurassic successions, and only minor faulting exists in the Cretaceous and overlying deposits. Above the Jurassic sequence lies the Cretaceous package. Reflectors in the east, towards the Øygarden Fault, appear to converge. The Cretaceous package is eroded by the Base Pleistocene Unconformity (located at the base of the light blue sequence). The sequence is affected by the Vette and Øygarden Faults, as well as minor faulting which disrupts the reflectors. The Tertiary package is found in the uppermost sector beneath the Quaternary fill and is eroded by the Base Pleistocene Unconformity. Reflectors are strong throughout this sequence, although heavily broken by faulting. The Vette and Øygarden Faults do not affect this sequence. The Quaternary package lies unconformably above the Tertiary, Cretaceous, and Jurassic sediments. Onlaps are observed towards the Øygarden Fault. Reflectors in this package are strong and continuous, and there is no disruption from faulting observed. Each interpreted reflector is displayed in Figure 4.6.

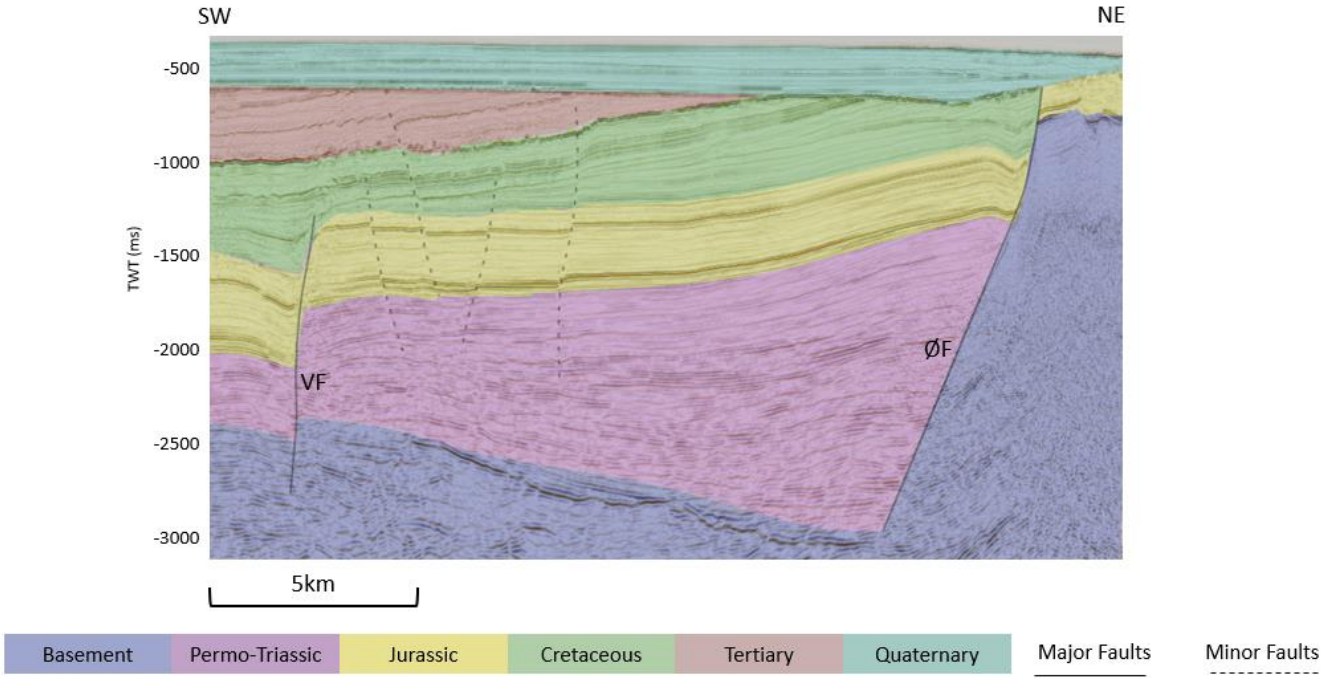

Figure 4.5: GN1101 cube, oriented from southwest to northeast. Colored areas represent the interpreted sections, with colored fill matching the correlating geologic time. VF: Vette Fault; ØF: Øygarden Fault.

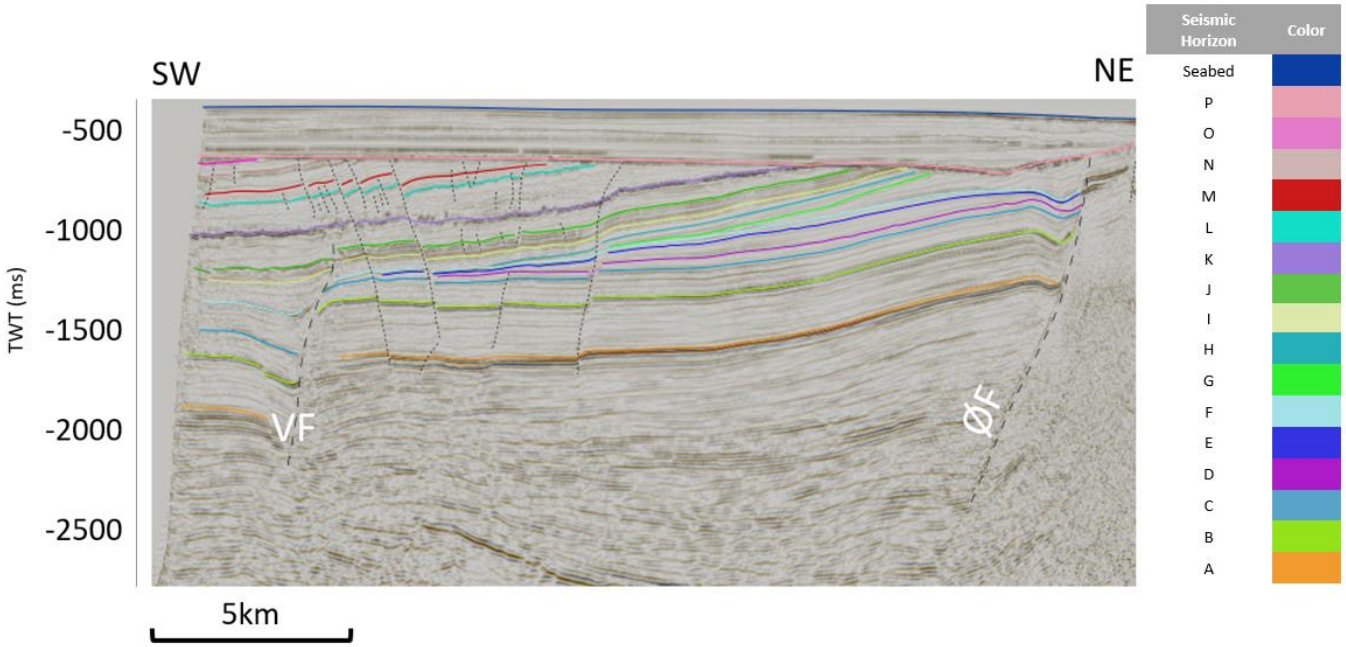

Figure 4.6: Interpreted Seismic Horizons of the GN1101 3D cube. VF: Vette Fault; ØF: Øygarden Fault.

Figure 4.7 displays overall thicknesses for each sequence. Jurassic sequences include Seismic Horizons A and B; Lower Cretaceous Sequences include Seismic Horizons C through J; Upper Cretaceous includes Seismic Horizon K; Tertiary includes Seismic Horizons L through O. The Jurassic package displays high amounts of thicker values, but a relatively uniform distribution. The Lower Cretaceous package displays a wider distribution as a result of erosion from the Base Pleistocene Unconformity. The Upper Cretaceous only includes the Shetland Group and therefore shows a more uniform distribution of lower values. The Tertiary package displays a wide distribution of values due to erosion from the Base Pleistocene Unconformity.

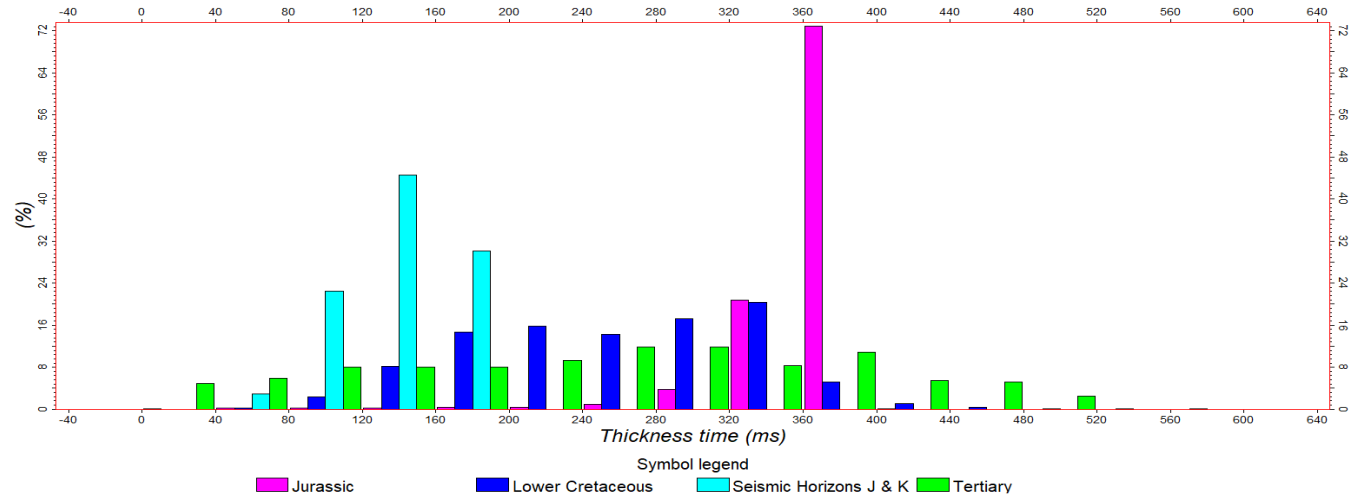

Figure 4.7: Histogram displaying thickness values from time-thickness maps. Jurassic: Seismic Horizons C and A, Lower Cretaceous: Seismic Horizons J and C, Upper Cretaceous: Seismic Horizons K and J, Tertiary: Seismic Horizons P and K.

4.2.1 Pre-Cretaceous

This section covers the Pre-Cretaceous units and horizons interpreted in this study, including Units/Seismic Horizons A and B. Seismic Horizon A represents the top of the Brent Group. Seismic Horizon B lies above this and represents a younger sequence. The surface maps display similarities in that they deepen to the west of the Vette Fault, and shallow towards the Øygarden Fault (Figure 4.8).

The surface map for Seismic Horizon A displays a deepening to the south, on the southwestern side of the Vette Fault (Figure 4.8). The overall dip trend is towards the southwest. The surface elevation time ranges from -1100 ms to -1600 ms between the Vette and Øygarden Faults but lowers to -1800 ms to the west of the Vette Fault, due to tectonic processes. There is a platform with lower elevation time values in the south, which is colored in dark blue. West of the Vette Fault, the formation deepens significantly due to the faulting. The differing surface values along Seismic Horizon A are primarily due to displacement across the major faults.

Seismic Horizon B correlates to the Jurassic Top Sognefjord. This reflector is continuous and strong, also existing throughout the 3D cube, west of the Vette Fault and east of the Øygarden Fault. The surface map for Seismic Horizon B displays a deepening to the southwest, especially west of the Vette Fault (Figure 4.8). The surface shows differentiation primarily due to faulting. Reflectors in Unit B are even and parallel in nature, and some subparallel reflectors are also seen deeper on the seismic data, towards Seismic Horizon A. At the lower boundary, a more gradational contact is observed due to the interfingering of the Heather Formation. Disruption in the reflector patterns is also due to faulting within the package.

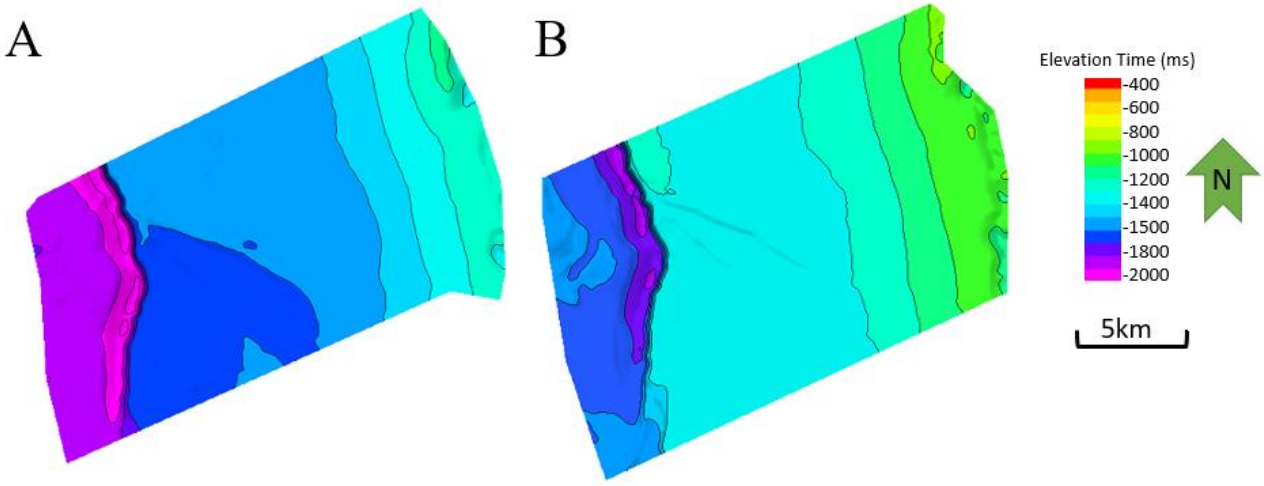

Figure 4.8: Seismic Horizons A and B surface maps. Both display lower values west of the Vette Fault, and a gradual deepening from the east to west direction. Values are scaled to show the same colors for each value on both maps, and values are shown in elevation time (ms).

Seismic Horizon A is continuous and strong, and exists throughout the 3D cube, including to the west of the Vette Fault and east of the Øygarden Fault. Reflectors in Unit A are parallel but become subparallel and eventually chaotic moving down the section towards the basement. Faulting throughout the package also disrupts the reflectors. Unit A also displays onlaps which terminate against an inclined reflector, as displayed in Figure 4.9.

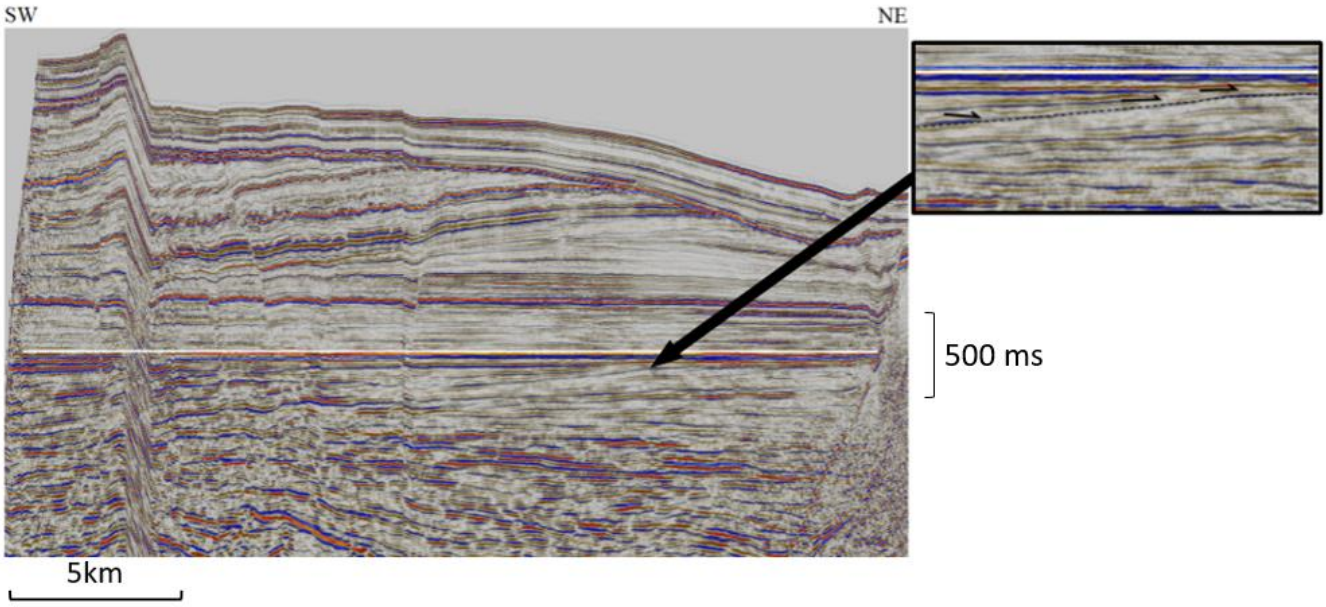

Figure 4.9: Flattened Seismic Horizon A with a smaller image displaying onlaps. The horizontal white line represents the Top Brent horizon. In the smaller image, the dotted black line outlines an inclined surface which reflectors are terminating against. The black arrows represent reflector terminations. Inline: 1291.

The RMS amplitude seismic attribute map for Seismic Horizon A (Figure 4.10) displays a high amount of amplitude variations, ranging from 0 up to approximately 8000. A delta is outlined in light blue and noted by the enlarged box (Figure 4.10) Generally, higher RMS values are associated with a greater amount of lithologic variation throughout the surface. The primary values for the RMS map are lower, between 2000 and 3000, but higher values are present near the delta and towards the west of the Vette Fault.

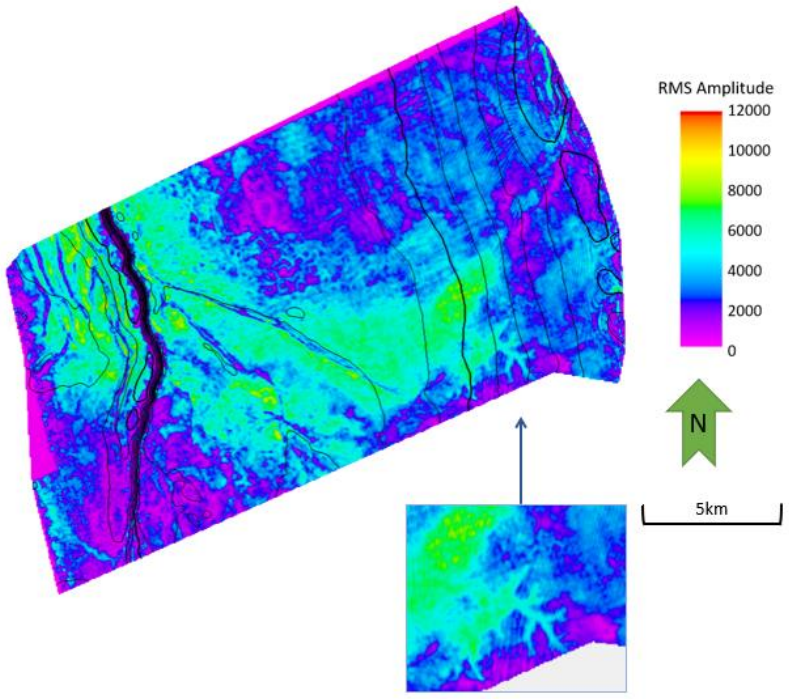

Figure 4.10: Seismic Horizons A (Top Brent) RMS amplitude attribute map with an enlarged image of parts of the Upper Brent delta.

The RMS amplitude attribute map for Seismic Horizon B (Figure 4.11) displays high RMS values in green NNW-SSE trending ribbons. The most common RMS values lie between 4000 and 7000, which are displayed by light blue.

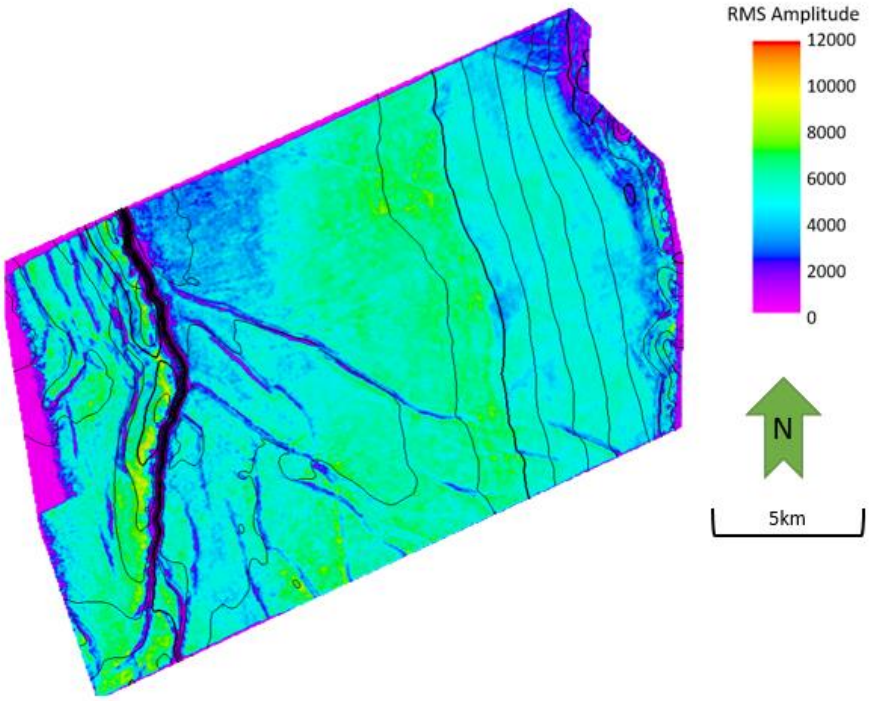

Figure 4.11: Seismic Horizons B (Top Sognefjord) RMS amplitude attribute map.

The time-thickness map for Unit B is displayed in Figure 4.12. It shows a relatively uniform thickness throughout the package, with variation at the Vette Fault. The thickness ranges from 150ms to 290ms.

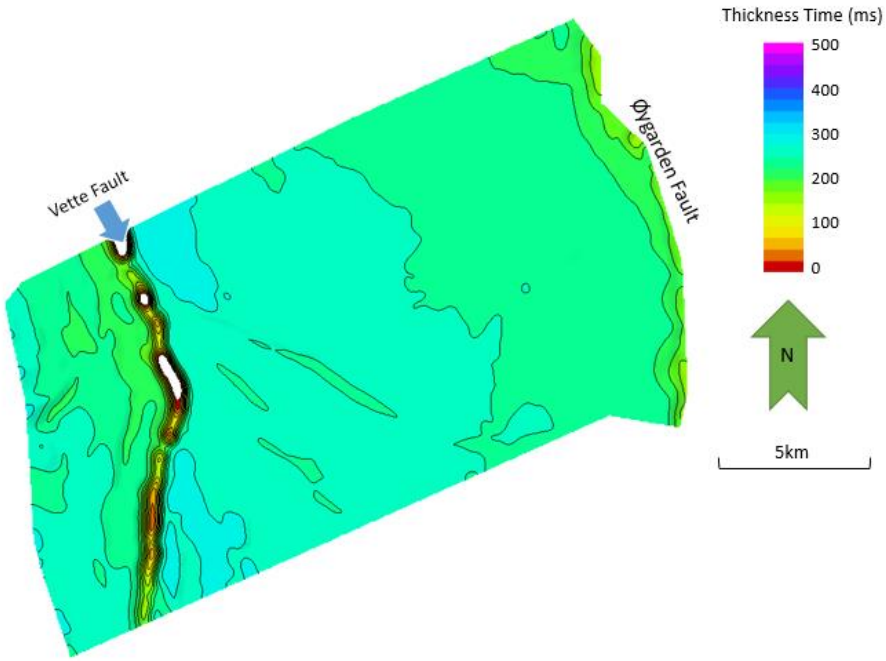

Figure 4.12: Time-thickness map for Unit B, between Seismic Horizons A (Top Brent) and B (Top Sognefjord).

Interpretation: Seismic Horizon A correlates to the Top Brent Surface, which is of the Jurassic sequence (Vollset and Doré, 1984). The Brent Group primarily consists of sandstones, siltstones, and shales, as confirmed by the high RMS values in Figure 4.10. The thickness of the Brent Group is seen to vary considerably, but on the Horda Platform the thickness is between 78 m and 159 m (Vollset and Doré, 1984). However, according to the well log for well 32/4-1, the thickness of the Brent Group is recorded as 30.5 m. As displayed in Figure 4.10, a delta from the Upper Brent exists in the southeast corner of the RMS amplitude map. The Brent sandstones represent a progradational delta which drained the central part of the northern North Sea towards a marine embayment between the Shetland and Horda Platforms (Faleide et al., 2015). Fluvial sedimentary processes belong to the fluvial delta facies with channels of the Ness Formation, which were deposited during a northward progradation of the Brent Delta. The Brent Group includes five formations, but according to well data, only the Ness and Tarbert Formations are present in the study area. The depositional environment can be interpreted as upper shoreface, and delta or coastal plains (well report). Unit A is part of the syn-rift development.

Unit B correlates to the Sognefjord Formation, which ranges in age from the Oxfordian to Kimmeridgian/Volgian (Vollset and Doré, 1984). A transgression in the Late Jurassic led to the deposition of the clayey Heather Formation, which interfingers with the sandier sediments of the Sognefjord. The thick sandstone bodies of the Sognefjord were initially interpreted by Whitaker (1984) and Hellem (1986) as offshore bars, formed by reworking regressive deposits by transgression. The formation was reinterpreted by Stewart (1995) and Dreyer (2005) to be a principally regressive shoreline to shelf system, particularly the “deposits of a coastal spit system, bordered to the east by a tidal backbasin” (Patruno, 2014). Well data from well 32/4-1 recognizes the top of the Sognefjord Formation by a decrease in gamma ray readings from above the Heather Formation. The RMS amplitude attribute map for Seismic Horizon B displays higher values in N-S trending strips (Figure 4.11), which correlate to clinoform tops. Sediment variations displayed on the RMS amplitude map are due to the interfingering of the Heather Formation. Reflectors directly beneath Seismic Horizon B are even and parallel in nature, and some subparallel reflectors are also seen lower down in the unit. Parallel reflectors suggest uniform rates of deposition. Unit B represents a change from the sandier sediments of the Sognefjord to the shalier sediments of the Draupne Formation which lies above it.

4.2.2 Cretaceous

The Cretaceous surfaces that were interpreted in this study are represented by Seismic Horizons C through K (Figure 4.13). Seismic Horizon C represents the Top of the Draupne Formation, and Seismic Horizon J represents the top of the Cromer Knoll Group. Seismic Horizon K represents the base of the Palaeocene and the Top of the Shetland Group. Each sequence is either truncated by the Øygarden Fault in the east or eroded by the Base Pleistocene Unconformity on the northeastern side of the surface. The surfaces display uniform characteristics in that they show decreased values in elevation to the southwest, especially west of the Vette Fault, for the surfaces that are present there. Seismic Horizons C through F display a similar angle of tilt, but the horizons following Seismic Horizon F are steeper.

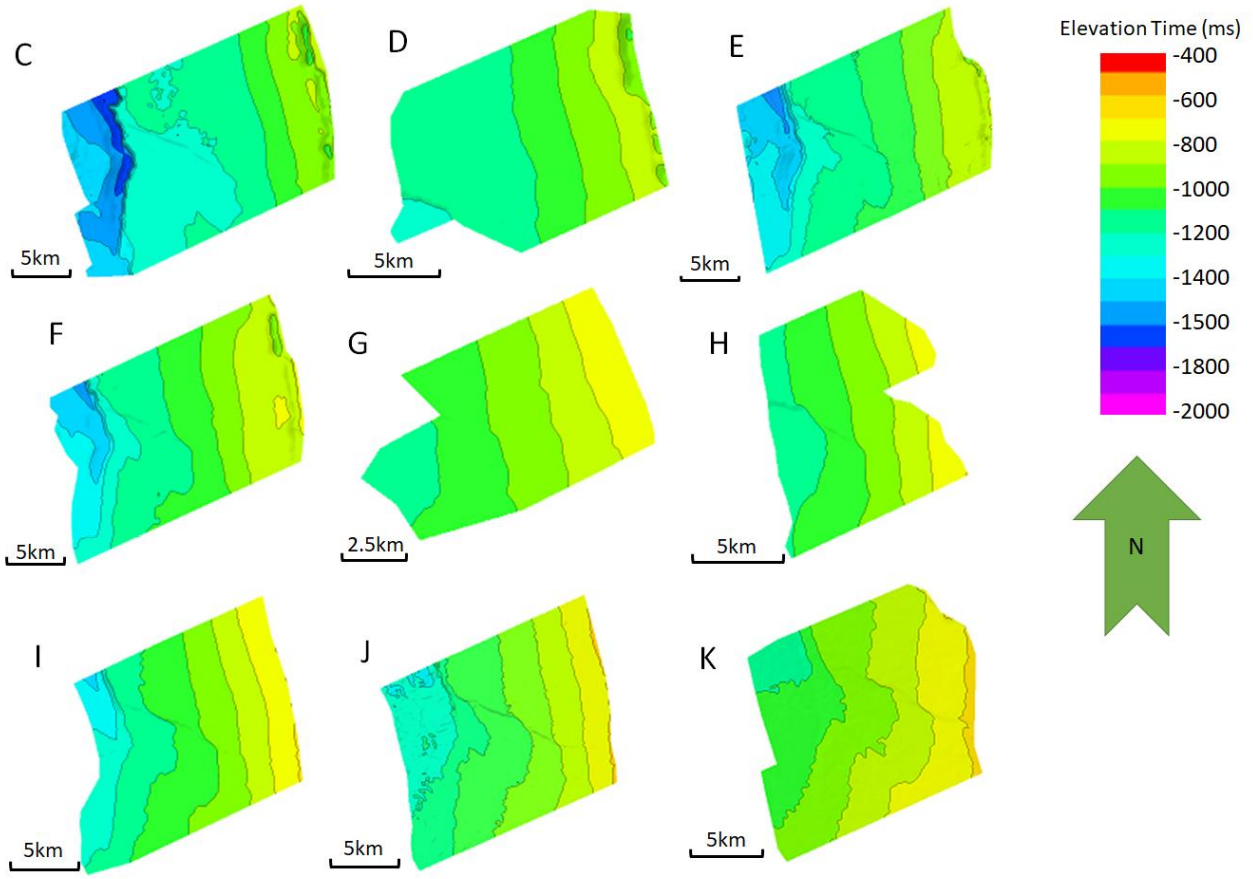

Figure 4.13: Compiled figure of all surface maps in order of descending depth and increasing age of the horizons within the Cretaceous succession. Values are scaled to show the same color for each value on all maps, and elevation time (ms) is displayed.

RMS Amplitude Maps

The RMS amplitude maps (Figure 4.14) are each scaled to show the same color variations. Seismic Horizon C shows low levels of variation in amplitude, with a similar trend as the time-thickness map of Unit C (Figure 4.15) where the unit thickens. Higher values also appear west of the Vette Fault. From Seismic Horizon D to Seismic Horizon F, there is an overall increase in values near the Vette and Øygarden Faults, and a slight increase in the center where the low values trend NNW-SSE. The values decrease again in Seismic Horizon G and the RMS map displays low values compared to the underlying Seismic Horizon F. Seismic Horizon H displays slightly higher values than Seismic Horizon G, but there is a sharp increase between Seismic Horizons H and I. In the RMS amplitude map for Seismic Horizon I, high values are displayed near the Øygarden Fault, but there is a gradual decrease towards the southwest. Seismic Horizon J displays a higher frequency of the same values as Seismic Horizon I, but the highest accumulation is in the northwest versus only at the Øygarden Fault, and the gradual decrease in values is primarily towards the south. Seismic Horizon K displays higher values, and a higher frequency of these high values, in a relatively even distribution throughout the surface.

Interpretation: Seismic Horizon C represents the Draupne Formation, which is primarily composed of shales with minor interbeds of sand (Vollset and Doré, 1984). From Seismic Horizon D to Seismic Horizon F, there is an overall increase in RMS values, especially near the Vette and Øygarden Faults, due to erosion at the faults which deposited coarser sediments in adjacent areas. Seismic Horizon G displays low values again, but there is another increase up to Seismic Horizon I where the values sharply become higher than underlying horizons, representing a deposition of coarser sediments. The values are highest near the Øygarden Fault, indicating deposition of coarse-grained sediment, but there is a more even spread of high values across the surface, with a gradual decrease towards the Vette Fault. Seismic Horizon J displays similar values as Seismic Horizon I, but the frequency of the values is higher, and the coarse sediment is accumulating in the northwest versus only at the Øygarden Fault, implying a higher distribution of similar sediments. A gradual decrease in values is also displayed, but primarily towards the south. Values increase again between Seismic Horizons J and K. In Seismic Horizon K, the values are higher than underlying horizons, and the frequency of the high values is also higher. Seismic Horizon K represents the Shetland Group which contained higher amounts of carbonate (Isaksen and Tonstad, 1989).

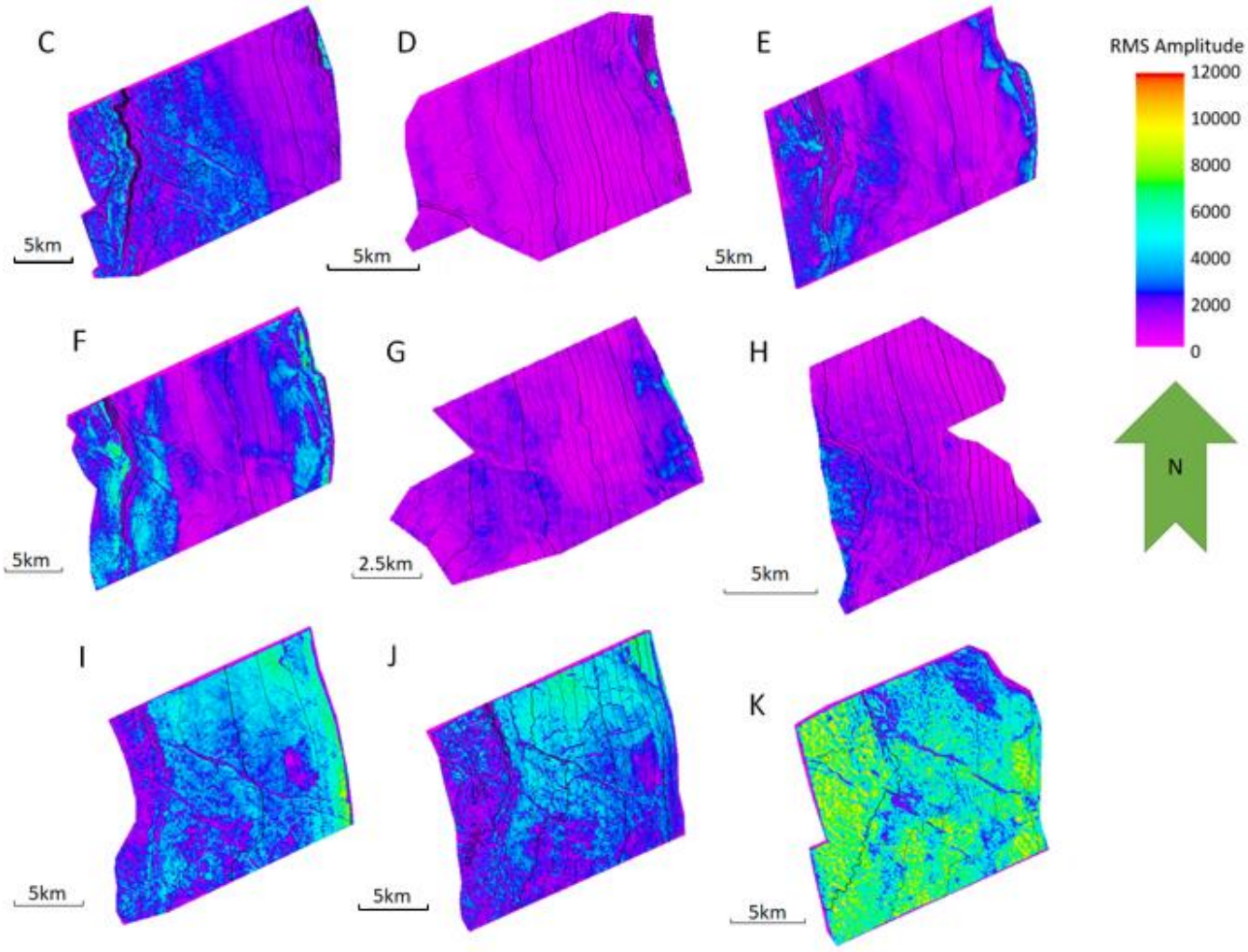

Figure 4.14: RMS amplitude maps for Seismic Horizons C (Top Draupne) through K (Top Shetland).

Time-Thickness Maps

The time-thickness map for Unit C displays a change in thickness towards the Øygarden and Vette Faults, especially to the west of the Vette Fault. Thickness across the surface maintains approximately 100 ms, but there is a thickened N-S trending package to 125 ms in the center. It also decreases towards the Vette and Øygarden Faults. West of the Vette Fault, the unit thickens to 150 ms, then decreases to 100 ms again west of that.

The time-thickness map for Unit D is displayed in (Figure 4.15). The thickness is relatively uniform at approximately 20 ms, but increases to 40 ms to the south, and decreases below 20 ms towards the Øygarden and Vette Faults. The time-thickness follows opposite of the pattern of the underlying sequences, which display a thickening on the time-thickness maps in the southern center, and instead displays a thinning in the south.

The time-thickness map for Units F through C is displayed in Figure 4.15. This time-thickness map displays an interval between the Øygarden and Vette Faults where the sequence thickens to 200 ms. Towards the Øygarden Fault, thickness decreases to 50 ms, and towards the Vette Fault, thickness significantly decreases to 25 ms. West of the Vette Fault, thickness is approximately 200 ms again, but decreases down to 75 ms. This sequence displays a thickening in the center, and a significant decrease in thickness towards the Vette Fault.

The time-thickness map for Units F through B is displayed in Figure 4.15. Thickness maintains approximately 180 ms, except towards the Vette Fault in the northwest section of the cube where it gradually decreases in thickness to approximately 40 ms. Thickness in the center ranges from 250 ms to 300 ms, correlating to the location of altered RMS values in the seismic attribute maps. Towards the Øygarden Fault, thickness values decrease gradually to 125 ms, and towards the Vette Fault, values decrease gradually to 75 ms. West of the Vette Fault, Values are much higher (350 ms) and then decrease gradually to 200 ms.

Unit G thins towards the southwest (Figure 4.15), changing from approximately 100 ms in the northeast to beneath 20 ms in the southwest. Late erosion due to the Base Pleistocene Unconformity is evident by the truncation of the tops of reflectors. In the southwest, reflectors terminate against the underlying Seismic Horizon F.

Due to the decreased area of underlying horizons due to their terminating against Seismic Horizon F, other horizons between Seismic Horizon I and F could not be used to effectively analyze the thickness of the sequence. Thickness is greatest in the northeast and decreases towards the southwest (Figure 4.15), but west of the Vette Fault the thickness increases again. Evidence of minor NW-SE trending faults is also displayed just south of the center of the time-thickness map. The sequence displays a wedge-shape geometry.

The time-thickness map between Units J through C (the Cromer Knoll Group; Figure 4.15) displays values of 375 ms in the east, and the values gradually decrease to 75 ms towards the Vette Fault. West of the Vette Fault, the sequence regains thickness and increases up to 450 ms and then quickly decreases down to 150 ms. This sequence displays a wedge shape geometry, which is characteristic for sediments which are infilling underlying rifted topography.

The time-thickness map for Unit K displays the change in sediment infill geometry between the sequences beneath Seismic Horizon J and the geometries above it. Values for the time-thickness map are approximately 50 ms, and gradually increase to -200 ms towards the Vette Fault. This is the first unit that is not heavily affected by the Vette Fault, and the sediments continue over it without having large variations in thickness. Unit K correlates to the Shetland Group, which represents the Upper Cretaceous succession.

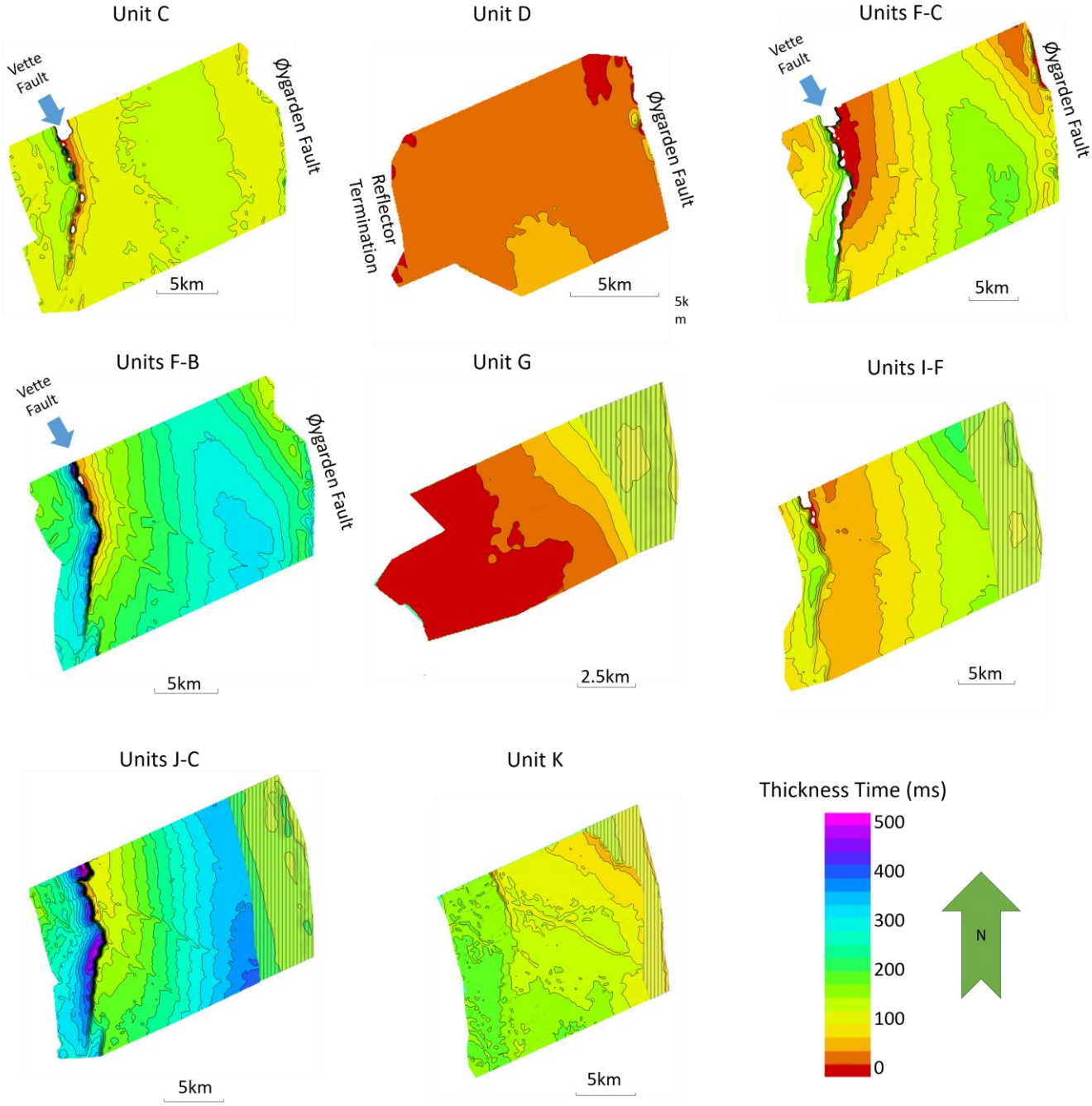

Figure 4.15: Compiled Figure of all time-thickness maps created within the Cretaceous succession. Note that the time-thickness maps are not for each unit and are sometimes compilations of multiple units.

Seismic Horizon C

Seismic Horizon C correlates to the top of the Draupne Formation, which is also the Base Cretaceous Unconformity (BCU). This reflector is continuous and intermediately strong, extending from the western wall of the Øygarden Fault to the west of the Vette Fault. Parallel and even reflection patterns exist throughout the package, although they become chaotic and terminate towards the Vette Fault, and the sequence displays a change in thickness to the west of the Vette Fault. Reflectors are truncated by the Øygarden Fault in the east.

Interpretation of this horizon was a challenging task due to the discontinuity of the reflector. Cretaceous sediments from above Seismic Horizon C onlap onto underlying Jurassic sediments (Figure 4.16). Upon flattening the surface, a wedge shape geometry is displayed. The surface map for Seismic Horizon C (Figure 4.13) displays deepening towards the southwest, following patterns of the underlying packages. Towards the Øygarden Fault, surface values are approximately -900 ms, and decrease gradually to -1200 ms. West of the Vette Fault, values decrease significantly to -1700 ms and increase gradually to -1400 ms.

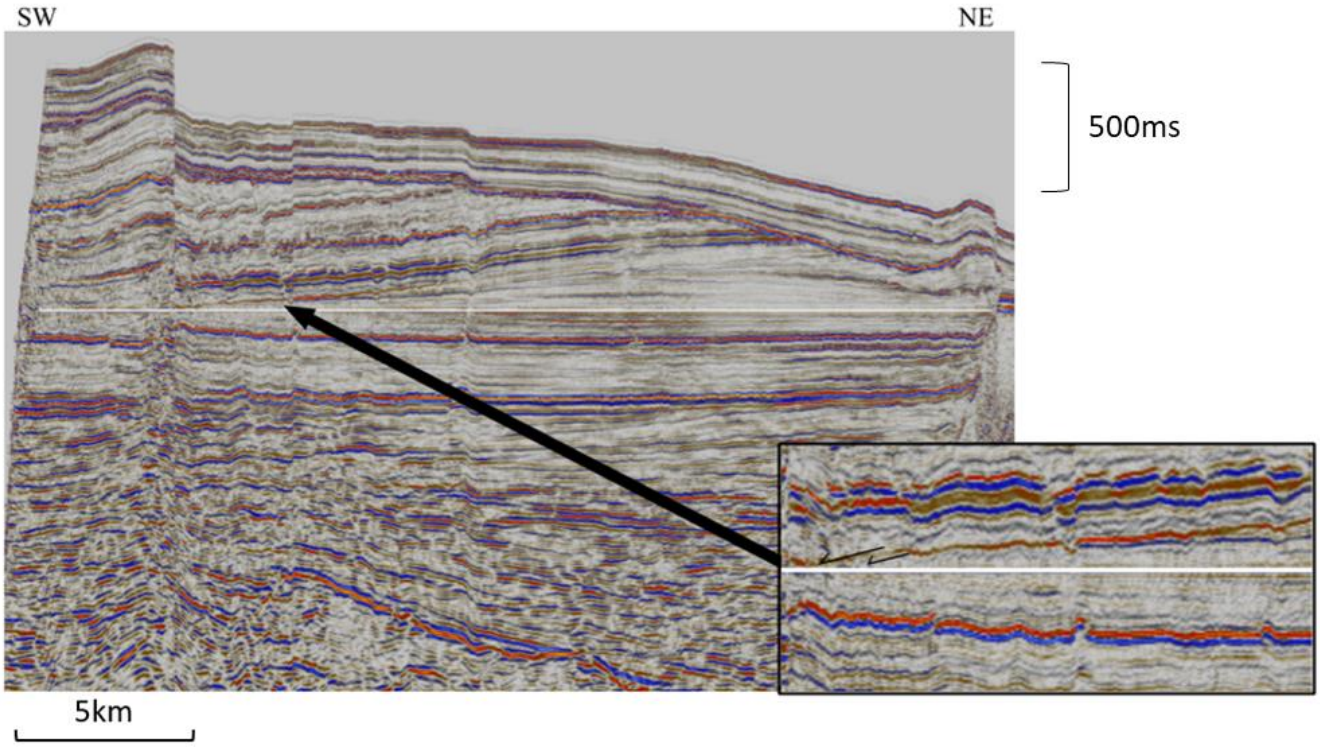

Figure 4.16: Flattened Seismic Horizon C (white line) with a smaller image showing overlying sequence downlapping onto the horizon. Inline: 1291

Interpretation: In the Late Jurassic (Middle Volgian to Early Barremian), over-deepened basins formed according to rifting topography, and poor bottom-water circulation led to the deposition of the organic-rich marine sediments of the Draupne Formation (Unit C), which also correlates to the Base Cretaceous Unconformity (Faleide et al., 2015). This unconformity is well-observed across transects throughout the North Sea and is displayed as a strong and continuous reflector. At the transition between Units B and C, tectonic activity shifted, leading to the termination of major faults at this horizon. The Draupne Formation (Unit C) displays

slight wedge-shaped geometry, thinning towards the Vette Fault in the west and thickening towards the Øygarden Fault in the east (Figure 4.15). This marks the shift between syn-rift and post-rift sedimentation. The deposition of these sediments continued into the Early Cretaceous. The RMS amplitude map indicates higher amounts of coarse sediment accumulation on the footwall, with more uniform distribution of sediment on the hanging wall between the Vette and Øygarden Faults. The low levels of amplitude variation correlate to lower porosity lithologies, such as shale. Sands were deposited as fans along rift boundaries during the Late Jurassic rift phase, potentially contributing to this variation in lithology (Faleide et al., 2015). The top of the Draupne Formation is marked in the well log for well 32/4-1 with an increase in gamma and a decrease in resistivity.

Seismic Horizon D

Seismic Horizon D represents the bottom-most sequence of the Cromer Knoll Group. The reflector representing Seismic Horizon D is weak and disrupted but was chosen according to adjacent reflector terminations. Truncations are observed below the horizon, as shown in Figure 4.17. Seismic Horizon D terminates against the overlying Seismic Horizon E and is truncated at the Øygarden Fault in the East. It does not appear to continue towards the Vette Fault, or to the east of the Øygarden Fault. Reflectors beneath Seismic Horizon D are parallel where they are present, but in most locations the reflectors are very weak and difficult to view.

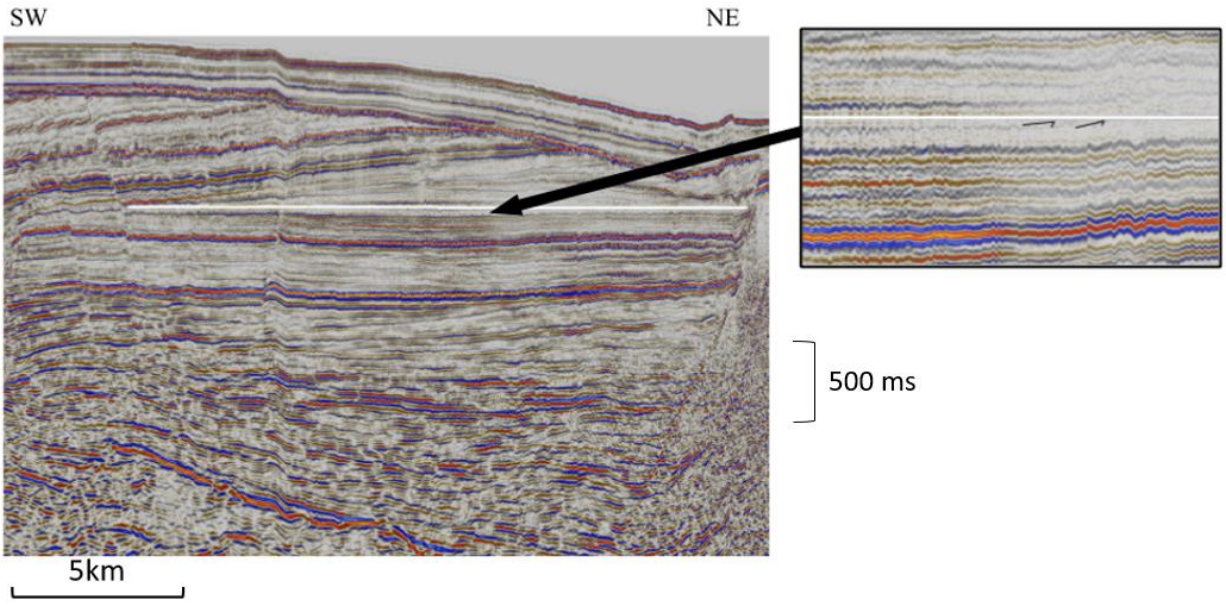

Figure 4.17: Truncations below Seismic Horizon D, which is indicated by the horizontal white line. Inline: 1291.

Interpretation: Due to the uplifted topography from the Jurassic, sediments during the Cretaceous were infilling the faulted, uneven topography, resulting in the abnormal wedge-shaped geometries (Figure 3.5) for Seismic Horizons from the Lower Cretaceous sequences. These sediments were deposited as part of the post-rift stage, and the sediment distribution is heavily influenced by it. Seismic Horizon D displays very low RMS values, implying a uniform lithology, reflecting the deposition of low energy and deep-marine shales in the Early Cretaceous (Faleide et al., 2015).

Seismic Horizon E

Seismic Horizon E is a weak reflector within the Lower Cretaceous sequence and shows disruption due to faulting throughout the 3D cube. It is truncated by the Øygarden Fault in the east and terminates against the overlying Seismic Horizon F towards the southwest (Figure 4.18). Reflectors beneath the horizon are not easily distinguishable, although they appear to be even in some places. In the east towards the Øygarden Fault, onlaps are observed against an inclined reflector (Figure 4.18).

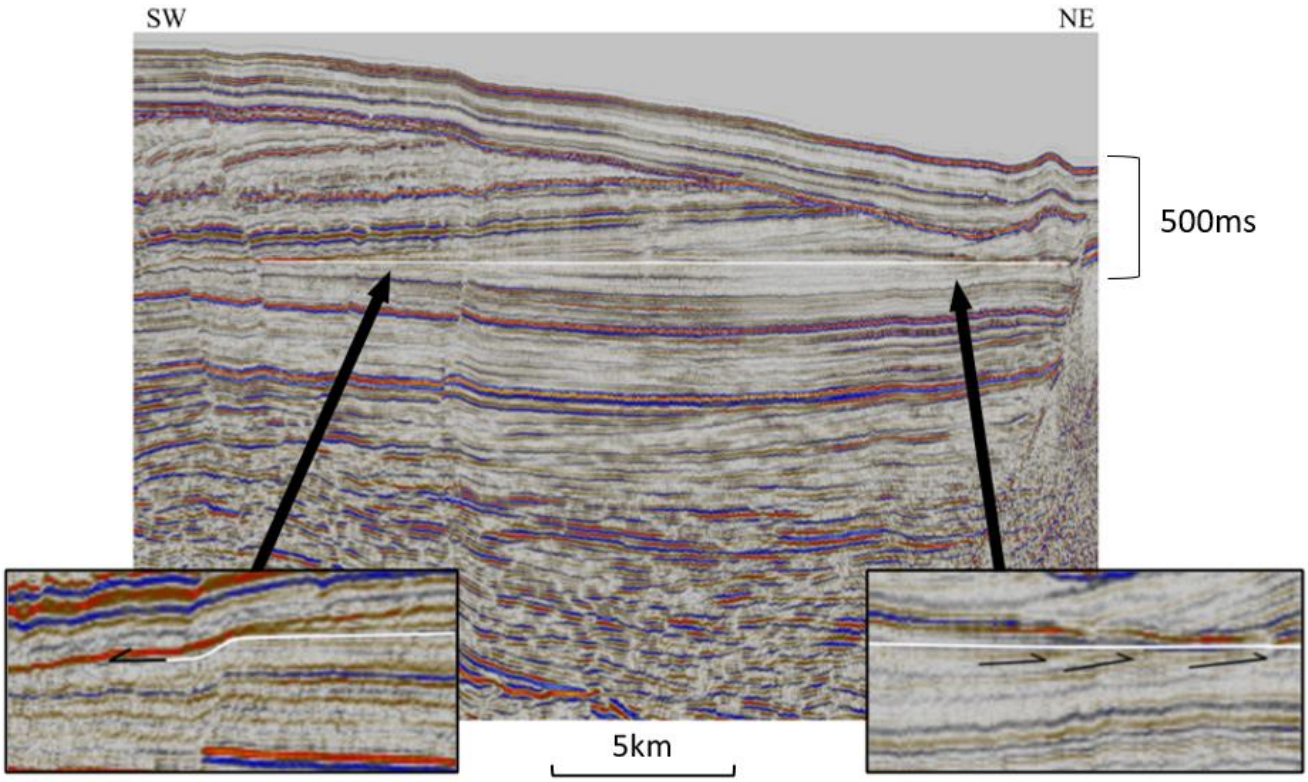

Figure 4.18: Flattened Seismic Horizon E (horizontal white line) with a smaller zoomed image showing black arrows as reflector truncations from the underlying reflectors (enlarged right image) and the termination of the horizon against the overlying Seismic Horizon F (enlarged left image). Inline: 1291.

Interpretation: Seismic Horizon E is within the Lower Cretaceous succession and part of the Cromer Knoll Group, and was interpreted due to toplaps from underlying reflectors. The RMS amplitude map displays higher RMS values than the underlying Seismic Horizon D, especially near the Vette and Øygarden Faults, implying a higher incorporation of sand.

Seismic Horizon F

Seismic Horizon F correlates to an erosional surface within the Lower Cretaceous sequence. The reflector displays continuity and an intermediate strength and is truncated by the Øygarden Fault but continues to the southwest of the Vette Fault. Beneath the horizon, onlaps and other reflector terminations are observed and displayed in Figure 4.19. These onlaps are part of the Seismic Horizon E section but are included in Figure 4.19 as well due to the close proximity of the horizons. There are also multiple downlaps which terminate onto the top of Seismic Horizon F. Reflectors within Unit F display very low amplitudes and are difficult to see and appear to disappear altogether in other parts of the sequence. However, some reflectors terminate towards the southwest (Figure 4.19, bottom right image) within Unit F.

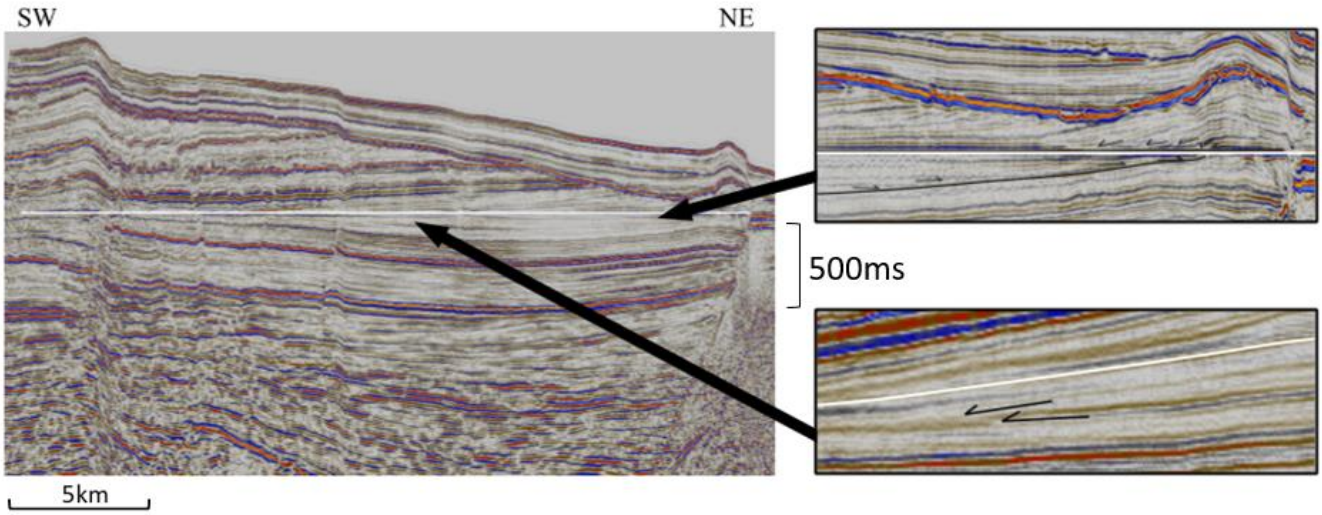

Figure 4.19: Seismic section displaying downlaps (upper enlarged image) onto Seismic Horizon F along with reflector terminations (lower enlarged image) within Unit F, which is indicated by the white line. Inline: 1291.

Interpretation: Seismic Horizon F is within the Early Cretaceous succession, and part of the Cromer Knoll Group. Between the Øygarden and Vette Faults, the package thickens in the center as a response to the subsidence that followed the Late Jurassic rifting phase, then thins towards the Vette Fault in the west. The thicker sediments in the center are a result of erosion near the faults, as uplifted structures in the Early Cretaceous were subaerially exposed (Faleide et al., 2015). Reflected within Unit F terminate within the sequence (Figure 4.19), and reflectors from the overlying Unit G downlap onto the surface. West of the Vette Fault, the package regains thickness and a wedge-shape geometry. This geometry is typical of rifting basins, and Seismic Horizon F is part of the post-rift geometry. Sediments were deposited at this time in a way that infilled the underlying topography, which had been deposited during the syn-rift phase, leading to an uneven distribution of sediment. Onlaps from the underlying Seismic Horizon E imply that Seismic Horizon F represents an erosional surface, or unconformity.

Seismic Horizon G

Seismic Horizon G is within the Lower Cretaceous sequence and is represented by a strong and continuous reflector. It is truncated by the Base Pleistocene Unconformity in the northeast and terminates against the underlying Seismic Horizon F in the southwest. It is not disrupted by faulting. Onlaps from the underlying sequence can be observed in Figure 4.20. The zoomed image in the figure shows the Seismic Horizon G surface unflattened to highlight the onlapping reflection behavior. The reflections beneath Seismic Horizon G are also shown in Figure 4.19. They are divergent, and often disappear or terminate onto the underlying Seismic Horizon F. The sequence itself displays a prominent wedge-shaped geometry.

The surface for Seismic Horizon G (Figure 4.13) displays a gradual deepening towards the southwest. Seismic Horizon G is truncated in the east by the Base Pleistocene Unconformity, and terminates onto the underlying Seismic Horizon F in the west. It does not reach the Vette Fault.

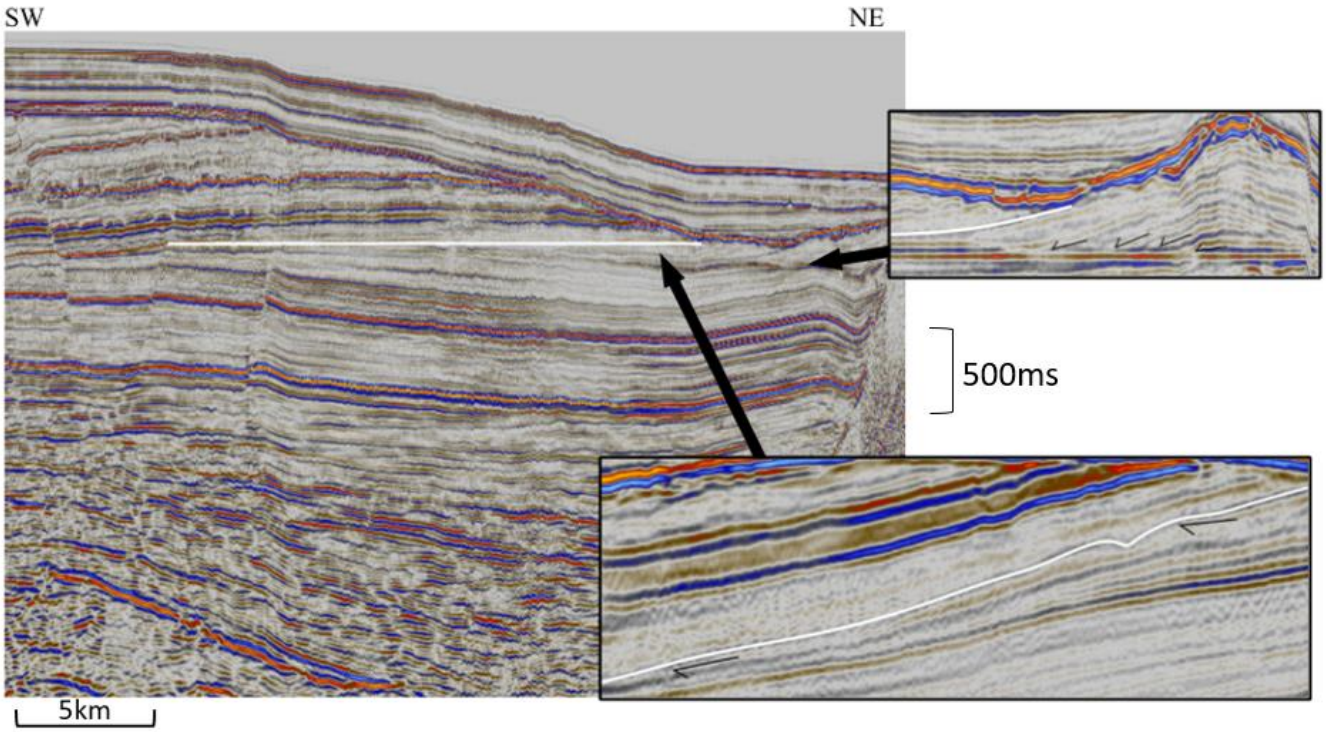

Figure 4.20: Seismic Horizon G (white line) flattened, with a focus on onlaps (lower zoomed image) and downlaps (upper zoomed image) from the underlying reflectors. The lower zoomed image is unflattened because the onlaps are more easily viewed this way. The upper enlarged image displays a flattened Seismic Horizon F. Inline: 1291.

Interpretation: Unit G displays multiple downlaps onto the underlying Seismic Horizon F, along with onlaps onto Seismic Horizon G itself (Figure 4.20). Higher values on the RMS map are present towards the east where erosion from the Base Pleistocene Unconformity occurred, and in the southeast.

Reflectors in Unit G display divergence and are skewed, and often disappear or downlap onto the underlying Seismic Horizon F. Inline 1031 is the most northwest inline on the 3D cube and displays the thickest variation of the reflectors. The package thins continuously to the SE, which is displayed by Inline 1531, and is shown in the time-thickness map of Unit G (Figure 4.15). On Inline 1031, the angles of the reflectors are higher, and they flatten towards inline 1531. Erosion due to the Base Pleistocene Unconformity is displayed by a dashed red line on the upper edge of the illustrations.

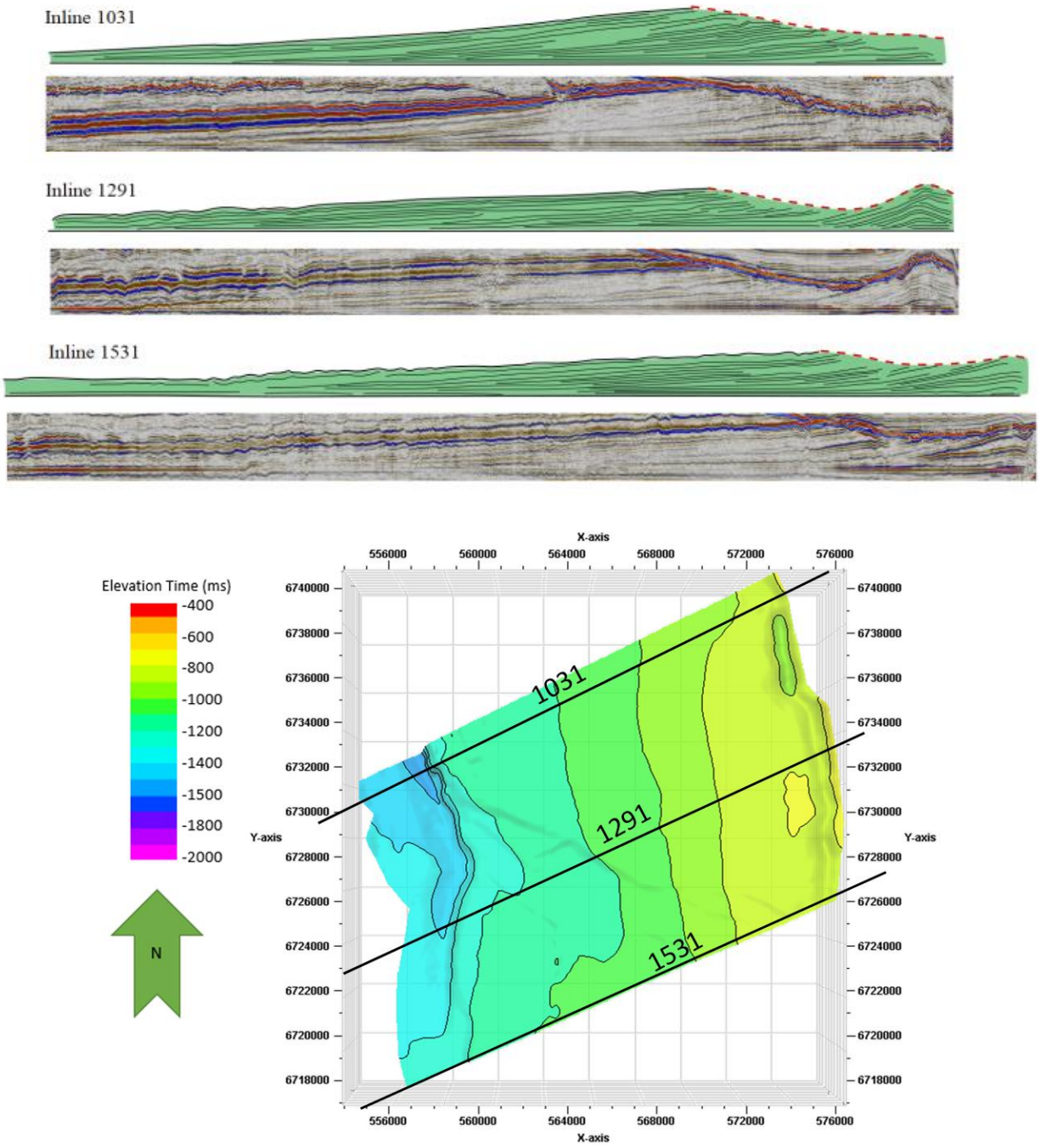

Figure 4.21: A figure displaying Unit G above a flattened Seismic Horizon F. The Base Pleistocene Unconformity eroded the tops of reflectors, as noted by the red dashed line. Inlines 1031, 1291, and 1531 are displayed to show lateral variation of this sequence.

Seismic Horizon H

Seismic Horizon H lies within the Lower Cretaceous sequence and displays an intermediately strong and continuous reflector. It is also truncated by the Base Pleistocene Unconformity in the northeast, and downlaps onto Seismic Horizon F in the southwest, which correlates to the erosional surface. It does not reach the Vette Fault, although it is disrupted by a minor fault within the sequence.

The surface map for this horizon (Figure 4.13) also displays a gradual deepening towards the southwest. Towards the Øygarden Fault, values on the surface are approximately -800 ms, and decrease to -1200 ms towards the west. Evidence of minor faults trending NW-SE are present on the surface by a diagonal shift in the surface values, following the trends of underlying surfaces.

Interpretation: Seismic Horizon H follows a similar pattern as Seismic Horizon G in terms of reflector strength and dip. The geometry is also similar to underlying sequences as it appears to conform to the rifting topography. The RMS map displays higher RMS values towards the southwest, indicating variations in lithology.

Seismic Horizon I

Seismic Horizon I is within the Lower Cretaceous sequence and is a strong and continuous reflector. It is truncated by the Base Pleistocene Unconformity in the northeast but continues to the southwest of the Vette Fault. This horizon is the first one above Seismic Horizon F that does not terminate onto Seismic Horizon F, and one of the few within the Lower Cretaceous succession that is redrawn west of the Vette Fault. Reflectors beneath Seismic Horizon I are chaotic and difficult to follow, although a few show continuities. The reflectors terminate against both the Vette and Øygarden Faults, and reflector behavior such as onlaps can be observed west of the Vette Fault (Figure 4.22).

The surface map for Seismic Horizon I (Figure 4.13) displays a gradual deepening towards the northwest. Evidence of faulting is also present, following the pattern of NW-SE trending minor faults from underlying surface maps. This is evidence by a diagonal shift in surface values on the map.

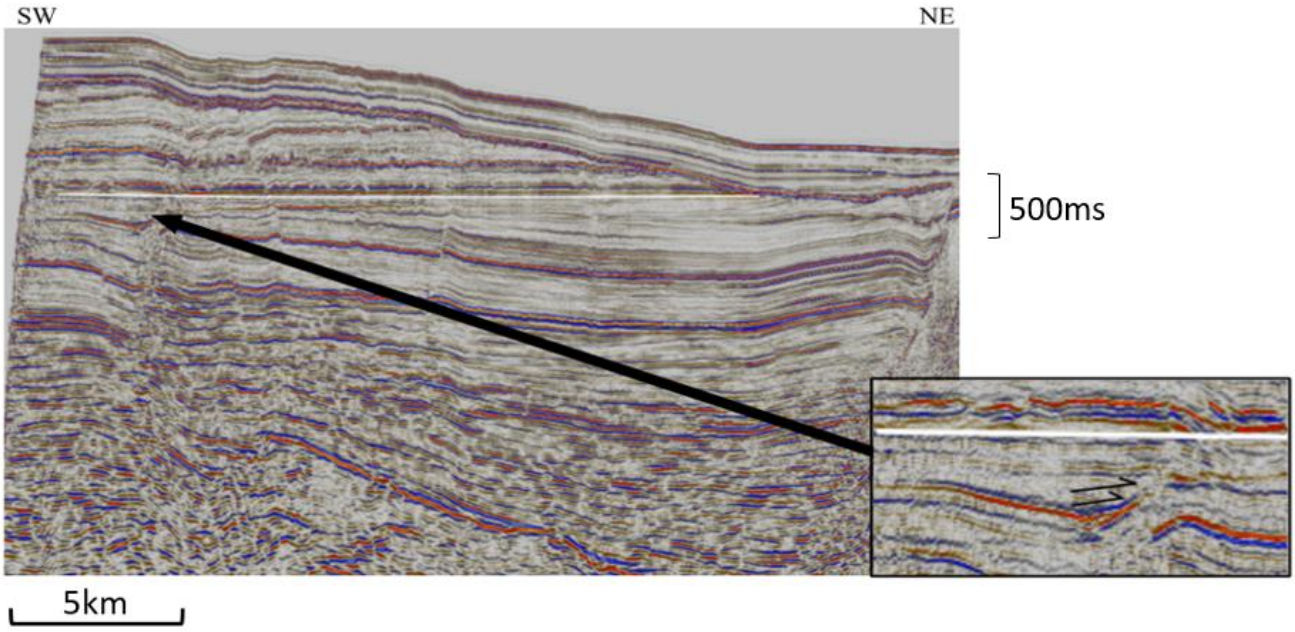

Figure 4.22: Flattened Seismic Horizon I with a zoomed image of onlaps west of the Vette Fault. Seismic Horizon I is noted by the horizontal white line. Inline: 1291.

Interpretation: Seismic Horizon I begins to display characteristics of a different phase in the post-rift sequence, as it is beginning to overstep the Vette Fault and show less of a wedge-shape geometry. It is still within the Cromer Knoll Group of the Early Cretaceous and represents part of the post-rift development. As the post-rift geometries develop, the underlying rift topography becomes infilled and drowned by sediments.

Seismic Horizon J

Seismic Horizon J s a continuous and strong reflector which is truncated by the Base Pleistocene in the northeast and is difficult to follow to the southwest of the Vette Fault. There are few noticeable reflectors between Seismic Horizon J and I, and therefore reflector terminations are not seen. The reflectors that are present between the two surfaces, however, are strong and continuous.

The surface map for Seismic Horizon J (Figure 4.13) displays a similar trend to underlying sequences in that it gradually deepens to the west. There is a small interval of deeper values shown by light blue in the northwestern corner of the surface map. Evidence of NW-SE trending faults is also displayed by the diagonal shift in values on the surface map at the center, following trends of underlying surface maps which also display similar faulting patterns.

Interpretation: Upon analyzing Seismic Horizon J (top Cromer Knoll Group), it is evident that the rift topography has been almost covered by sediments, and the sedimentation pattern no longer follows the rifting topography. This boundary occurs between the Lower and Upper Cretaceous sequences. The horizon oversteps the Vette Fault and displays a more even, uniform surface. The RMS amplitude attribute map for Seismic Horizon J (Figure 4.14) displays relatively high values. The map is dominantly covered in light blue, representing an intermediate amount of lithologic variation, especially towards the north and near the rifts.

Seismic Horizon K

Seismic Horizon K is a strong and continuous reflector, although it is heavily disrupted by faulting. It is truncated by the Base Pleistocene Unconformity in the northeast, but continues to the southwest of the Vette Fault, which it is not affected by.

The surface map for Seismic Horizon K (Figure 4.13) displays a similar pattern as underlying surfaces in that it deepens to the west, and particularly to the northwest. Values in the east where it is eroded by the Base Pleistocene Unconformity are approximately -50 ms, and these values gradually decrease to -1100 ms to the northwest. Evidence of NW-SE trending faults is also shown by the diagonal shifting in surface values. Reflectors beneath Seismic Horizon K are divergent and skewed, partially due to faulting. The package visibly thins towards the east, but reflector terminations are difficult to observe. The time-thickness map between Seismic Horizons K and J is displayed in Figure 4.15.

Interpretation: Seismic Horizon K represents the top of the Shetland Group, and the top of the Cretaceous sequence. The Shetland Group is dated from the Cenomanian to Danian (Isaksen and Tonstad, 1989), and is represented by multiple formations which are not interpreted in this study, including the Jorsalfare, Kyrre, Tryggvason, Blodløks, and Svarte Formations. The RMS amplitude map displays high values, reflecting a change in lithology from the underlying more uniform lithologies to one that is higher in calcareous content. The Shetland Group contains a higher amount of limestone on the Horda Platform than in the Viking Graben (Isaksen and Tonstad, 1989), reflected by the high RMS values. Well 32/4-1 displays and overall increase in gamma readings throughout the Shetland Group, and reflects an open marine depositional environment. The time-thickness map for Unit K displays the change in infill geometry from the wedge and irregular shapes of underlying sequences to a more uniform shape (Figure 4.15).

4.2.3 Post-Cretaceous

The Cenozoic surfaces interpreted in this study include Seismic Horizons L through P (Figure 4.23). Seismic Horizon P represents the Base Pleistocene Unconformity. Surfaces for Seismic Horizons L through O display a similar appearance to underlying surfaces in that they deepen towards the southwest. Surfaces for Seismic Horizons L and M also display faults that trend NW-SE, similarly, to underlying sequences. Each of the horizons beneath Seismic Horizon P are eroded by the Base Pleistocene Unconformity, which is represented by Seismic Horizon P. They are not affected by the Vette Fault, but do show some disruption from minor faulting. During the Eocene, the surfaces were tilted towards the east (Kolnes, 2019).

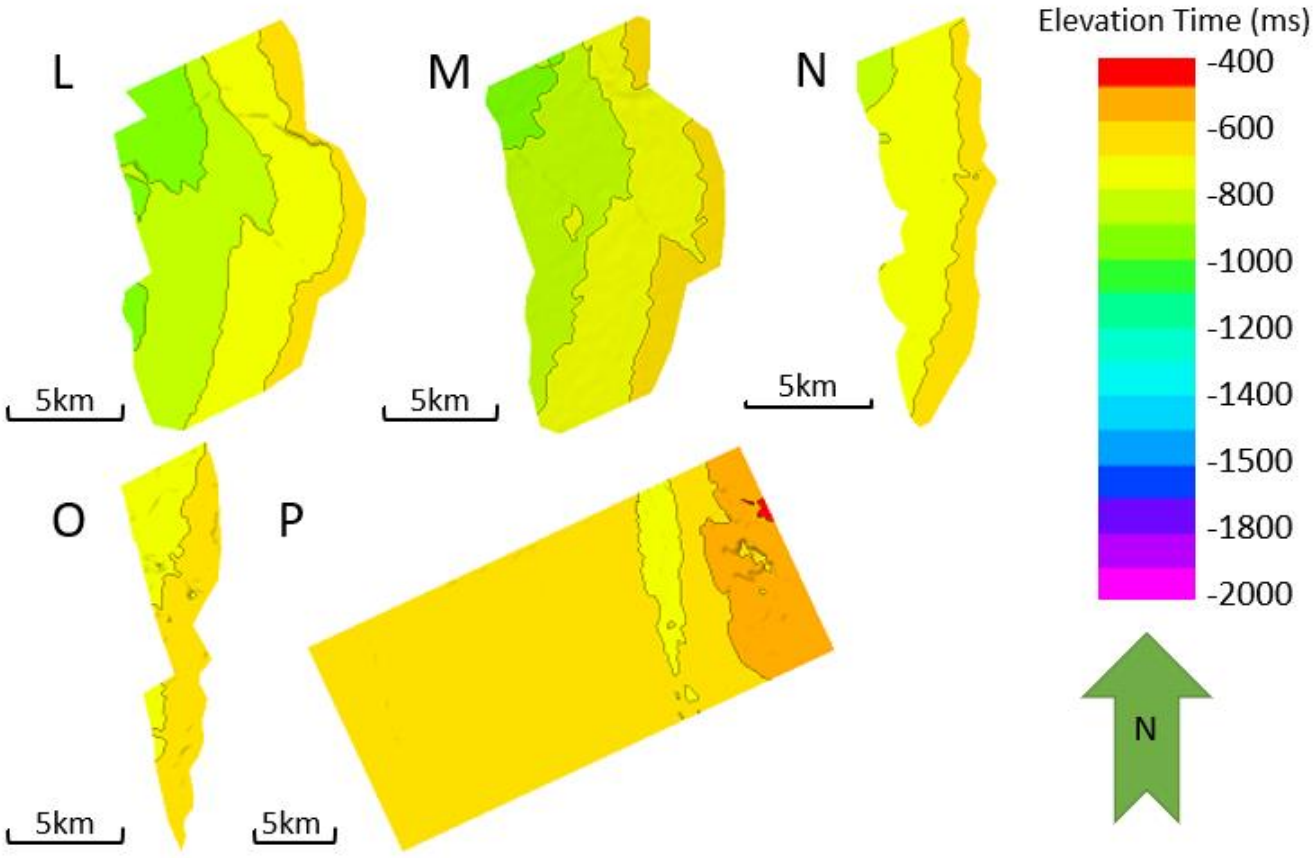

Figure 4.23: Compiled figure of all Cenozoic surfaces, from Seismic Horizons L through P.

RMS Amplitude Maps

The RMS amplitude attribute map for Seismic Horizon L (Figure 4.24) displays a mottled texture at the surface, and higher levels of lithologic variation. RMS values decrease in Seismic Horizon M, then show a slight increase in the south at Seismic Horizon N. In Seismic Horizon O, values increase in the north. Seismic Horizon P displays high values in a relatively even and frequent spread across the surface.

Interpretation: Seismic Horizon L represents the Lista Formation, which is composed of laminated shales with minor interbeds of sand (reference). The values decrease in Seismic Horizon M, indicating a higher amount of fine grained sediments, and then the values increase again in Seismic Horizon N. Seismic Horizon N represents the Sele Formation, which is primarily composed of shales with interbeds of sand, which is displayed by the small amounts of lithologic variation on the RMS map. Seismic Horizon O also displays a few patches of high values, indicating coarser sediment deposition. Seismic Horizon P represents the Base Pleistocene Unconformity and displays large amounts and frequencies of high RMS values. N-S trending striations from glacial activity on the surface are displayed on the RMS amplitude map and emphasized in the variance map (Figure 4.27).

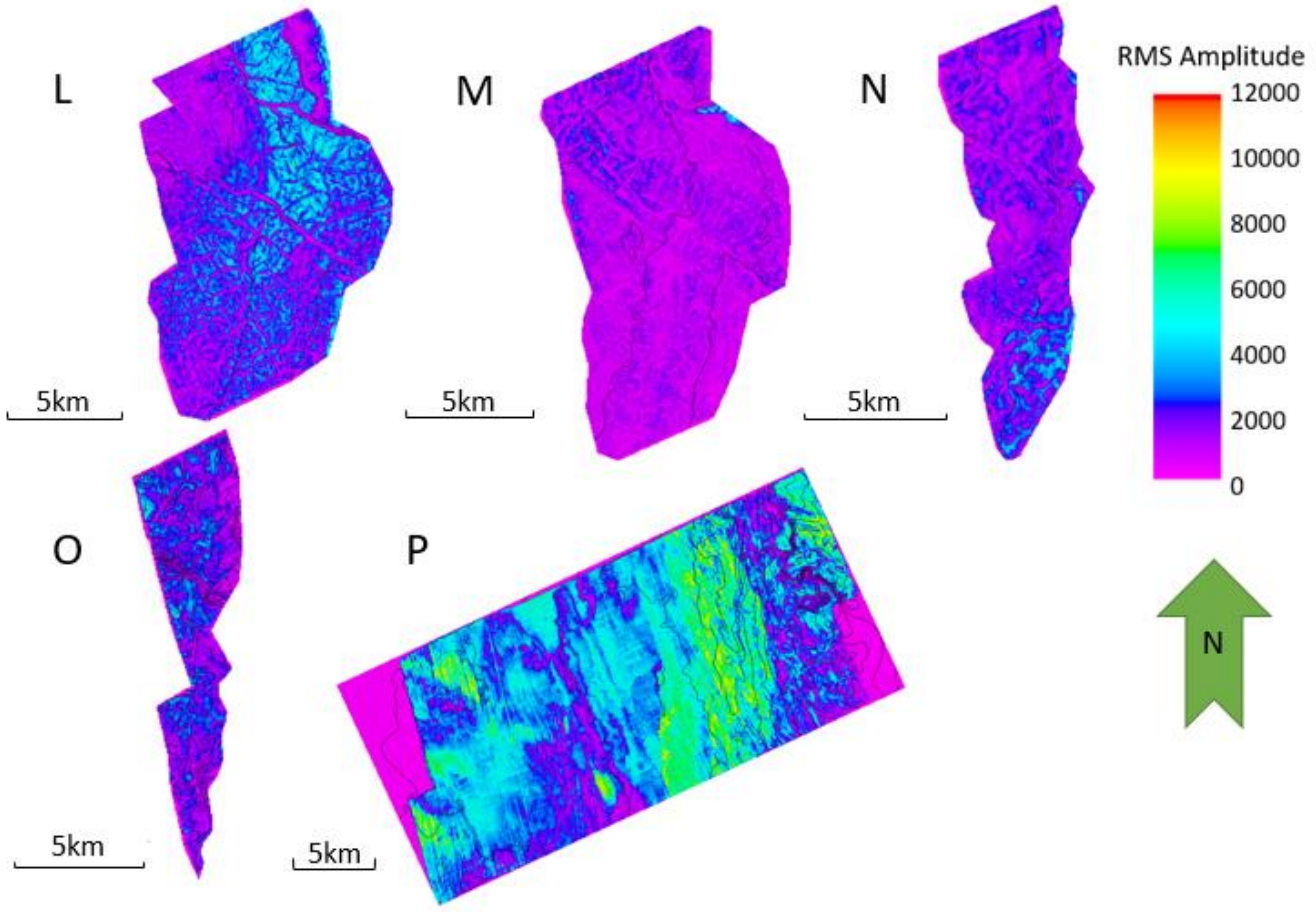

Figure 4.24: RMS amplitude maps for Seismic Horizons L through P.

Seismic Horizon L

Seismic Horizon L is a strong and continuous reflector within the Palaeogene sequence, which is also disrupted by minor faulting. It is truncated in the east by the Base Pleistocene Unconformity. Reflection terminations are difficult to observe, outside of the truncation against the Base Pleistocene Unconformity.

The surface for Seismic Horizon L (Figure 4.23) displays a similar pattern to underlying surfaces, in that it deepens towards the northwest. Surface values towards the Base Pleistocene Unconformity are approximately -700 ms and decrease to -1100 ms towards the west. NW-SE trending faults are also visible by the diagonal shifting in the surface values.

The time-thickness map for Unit L (Figure 4.25) displays thickening towards the northeast. In the southwest, thickness is approximately 100 ms, but this increases gradually to approximately 200 ms in the northeast.

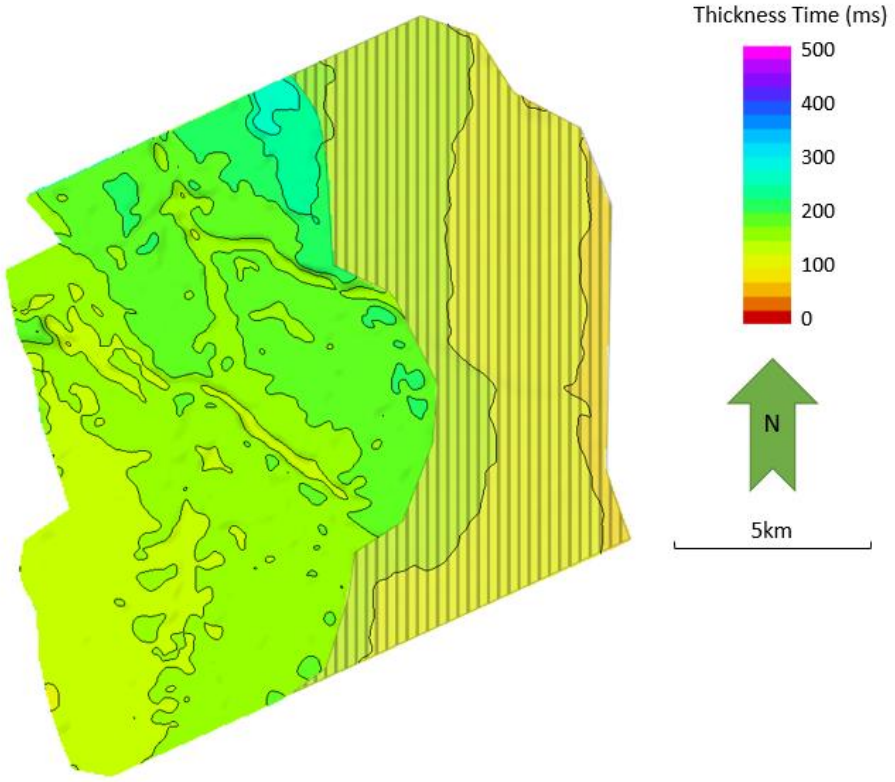

Figure 4.25: time-thickness map for Unit L, between Seismic Horizons L and K. Lines on the left image represent the eroded section over the surface of Seismic Horizon K.

Interpretation: Unit L is part of the Rogaland Group, which is dated to the Early to Late Palaeocene. The Rogaland Group includes Units L through O and is comprised of marine sediments such as shales with interbedded sandstones (Isaksen and Tonstad, 1989). The RMS map displays high values, potentially reflecting the sand components. The Rogaland Group was deposited in a deep marine environment. Seismic Horizon L may be correlated to the top of the Våle Formation, as the well data displays a decrease in gamma ray values, and a composition of deep marine limestone and mudstone.

Seismic Horizon M

Seismic Horizon M is an intermediate strength reflector which is disrupted by faulting and truncated by the Base Pleistocene Unconformity in the northeast. Reflectors in Unit M are difficult to view, but appear to be parallel, implying uniform deposition. The surface and underlying reflectors are mildly disrupted by minor faults.

The surface map for Seismic Horizon M (Figure 4.23) displays a deepening towards the northwest. There is some evidence of faults which trend NW-SE, following the pattern of underlying sequences, and is displayed on the surface by a diagonal shift in values.

Interpretation: Seismic Horizon M is included in the Rogaland Group. It may be correlated to the Lista Formation, which was deposited in a deep water, low-energy environment and is composed of non-tuffaceous and non-laminated shales with minor interbeds of sand (Isaksen and Tonstad, 1989). The RMS amplitude map displays mostly lower values, reflecting lower variance in lithology, as well as some locations where values are relatively high, which may represent the minor interbeds of sand. The well log describes lower gamma ray values along with a composition of siltstone and claystone at the top of the Lista Formation.

Seismic Horizon N

Seismic Horizon N is a weak reflector which is truncated by the Base Pleistocene Unconformity in the northeast. Reflector terminations are not observed directly above or below this horizon. Reflectors beneath Seismic Horizon N are disrupted by minor faulting and are subparallel in behavior. The amplitudes are low, and the reflectors are difficult to observe.

The surface map for Seismic Horizon N displays a deepening towards the northwest, similarly, to underlying surfaces. In the east, it is eroded by the Base Pleistocene unconformity.

Interpretation: Seismic Horizon N represents the Sele Formation of the Rogaland Group, and is dated to the Late Palaeocene (Isaksen and Tonstad, 1989). It is primarily composed of shales and siltstones, with minor interbeds of sandstones which were deposited in a deep marine section, as reflected by the small amount of high RMS values in Figure 4.24. The well log for well 32/4-1 describes lower values on the gamma ray log, as reflected by higher values on the RMS amplitude map.

Seismic Horizon O

Seismic Horizon O is a strong and continuous reflector which is truncated by the Base Pleistocene Unconformity in the northeast. Reflector terminations are not observed directly above or below this horizon. Reflectors are not easily visible and have very low amplitudes, making them difficult to observe.

The surface map for Seismic Horizon O (Figure 4.23) is very small due to the nature of the reflector's location in the upper corner of the 3D cube beneath the Base Pleistocene Unconformity. However, it follows the same pattern as underlying reflectors in that it deepens to the northwest. On the eastern side near where it is eroded by the Base Pleistocene Unconformity, the surface values are approximately -700 ms, then decrease to -800 ms in the west.

Interpretation: Seismic Horizon O lies beneath the Base Pleistocene Unconformity, and is of Late Palaeocene age. It is within the Rogaland Group. The RMS amplitude map displays a similar level of values to underlying horizons in that there is a variety of low and intermediate levels.

Seismic Horizon P

Seismic Horizon P is a strong and continuous reflector which truncates the underlying Seismic Horizons G through O. It continues across the cube, through the Vette and Øygarden Faults. Onlaps are observed near the Øygarden Fault directly above the horizon, as shown in Figure 4.26. The surface map for Seismic Horizon P displays a shallowing towards the northeast, to the east of the Øygarden Fault.

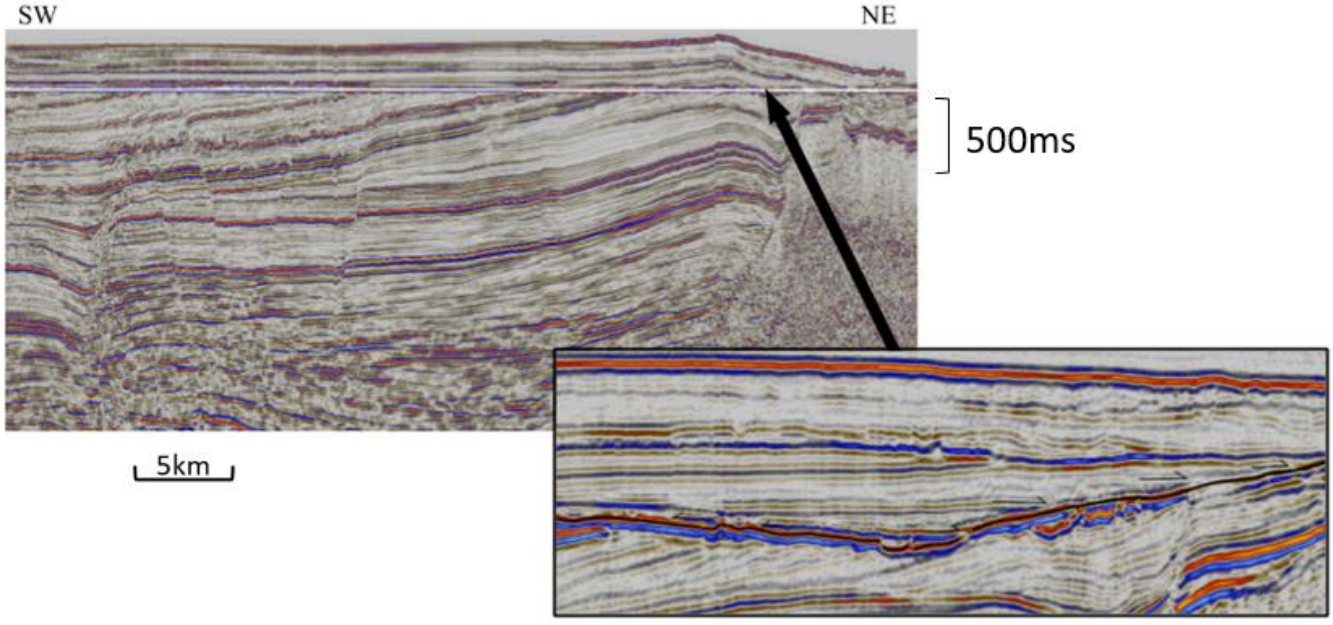

Figure 4.26: Onlaps from above Seismic Horizon P, which is represented by the continuous black line. Inline: 1291.

Interpretation: Seismic Horizon P represents the Base Pleistocene Unconformity. The RMS amplitude map displays intermediate to high levels of variation, along with evidence of glacial

features, which are displayed as N-S trending lines. Onlaps are observed near the Øygarden Fault directly above the horizon, as shown in Figure 4.26. These onlaps from the Quaternary succession on both sides of the depression suggest that the depression existed at the time of deposition.

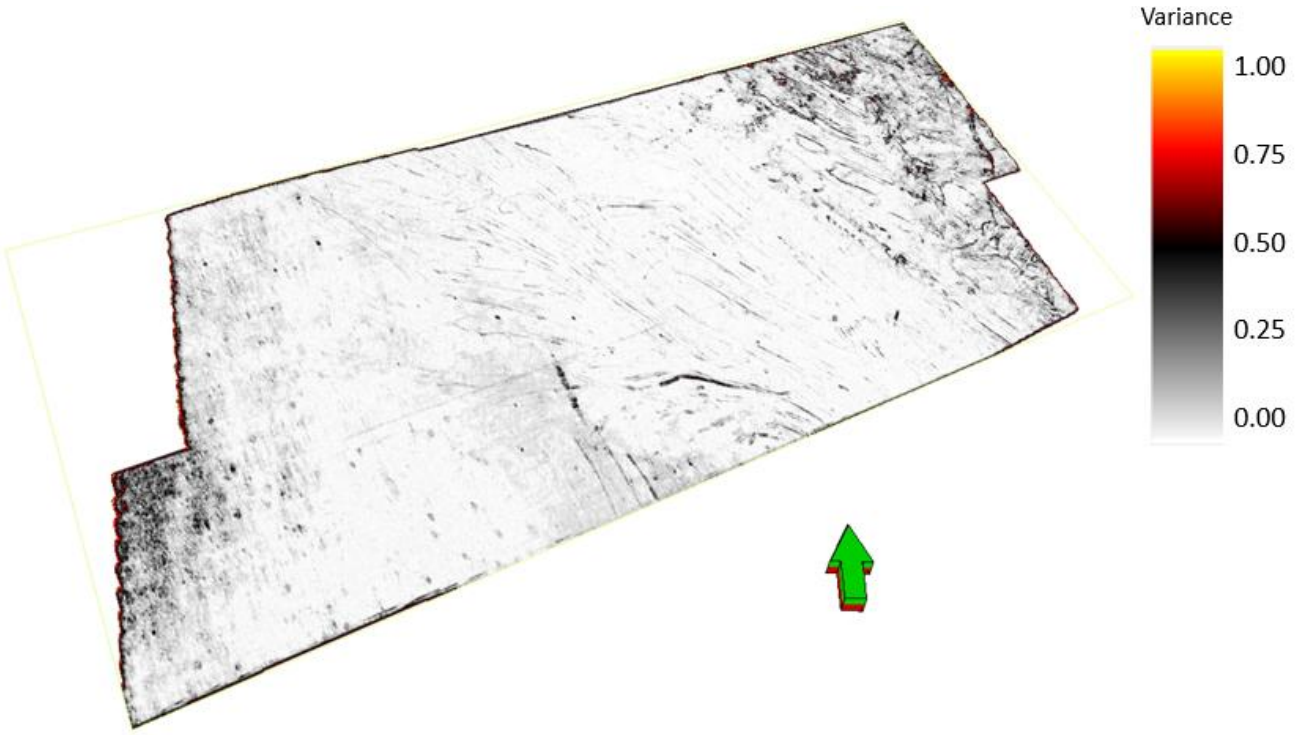

Figure 4.27: Variance map for Seismic Horizon P.

Chapter 5

5 Discussion

The seismic horizons of focus represent the Lower Cretaceous Cromer Knoll Group, and the Upper Cretaceous Shetland Group. The start of the Cretaceous is marked by the Base Cretaceous Unconformity, which correlates to the Top Draupne (Seismic Horizon C). The transition between Lower and Upper Cretaceous is marked by Seismic Horizon J, which correlates to the top of the Cromer Knoll Group. The end of the Late Cretaceous is represented by the Shetland Group (Seismic Horizon K). Multiple seismic horizons are identified within this package based on reflection strength and terminations of reflections surrounding a horizon, such as onlaps, toplaps, and downlaps. Time-thickness maps were made between multiple horizons based on appearance of differing thicknesses on the seismic cube. Points of discussion in this study will include a discussion of sedimentological development in the Pre-Cretaceous and Post-Cretaceous periods, along with a detailed analysis of Cretaceous Seismic Horizons C through K, interpretation of uplift and subsidence events affecting Smeaheia, and the impact of the development on CO_2 storage.

5.1 Pre-Cretaceous Infill and Development

Throughout the Jurassic, the Horda Platform was supplied with clastic sediments from the eastern side of the developing graben system, leaving a record of transgressions and regressions (Stewart et al., 1995). Subsidence occurred in the Late Jurassic (Underhill, 1998; Brekke, 2000) along with the rotation of basement blocks and overlying sediments due to faulting along the Viking Graben (Faleide et al., 2015). Rotation led to the exposure of the fault blocks, causing erosion of Lower-Middle Jurassic and some Upper Triassic sediments.

The deposition of the Brent Group (Unit A) in the Jurassic represented a change from margin-fed shallow marine environments to an axial system which prograded and retrograded in north-south directions (Martinsen and Dreyer, 2001), which is displayed by the composition of sandstone, siltstones, and shales (Vollset and Doré, 1984). During deposition of the Brent Group, tectonic activity shifted from being limited to relatively uniform, subsidence increased, and fault block rotation occurred (Stewart et al., 1995). Syn-rift clastic wedges and shallow marine sands of the Upper Jurassic are associated with deltas and coastal plains, and likely originated from crests of rotated fault blocks (Brekke, 2001).

Unit B represents the Sognefjord Formation, which consists of high-energy shallow marine sheet sands believed to be derived from the fronts of deltas or coastal plains (Brekke, 2001). The time-thickness map for Unit B (Figure 4.15) displays a slight lensoid shape with a thicker package of sediment in the center and thinning towards the faults, potentially due to the orientation of sediment in depressions caused by Late Jurassic subsidence. At the time of deposition of the Sognefjord Formation, fault blocks on the Horda Platform were tilted to the east, and faulting was dominantly north-south (Stewart et al., 1995).

Unit C represents the Draupne Formation, which was deposited in the Late Jurassic as an organic rich source rock due to a high sedimentation rate and poor bottom water circulation in over-deepened basins which formed according to the rifting topography (Bugge, 2001). The unit is fairly homogenous, with a primary composition of clay-fraction sediments, and traces of coarse-grained sediments primarily in the area between the Vette and Øygarden Faults (Figure 4.14).

5.2 Cretaceous Infill and Development

A rifting event occurred during the Mid to Late Jurassic to early Cretaceous, controlling the sedimentary effects of the Cretaceous development on the Horda Platform (Cowie et al., 2005; Færseth et al.,1997; Færseth and Ravnås,1998; Gabrielsen et al.,1990). Major uplift and erosion in the Late Volgian to Ryazanian caused the formation of isolated sedimentary basins where deposition occurred, and the structural highs were exposed to erosion. Seismic Horizon C (Top Draupne) represents a major unconformity, noted as the Base Cretaceous Unconformity, which exists between the Cretaceous and Jurassic units, except towards the deeper parts of the rift where continuous sedimentation may have occurred (Faleide et al., 2015). The unconformity marks a strongly diachronous shift from syn-rift to post-rift configurations. The Cretaceous is characterized by the onlapping of sedimentary units onto basin flanks, infilling relief created by the preceding rifting phase (Kjennerud et al., 2001). The Cromer Knoll Group (Seismic Horizons C through J) contains fine-grained marine sediments with varying amounts of calcareous material (Isaksen and Tonstad, 1989). Sediments throughout the Lower Cretaceous were transported in suspension and sourced from erosion of the Shetland Platform and from southern Norway in the east. (Øvrebø et al., 2001). The thickness of the deposits varies considerably, due to deposition in response to a tectonic phase in the Late Jurassic. The Cromer Knoll Group is involved in *the incipient post-rift phase* as defined by Faleide et al. (2015) (see Section 2.3.6), where the basin configuration is primarily dependent on the structural features such as crests of rotated fault blocks and sub-platforms which were formed in the syn-rift phase. The group displays thickening towards the Øygarden Fault where it is eroded along the Base Pleistocene Unconformity, and thinning towards the Vette Fault, indicating exposure to erosion on the eastern side. However, the package regains thickness to the west of the Vette Fault.

Regression occurred from the mid-late Aptian, along with movement of the North Sea rifts. In the deeper-marine areas, sedimentation shifted from calcareous-rich to organic-rich. Erosion along structural highs led to deposition of some sands as submarine fans along the rifts, as seen in RMS amplitude maps which display higher levels of lithologic variation near the rift boundaries (e.g. Figure 4.14 of Seismic Horizon F), and thicker packages of sediments as displayed on the time-thickness maps. This regression was followed by a regional transgression in the Albian, where the sea level was raised above most parts of the structural highs, and the carbonate content continued to increase (Isaksen et al., 1989), which is reflected by the increase in RMS amplitude values towards the top of the Cromer Knoll Group.

At the end of the Early Cretaceous in the late Albian to early Cenomanian, another regressive event caused erosion and/or non-deposition of sediments near structural highs (Faleide et al., 2015). Overall, periods of transgression and regression dominated throughout a period of

overall transgression, and the deposition of shallow to deep marine mudstones with small amounts of sand was the primary component of sedimentation (Skibeli et al., 1995). These cycles between regression and transgression are reflected in the RMS amplitude maps by shifts between increasing and decreasing values, indicating a change in grain size. Tilted fault blocks were exposed to erosion, and sediments were deposited near fault boundaries as coarser-grained sediments, as displayed by the higher RMS values near faults. During the Late Cretaceous, southern Norway was exposed to erosion due to an approximately 200 m drop in sea level (Haq et al., 1987). Isostatic rebound was initiated, and the resulting isostatic uplift is estimated to be 400-600 m (Hay and Southam, 1977). In Figure 4.15, which displays Seismic Horizon J, it becomes evident by the uniform thickness that the rift topography is being drowned by sediments, subsidence has ceased, and the sedimentation pattern no longer follows that of the underlying rift features, which is in accordance with the work of Faleide et al., 2015. Therefore, Seismic Horizon K (Top Shetland Group) is included in *the mature phase* (see Section Cretaceous 2.3.6).

5.3 Post-Cretaceous Infill and Development

The Cenozoic era is characterized by shifts in outbuilding directions and sediment provenance in relation to uplift, subsidence, and erosion. Cenozoic sediments in the North Sea are grouped into the Rogaland, Hordaland, and Nordland Groups and have been thoroughly documented (e.g. Jordt et al., 1995; Michelsen, 1994; Michelsen et al., 1995; Nielsen et al., 1986; Stewart, 1987), but the specific effects of erosion and tectonic development are still subjects of debate.

Uplift occurred in the Palaeocene to Eocene on the East Shetland Platform, followed by subsidence and the infill of siliciclastic sediments in the North Sea during the Eocene (e.g. Anell et al., 2009; Faleide et al., 2002; Gabrielsen et al., 2005, 2010; Goledowski et al., 2012; Jordt et al., 1995, 2000). Uplift is related to igneous activity in the North Atlantic Igneous Province (Knox and Morton, 1988) and an overall change from shallow marine to deep marine Palaeogene sediments (Kyrkebø et al., 2001; Michelsen, 1994). In the Eocene to Early Oligocene, a combination of uplift and subsidence along with climatic change led to a new basin infill pattern, along with tilting of fault blocks (Figure 5.2, *Stage 6*). The Beta Structure of Smeaheia was tilted and placed in a new configuration where it was shallower than the Alpha Structure (Kolnes, 2019). From the Palaeocene to Eocene, the main sediment transport direction was eastwards, but that shifted to westwards during the Neogene (Jordt et al., 1995). During the Quaternary, a global cooling event resulted in glaciations, causing glacial erosion and incision in southern Norway, the remnants of which can be seen on the Base Pleistocene Unconformity (Figure 4.27). Erosion along the Base Pleistocene Unconformity can be seen at the northeast edges of the Cretaceous and Tertiary units in the study area.

5.4 Development

The development of the study area is divided into 8 stages based on observed major changes such as faulting, uplift, erosion, or shifts in sediment influx. Figure 5.2 and Figure 5.2 display a schematic illustration of the development.

Stage 1: Middle to Upper Jurassic units are deposited, followed by faulting which creates accommodation space for the Upper Jurassic units (Faleide et al., 2015).

Stage 2: Upper Jurassic units are deposited, and normal faulting occurs, displacing the units. The boundary between the Upper Jurassic and the Lower Cretaceous units is the Base Cretaceous Unconformity. Subsidence in the Late Jurassic (Brekke, 2000) led to the deposition of units which are slightly thicker between the Vette and Øygarden Faults.

Stage 3: Lower Cretaceous units are deposited, filling in the resulting topography from normal faulting, as shown by the black lines in the depression next to the Øygarden Fault. Erosion of western and eastern parts of the Lower Cretaceous units occurs due to uplift (Øvrebø et al., 2001) and a drop in sea level (Haq et al., 1987), leaving a thicker unit of sediment between the faults. This erosional surface represents an unconformity in the Lower Cretaceous, which is informally called the "Mid-Cretaceous Unconformity" and has not been discussed in some previous studies (e.g. Gassnova, 2012).

Stage 4: Sediments are deposited in the Lower Cretaceous after the Mid-Cretaceous Unconformity and display a progradational pattern of influx and a wedge-shape that does not reach the Vette Fault in the west.

Stage 5: The Late Cretaceous unit is deposited, overstepping the underlying rifting topography and marking the shift from early post-rift to late post-rift.

Stage 6: Deposition of Tertiary sediments occurs over the Late Cretaceous unit. Uplift of Norway occurs in the Eocene-Oligocene (Anell et al., 2009), paired with subsidence in the Viking Graben, resulting in the tilting of successions and exposing them to erosion.

Stage 7: Tilted units are partially eroded, and further erosion and isostatic uplift of Norway occur, primarily due to glacial activity. The units now dip to the southwest rather than the former configuration of dipping to the east. Subsequently, the Base Pleistocene unconformity erodes sediments from the Tertiary, Cretaceous, and Jurassic units.

Stage 8: Present-day configuration. Units above the Permian-Triassic sequence are dipping to the southwest, with the Lower-Cretaceous to Tertiary units dipping more steeply. Quaternary sediments lie unconformably above the Tertiary, Upper Cretaceous, and Lower Cretaceous units, and above the Upper Jurassic units to the east of the Øygarden Fault.

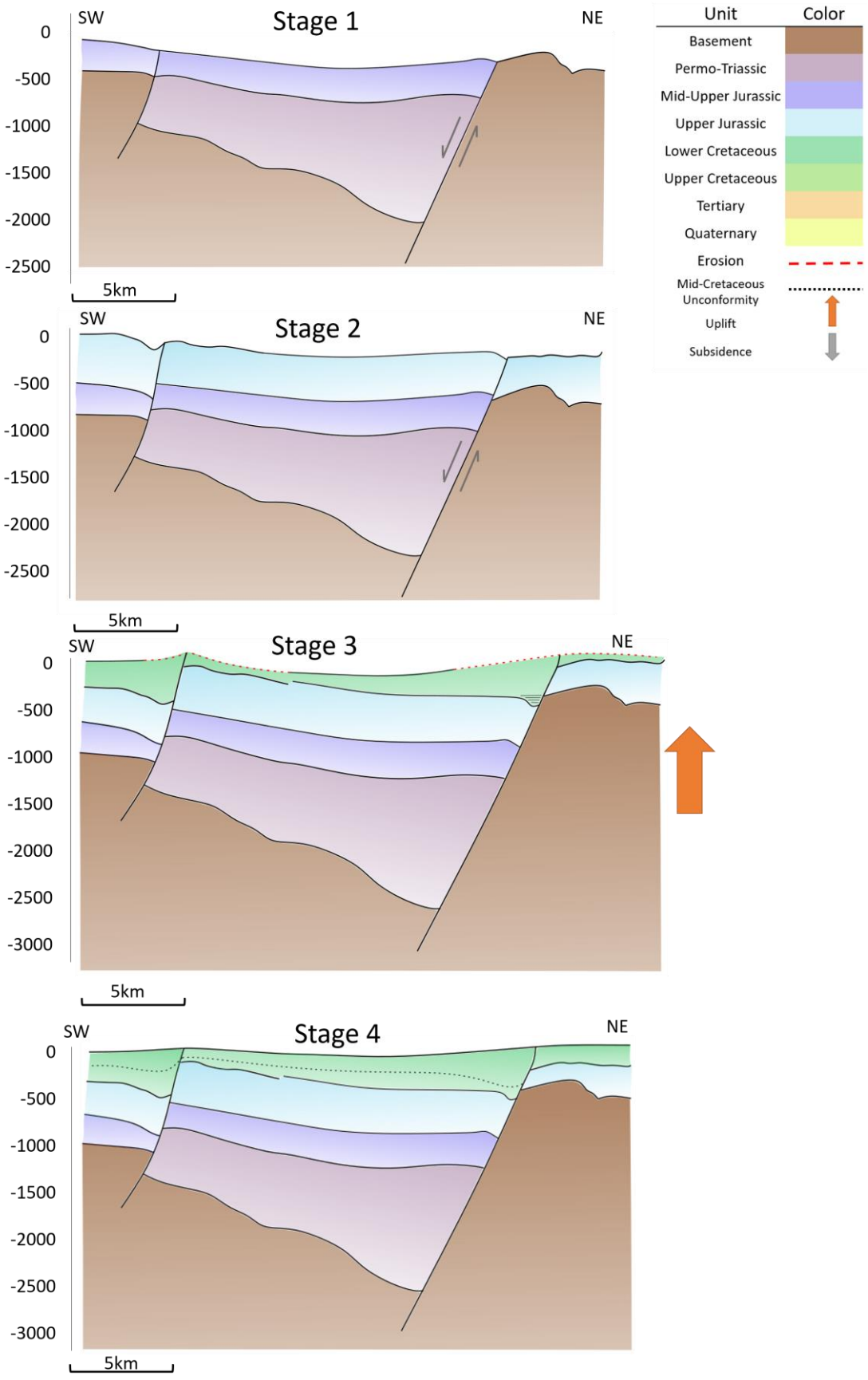

Figure 5.1: Stages one through four of the compiled figure of developmental stages of the study area. Y axis represents approximate depth (m). Each figure is bound in the west by the Vette Fault, and in the east by the Øygarden Fault.

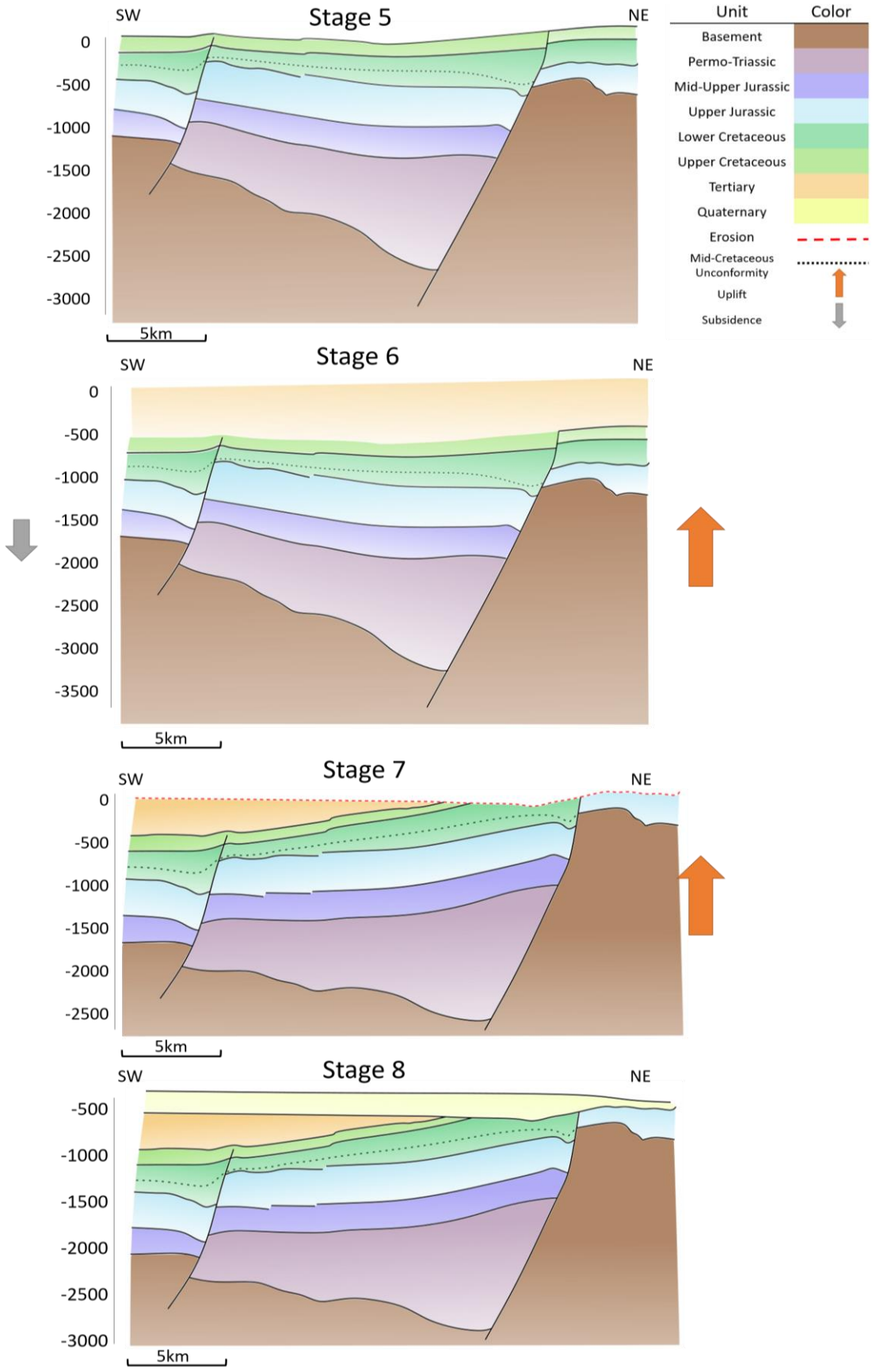

Figure 5.2: Stages five through eight of the compiled figure of developmental stages of the study area. Y-axis represents approximate depth (m). Each figure is bound in the west by the Vette Fault, and in the east by the Øygarden Fault.

5.5 Implications for CO_2 Storage

One of the purposes of this study was to outline potential for CO_2 storage in Smeaheia, which is a potential subsurface storage site on the Horda Platform in the North Sea (blocks 32/4 and 32/1). Two prospects have been defined, one being the Alpha structure (primary target) in the footwall of the Vette Fault, and the other being the Beta structure in the hanging wall of the Øygarden Fault, updip of the Alpha structure (Figure 5.3).

Injection and storage of CO_2 will potentially occur in the shallow-marine sediments of the Viking Group (Jurassic), specifically in the Sognefjord Formation. According to this study, the sediments over the Beta structure are fine-grained (Figure 4.11), but the sediments over the Alpha structure are likely coarser based on the RMS amplitude maps.

The primary seal consists of the Upper Jurassic Draupne shale, which is a marine, organic rich claystone that displays very low permeability (Mondol et al., 2018) The RMS amplitude map for Seismic Horizon C (the Draupne Formation) displays high values between the Vette and Øygarden Fault, but low values at the fault boundaries, indicating coarse sediment in the center and fine-grained sediments near the faults at the location of the Alpha and Beta Structures. Finer-grained sediments pose as better seals due to lower porosity and permeabilities, so the presence of these sediments over the potential storage site is beneficial as a primary seal.

The Cretaceous limestones and shales of the Shetland and Cromer Knoll Groups are also components of secondary storage. In this study, the Cromer Knoll Group is observed to contain primarily fine-grained sediments with cycles of increasing and decreasing grain size of sediments, with a high likelihood for coarse-grained sediments at the upper boundary of the secondary storage unit. Some of the horizons display a homogeneous sedimentary distribution, such as Seismic Horizons D, G, and H. However, Seismic Horizons E and F display higher RMS values, especially near the fault boundaries, which indicates coarser sediment distribution. The RMS values also indicate coarse sediments in the east where the surfaces have been eroded by the Base Pleistocene Unconformity, which could serve as a potential leakage zone if the primary seal fails. The Quaternary sediments are loosely compacted, so exposure of these sediments to CO_2 could lead to further leakage. However, this location lies over the Beta Structure, which is not being considered as a CO_2 storage site. Over the Alpha Structure, the Cretaceous sediments display a similar configuration of coarse-grained sediments near the fault zone but are not directly exposed to the Quaternary sediments.

Wells have been drilled into the Smeaheia area, including well 32/4-1 and 32/2-1. Well 32/4-1 discovered 68 m of Sognefjord Formation sands, while 114 m was found in well 32/2-1 (Mondol et al., 2018). A petrophysical analysis and rock physics diagnosis was done for the Sognefjord Formation by Mondol et al. (2018). The reservoir quality was found to be consistent due to the clean sandstone, which is mostly uncemented, contains little clay, and does not show high compaction effects. The diagenetic maturity was very low according to chemical and physical alterations of the sediment. The porosity has been mostly preserved, and the sediments show consistency with present day sediments at shallow burial depths of less than 1500 m (Mondol et al., 2018).

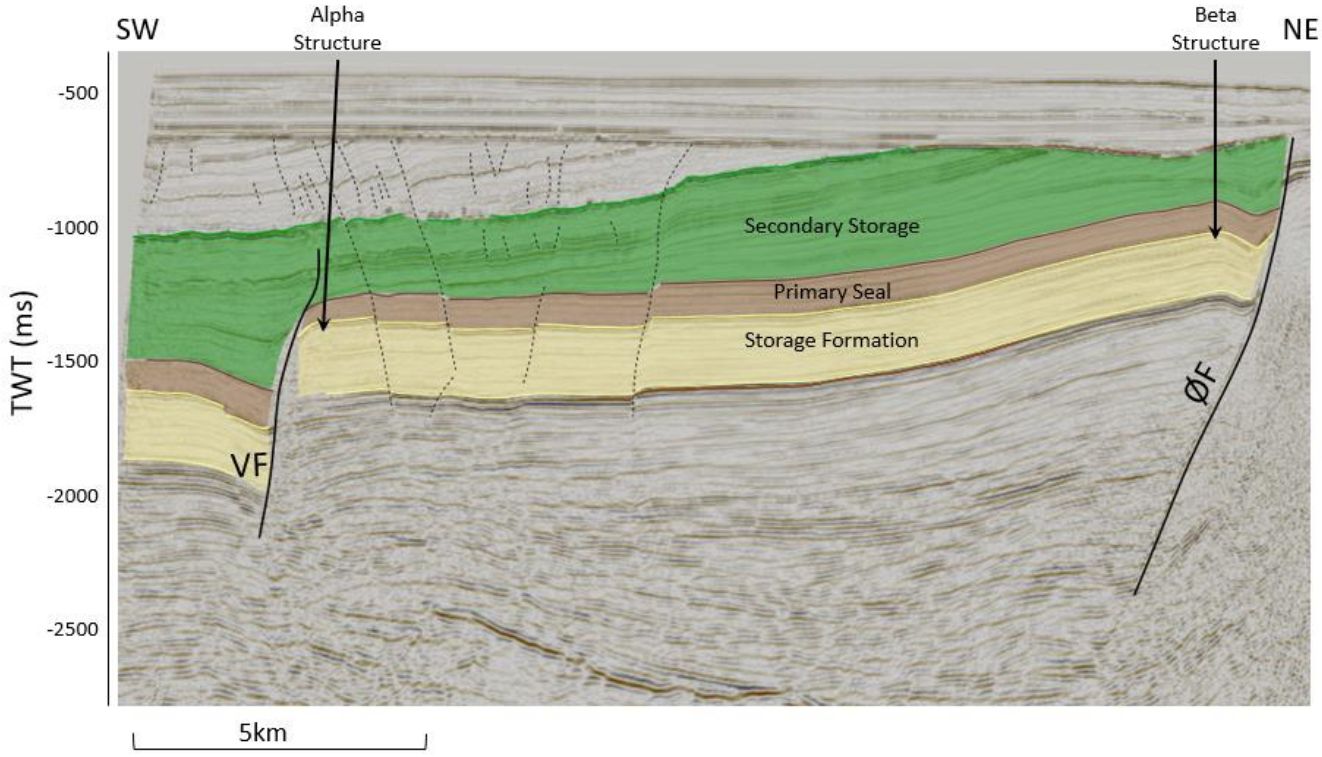

Figure 5.3: GN1101 cube displaying storage formation (Sognefjord Formation), primary seal (Draupne Formation), and secondary storage (Cretaceous units). Alpha and Beta structures are noted by arrows. VF: Vette Fault; ØF: Øygarden Fault.

CO_2 capture and storage in Smeaheia has been studied previously (Gassnova, 2016; Riis and Halland, 2014; Sundal et al., 2014) along with similar sites in the Norwegian North Sea. The total area for Smeaheia is 1.180 km^2 (Sacco, 2018). A potential formation for injection is the Sognefjord Formation, which is a tilted reservoir, favoring migration of CO_2 to the north within the Sognefjord Formation. The tilting also assists with dissolution due to higher contact area with formation water (Bachu, 2015; Hermanrud et al., 2009; Pruess and Nordbotten, 2011). The sedimentary architecture observed at Smeaheia is dominated by porous and permeable shallow-marine sandstones of the Sognefjord, Fensfjord, and Krossfjord Formations. The Heather Formation interfingers the sandstone, causing a contrast between the sandstones and claystones to potentially improve the success of trapping mechanisms (Bachu, 2015; Nordbotten et al., 2005).

Estimates of net erosion over the Alpha and Beta structures in Smeaheia have been conducted by Kolnes (2019). The results show a net-erosion estimate of 900 m over the Alpha structure, and 1700 m over the Beta structure, with a steep rate of increase towards the west (Kolnes, 2019). Maximum burial depths were also calculated to be 2213 m for the Beta Structure and 1540 m for the Alpha Structure approximately 10 Ma. Following this, the Beta and Alpha structures were uplifted 1800 m and 800 m respectively, and a significant uplift event is estimated to have occurred in the Eocene-Oligocene (Kolnes, 2019). In conclusion, the Beta structure has seen greater burial depths and uplift, has potentially undergone faster mechanical compaction, and possibly chemical compaction. Therefore, the characteristics of the Beta and Alpha structures, such as porosity, permeability, and storage capacity, likely differ. At higher

burial depths, it is possible for sediments to undergo chemical compaction. The Draupne Formation overlying the Beta Structure may have developed micro-quartz under chemical compaction and is more prone to brittle deformation and fracturing. However, such effects are not likely to occur over the Alpha Structure due to a lower maximum burial depth (Kolnes, 2019). Additionally, CO_2 leakage along the Øygarden Fault is a potential risk due to a potential reduction in porosity and permeability from compaction in the reservoir formation.

The Cretaceous units have undergone the same burial and uplift history as the reservoirs, but at shallower depths. The units were not buried deeply enough to be exposed to chemical compaction, but mechanical compaction may have had an effect. Some Cretaceous units observed in this study through RMS amplitude maps display homogeneity while others are more laterally varied, including a mix of fine and coarse grained sediments, especially near fault boundaries. Fine grained or clay fraction sediments may form baffles, or impermeable obstacles, which the CO_2 might flow around upon contact. Multiple units observed in the Cretaceous package display coarse-grained sediments near the fault boundaries above the Alpha and Beta Structures, but a homogenous section of fine-grained sediments in the center. This section of fine-grained sediments may provide baffles against the CO_2. However, if the CO_2 were to migrate upwards towards the contact between the Cretaceous units and the Base Pleistocene Unconformity, coarse-grained sediments may be reached, and the direct contact to loosely compacted Quaternary sediments may be a potential risk for leakage.

Chapter 6

6 Conclusions

The focus of this study was to understand the specific uplift and subsidence history of the proposed injection site, Smeaheia, which lies on the Horda Platform in the North Sea. Seismic interpretation, the use of seismic attributes and time-thickness maps, and analysis of reflector terminations have been completed to compile the tectonostratigraphic history. It has become evident that the uplift and subsidence history has significant impacts on sedimentological successions, and the results of this study may give implications for the quality of reservoir, primary seals, and secondary storage of the proposed storage site.

- Throughout the Pre-Cretaceous development on the Horda Platform, the primary sediment supply was clastic sediments from the east, providing the sandy sediments for the reservoir of Smeaheia. Fault block rotation led to erosion of Jurassic and Triassic sediments, and subsidence occurred in the Late Jurassic. A rise in sea level at the end of the Jurassic Period led to the deposition of the fine-grained Draupne shales which make up the primary seal for the potential storage site.
- In the Early Cretaceous, erosion related to a drop in sea level occurred within the Cromer Knoll Group, marked by an unconformity which is informally called the "Mid-Cretaceous Unconformity". Erosion occurred primarily near the Vette and Øygarden Faults. Overlying sediments filled in with a progradational, wedge-shaped pattern.
- Regional tilt and uplift in the Eocene-Oligocene resulted in a shift of the units from an east-dipping direction to a west-dipping direction. The Beta Structure of Smeaheia was uplifted higher than the Alpha Structure, contrasting the former configuration of being buried deeper.
- The main reservoir for the potential CO_2 storage site displays primarily coarse-grained sediments, with some finer-grained sediments at the contact between the reservoir and primary seal.
- The primary seal consists of the Upper Jurassic Draupne Formation (Unit C), which is shown to contain primarily fine-grained sediments with minor interbeds of sand. Low RMS amplitude values at the fault boundaries indicate fine-grained sediments above the proposed CO_2 injection and storage site, which implies adequate primary seal functionality.
- Secondary storage consists of the Cromer Knoll and Shetland Groups (Cretaceous) and contains coarse-grained sediments in the east where the Cromer Knoll Group has been eroded by the Base Pleistocene Unconformity, which could serve as a potential leakage site for CO_2, as the group directly contacts loosely compacted Quaternary sediments. However, this contact lies over the Beta Structure, and although some coarse-grained sediments are present above the Alpha Structure in the secondary storage, there is no direct contact with Quaternary sediments there. RMS amplitude

maps display some homogeneous units with coarse-grained sediments at fault boundaries, while some other units display more lithologic variation and may form baffles to the CO_2, in the case that it reaches the secondary storage.

7 References

Andersen, T.B. (1998). Extensional tectonics in the Caledonides of southern Norway, an overview. Tectonophysics 285, 333–351. https://doi.org/10.1016/S0040-1951(97)00277-1.

Andersen, M.S., Sørensen, A.B., Boldreel, L.O., Nielsen, T. (2002). Cenozoic evolution of the Faroe Platform comparing denudation and deposition. In: Doré, A.G., Cartwright, J.A., Stoker, M.S., Turner, J.P., White, N. (Eds.), Special Publication of the Geological Society of London, 196, pp. 291– 311.

Anderton, R., Bridges, EH., Leeder, M.R. and Sellwood, B.W. (1979). A Dynamic Stratigraphy of the British Isles. A Study in Crustal Evolution. George Allen and Unwin Ltd., London, 301 pp.

Anell, I., Thybo, H., and Artemieva, I. (2009). Cenozoic Uplift and Subsidence in The North Atlantic Region: Geological evidence revisited. Tectonophysics, 474 (1-2):78– 105.

Anell, I., Thybo, H. and Stratford, W. (2010) Relating Cenozoic North Sea sediments to topography in southern Norway: The interplay between tectonics and climate. Earth Planet. Sci. Lett., 300, 19–32.

Bachu, S., Adams, J.J. (2003). Sequestration of CO_2 in geological media in response to climate change: capacity of deep saline aquifers to sequester CO_2 in solution. Energy Convers. Manag. 44, 3151–3175. https://doi.org/10.1016/S0196-8904(03)00101-8.

Bachu, S. (2015). Review of CO_2 storage efficiency in deep saline aquifers. International Journal of Greenhouse Gas Control, 40, 188-202.

Baig, I., Faleide, J. I., Jahren, J., and Mondol, N. H. (2016). Cenozoic Exhumation on the Southwestern Barents Shelf: Estimates and Uncertainties Constrained from Compaction and thermal maturity analyses. Marine and Petroleum Geology, 73:105–130.

Blystad, E, Brekke, H., Færseth, R.B., Larsen, B.T., Skogseid, J. and Tørudbakken, B. (1995). Structural elements of the Norwegian continental shelf. Part II: The Norwegian Sea Region. Norwegian Petroleum Directorate Bulletin, 8. The Norwegian Petroleum Directorate, Stavanger, 45 pp.

Blythe, A.E., Kleinspehn, K.L. (1998). Tectonically versus climatically driven Cenozoic exhumation of the Eurasian plate margin Svalbard: fission track analyses. Tectonics 17, 621– 639.

Bolle, L. (1992). Troll Field. Norway's Giant Offshore Gas Field, Giant Oil and Gas Fields of the Decade 1978-1988, Vol. M 54, A/S Norske Shell, chapter 28, pp. 447–458.

Bonow, J.M., Lidmar-Bergstrom, K., Japsen, P. (2006). Palaeosurfaces in central West Greenland as reference for identification of tectonic movements and estimation of erosion. Glob. Planet. Change 50, 161– 183.

Brekke, H., Dahlgren, S., Nyland, B. and Magnus, C. (1999). The prospectivity of the Vøring and Møre basins on the Norwegian Sea continental margin. In: A.J. Fleet and S.A.R. Boldy (Editors), Petroleum Geology of Northwest Europe: Proceedings of the 5th Conference. Geological Society, London, pp. 261-274.

Brekke, H. (2000). The tectonic evolution of the Norwegian Sea Continental Margin with emphasis on the Vøring and Møre Basins. In: A. Nøttvedt et al. (Editors), Dynamics of the Norwegian Margin. Geol. Soc., London, Spec. Publ., 167: 327-378.

Brekke, H., Sjulstad, H.I., Magnus, C. and Williams, R.W. (2001). Sedimentary environments offshore Norway — an overview. In: Martinsen, O.J. and Dreyer, T. (Eds) Sedimentary Environments Offshore Norway — Palaeozoic to Recent, NPF Special Publication 10, pp 7-37. DOI: 10.1016/S0928-8937(01)80006-0.

Brown, R. W. (1991). Backstacking apatite fission-track 'stratigraphy': a method for resolving the erosional and isostatic rebound components of tectonic uplift histories. Geology 19, 74-77.

Brown, A. R. (ed.) (1999). Interpretation of Three-Dimensional Seismic Data , 6th edn, AAPG Memoir 42 and SEG, Tulsa, Oklahoma.

Brown, A.R. (2001). Data polarity for the interpreter. The Leading Edge 20, 549–549. https://doi.org/10.1190/1.1438994

Bugge, T., Tveiten, B., Bäckström, S. (2001). The depositional history of the Cretaceous in the northeastern North Sea, in: Norwegian Petroleum Society Special Publications. Elsevier, pp. 279–291. https://doi.org/10.1016/S0928-8937(01)80018-7.

Clausen, O.R., Nielsen, O.B., Huuse, M., Michelsen, O. (2000). Geological indications for Palaeogene uplift in the eastern North Sea Basin. Glob. Planet. Change 724,175– 187. Clift, P., 1996. Plume tectonics as a cause of mass wasting on the southeast Greenland continental margin. Mar. Pet. Geol. 13, 771– 780.

Collinson, J.D. (1988). Controls on Namurian sedimentation in the Central Province basins of northern England. In: B.M. Besly and G. Kelling (Editors), Sedimentation in a Synorogenic Basin Complex: The Upper Carboniferous of Northwest Europe. Blackie, Glasgow, pp. 85-101.

Cook, P.J. (1999). Sustainability and nonrenewable resources. Environmental Geosciences, 6 (4), 185–190.

Corfield, S.M., Gawthorpe, R.L., Gage, M., Fraser, A.J. and Besly, B.M.(1996). Inversion tectonics of the Variscan Foreland of the British Isles. J. Geol. Soc., London, 153: 17-32.

Coward, M. P., Dewey, J. F., Hempton, M. and Holroyd, J. (2003). Tectonic evolution. 17-33 in The Millennium Atlas: Petroleum geology of the central and northern North Sea. Evans, D., Graham, C., Armour, A. and Bathurst, P. (editors and coordinators). (London: The Geological Society of London).

Cowie, P. A., Underhill, J. R., Behn, M. D., Lin, J. and Gill, C. E. (2005). Spatiotemporal evolution of strain accumulation derived from multi-scale observations of late jurassic rifting in the northern North Sea: A critical test of models for lithospheric extension, Earth and Planetary Science Letters234: 401–419.

Daber, R., Ditcha, E. M., Gustafsson, L. E., Knudsen, E., Pepper, R., Bejarano, G. (2008). Seismic-to-Simulation Software – Interpreter's Guide to Seismic Attributes. Houston: Schlumberger Information Solutions.

Dahlgren, S. and Corfu, F. (2001). Northward sediment transport from the late Carboniferous Variscan Mountains: zircon evidence from the Oslo Rift, Norway. J. Geol. Soc., London, 158: 29-36.

Danielsen, M., Michelsen, O., Clausen, O.R. (1998). Oligocene sequence stratigraphy and basin development in the Danish North Sea sector based on log interpretations. Mar. Pet. Geol. 14, 931– 950.

Deegan, C.E. and Scull, B.J. (1977) A standard lithostratigraphic nomenclature for the Central and Northern North Sea. Institute of Geological Sciences, 1 , 36 pp.

Doré, A.G., Lundin, E.R., Jensen, L.N., Birkeland, O., Eliassen, P.E. and Fichler, C. (1999). Principal tectonic events in the evolution of the northwest European Atlantic margin. In: Fleet, A.J. and Boldy, S.A.R. (eds.), Petroleum Geology of Northwest Europe: Proceed

Duffy, O., Bell, R., Jackson, C., Gawthorpe, R., Whipp, P. (2015). Fault growth and interactions in a multiphase rift fault network: Horda Platform, Norwegian North Sea. Journal of Structural Geology 80 (2015) 99-119.

Dreyer, T., Whitaker, M., Dexter, J., Flesche, H., and Larsen, E. (2005). From spit system to tide-dominated delta: integrated reservoir model of the Upper Jurassic Sognefjord Formation on the Troll West Field. In: Doré, A.G. and Vining, B.A. (Eds) Petroleum Geology: North-West Europe and Global Perspectives – Proceedings of the 6th Petroleum Geology Conference. Geological Society, London, Petroleum Geology Conference series, 6, 423-448.

Eidvin, T., Jansen, E., Riis, F. (1993). Chronology of Tertiary fan deposits off the western Barents Sea: implications for the uplift and erosion history of the Barents Shelf. Mar. Geol. 112, 109– 131.

Faleide, J.I, Kyrkebø, R., Kjennerud, T., Gabrielsen, R.H., Jordt, H., Fanavoll, S., Bjerke, M.D. (2002). Tectonic impact on sedimentary processes during the Cenozoic evolution of the North Sea and surrounding areas. In: Doré, A.G., Cartwright, J.A., Stoker, M.S., Turner, J.P., White, N. (Eds.), Exhumation of the North Atlantic Margin: Timing, Mechanisms and Implications for Petroleum Exploration. Geol. Soc. Spec. Publ., vol. 196, pp. 235– 269.

Faleide, J.I., Bjørlykke, K. and Gabrielsen, R.H. (2015). Geology of the Norwegian Continental Shelf. In: Bjørlykke, K. (Ed) Petroleum Geoscience - From Sedimentary Environments to Rock Physics. Springer, Berlin. pp. 603-620 DOI: 10.1007/978-3-642-34132-8_25.

Folkestad, A., Steel, R.J. (2001). The alluvial cyclicity in Hornelen basin (Devonian Western Norway) revisited: a multiparameter sedimentary analysis and stratigraphic implications, in Norwegian Petroleum Society Special Publications. Elsevier, pp. 39–50. https://doi.org/10.1016/S0928-8937(01)80007-2.

Fraser, S. I., Robinson, A. M., Johnson, H. D., Underhill, J. R., Kadolsky, D. G. A., Connell, R., Johannesen, P., and Ravnås, R. (2003). Upper Jurassic. In D. Evans, C. Graham, A. Armour and P. Bathurst (Eds.), The Millennium Atlas: Petroleum geology of the central and northern North Sea. (p. 157-189) London: The Geological Society of London.

Færseth, R. (1996). Interaction of permo-triassic and jurassic extensional fault-blocks during the development of the northern North Sea. Journal of the Geological Society, 153(6):931–944.

Færseth, R. B., Knudsen, B.-E., Liljedahl, T., Midbøe, P. S. and Søderstrøm, B. (1997). Oblique rifting and sequential faulting in the Jurassic development of the northern North Sea: Journal of Structural Geology19: 1285–1302.

Færseth, R. B. and Ravnås, R. (1998). Evolution of the Oseberg Fault-Block in context of the northern North Sea structural framework, Marine and Petroleum Geology15: 467–490.

Gabrielsen, R.H., Færseth, R.J., Steel, R.J., Idil, S. and Kløvjan, O.S. (1990) Architectural styles of basin fill in the northern Viking Graben. In: Tectonic evolution of the North Sea Rift (Eds D.J. Blundell and A.D. Gibbs), Oxford University Press, Oxford. 158–179.

Gabrielsen, R.H., Odinsen, T. and Grunnaleite, I. (1999). Structuring of the Northern Viking Graben and the Møre Basin; the influence of basement structural grain and the particular role of the Møre-Trøndelag fault Complex. Marine and Petroleum Geology 16, 443–465.

Gabrielsen, R.H., Braathen, A., Olesen, O., Faleide, J. I., Kyrkjebø, R. and Redfield, T. F. (2005) Vertical movements in south-western Fennoscandia: a discussion of regions and processes from the present to the Devonian. In: Onshore-Offshore Relationships on the North Atlantic Margin (Eds B.T.G. Wandas, J.P. Nystuen, E. Eide and F. Gradstein), Norwegian Petroleum Society Special Publication, 12, 1–28.

Gabrielsen, R.H., Faleide, J.I., Pascal, C., Braathen, A., Nystuen, J.P., Etzelmuller, B and O'Donnell, S. (2010) Latest Caledonian to Present tectonomorphological development of southern Norway. Mar. Petrol. Geol., 27, 709–723.

Gassnova. (2012). Troll Kystnær Subsurface Status Report.

Gassnova. (2016). Feasibility study for full-scale CCS in Norway.

Ghazi, S.A. (1992). Cenozoic uplift in the Stord Basin and its consequences for exploration. Nor. Geol. Tidsskr. 72, 285– 290.

Glennie, K.W. (1998). Lower Permian-Rotliegend. In: K.W. Glennie (Editor), Petroleum Geology of the North Sea. Basic Concepts and Recent Advances. 4th ed., Blackwell Science Ltd., London, pp. 137-173.

Glennie, K.W. and Underhill, J.R. (1998). Origin, development, and evolution of structural styles. In: K.W. Glennie (Editor), Petroleum Geology of the North Sea. Basic Concepts and Recent Advances. 4th ed., Blackwell Science Ltd., London, pp. 42-84.

Goledowski, B., Nielsen, S. B., and Clausen, O. R. (2012). Patterns of Cenozoic sediment flux from western Scandinavia. Basin Research, 24, 377–400.

Gong, C., Wang, Y., Steel, R.J., Olariu, C., Xu, Q., Liu, X., Zhao, Q. (2015). Growth Styles of Shelf-Margin Clinoforms: Prediction of Sand- and Sediment-Budget Partitioning into and Across the Shelf. Journal of Sedimentary Research, vol. 85, no. 3, 2015, pp. 209–229., doi:10.2110/jsr.2015.10.

Google Earth. Map showing location of Norway. Google Earth, earth.google.com/web/. [last accessed: May 2019]

Grayson, R.F. and Oldham, L. (1987). A new structural framework for the northern British Dinantian as a basis for oil, gas and mineral exploration. In: J. Miller, A.E. Adams and V.E Wright (Editors), European Dinantian Environments. Wiley, Chichester, pp. 33-60.

Gradstein, F. M., Kaminski, M. A., Berggren, W. A., Kristiansen, I. L. and D'ioro, M. A. (1994). Cenozoic biostratigraphy of the North Sea and Labrador Shelf Micropaleontology Suppl. 40, 152.

Hamann, N.E., Whittaker, R.C., Stemmerik, L. (2005). Structural and geological development of the North East Greenland shelf. In: Doré, A.G., Vinning, B.A. (Eds.), Petroleum Geology: North-West Europe and Global Perspectives — Proceedings of the 6th Petroleum Geology Conference. Geological Society, London, pp. 887– 902.

Haq, B. U., Hardenbol, J., and Vail, P. R. (1987). Chronology of fluctuating sea levels since the Triassic. Science, 235(4793):1156–1167.

Heeremans, M. and Faleide, J.I. (2004). Permo-Carboniferous rifting in the Skagerrak, Kattegat and the North Sea: Evidence from seismic and borehole data. In: Wilson, M., Neumann, E.-R., Davies, G., Timmerman, M.J., Heeremans, M. and Larsen, B.T. (eds.), Permo-Carboniferous Rifting in Europe. Geological Society Special Publication 223, pp. 159–177.

Hellem, T., Kjemperud, A., and Øvrebø, O.K. (1986). The Troll Field; a geological/ geophysical model established by the PLO85 Group. In: Spencer, A.M. (Ed.) Habitat of hydrocarbons on the Norwegian continental shelf; proceedings of an international conference. Graham and Trotman. London, United Kingdom, 217-238.

Henriksen, S., Fichler, C., Grønlie, A., Henningsen, T., Laursen, I., Løseth, H., Ottesen, D., Prince, I. (2005). In: Wandås, B.T.G., Nystuen, J.P., Eide, E.A., Gradstein, F.M. (Eds.), Onshore– Offshore Relationships on the North Atlantic Margin. NPF Spec. Publ., vol. 12, pp. 111– 133.

Hermanrud, C., Andresen, T., Eiken, O., Hansen, H., Janbu, A., Lippard, J., Bolås, H. N., Simmenes, T. H., Teige, G. M. G. and Østmo, S. (2009). Storage of CO_2 in saline aquifers–lessons l earned from 10 years of injection into the Utsira Formation in the Sleipner area. Energy Procedia, 1, 1997-2004.

Hellevang, H. (2015). Carbon capture and storage (CCS). In Petroleum Geoscience, pages 591–602. Springer.

Hesjedal, A. and Hamar, G.E (1983). Lower Cretaceous stratigraphy and tectonics of the south-southeastern Norwegian offshore. In: J.EH. Kaasschieter and T.J.A. Reijers (Editors), Petroleum Geology of the Southeastern North Sea and the Adjacent Onshore Areas. Geol. Mijnbouw, 62: 135-144.

Hodson, G.M. (1975): Some aspects of the geology of the Middle Jurassic in the northern North Sea, with particular reference to electro-physical logs. In, Jurassic northern North Sea Symposium. Norsk Petroleumsforening, Stavanger.

IPCC. (2005). IPCC Special Report on Carbon Dioxide Capture and Storage. Prepared by Working Group III of the Intergovernmental Panel on Climate Change [Metz, B., O. Davidson, H. C. de Coninck, M. Loos, and L. A. Meyer (eds.)]. Cambridge University Press, Cambridge, United Kingdom and New York, NY, USA, 442 pp.

Isaksen, D. and Tonstad, K. (1989) A revised Cretaceous and Tertiary lithostratigraphic nomenclature for the Norwegian North Sea. NPD Bulletin 5, 59 pp.

Jackson, C.A.-L., Larsen, E. (2008). Temporal constraints on basin inversion provided by 3D seismic and well data: a case study from the South Viking Graben, offshore Norway: Temporal constraints on basin inversion provided by 3D seismic and well data. Basin Research 20, 397–417. https://doi.org/10.1111/j.1365-2117.2008.00359.x

Japsen, P., Chalmers, J., (2000). Neogene uplift and tectonics around the North Atlantic: overview. Global and Planetary Change 24 (2000) 165–173.

Japsen, P., Green, P.F., Chalmers, J.A. (2005). Separation of Palaeogene and Neogene uplift on Nussuaq, West Greenland. J. Geol. Soc. London 162, 299.314.

Japsen, P., Bonow, J.M., Green, P.F., Chalmers, J.A., Lidmar-Bergström, K. (2006). Elevated passive continental margins: long-term highs or Neogene uplifts? New evidence from West Greenland. Earth Planet. Sci. Lett. 248, 330– 339.

Jarsve, E.M., Faleide, J.I., Gabrielsen, R.H., Nystuen, J.P., 2014. Mesozoic and cenozoic basin configurations in the North Sea, in: Martinius, A.W., Ravnås, R., Howell, J.A., Steel, R.J., Wonham, J.P. (Eds.), From Depositional Systems to Sedimentary Successions on the Norwegian Continental Margin. John Wiley & Sons, Ltd, Chichester, UK, pp. 417–452. https://doi.org/10.1002/9781118920435.ch15

Jensen, T.F., Holm, L., Frandsen, N., and Michelsen, O. (1986) Jurassic – Lower Cretaceous lithostratigraphic nomenclature for the Danish Central Trough. *Danmarks Geologiske Undersøgelse, Serie A.* 12, 65 pp.

Jensen, L.N., Riis, F., Boyd, R., (1990). Post-cretaceous uplift and sedimentation along the western fennoscandian shield 120.

Jensen, L.N., Schmidt, B.J. (1992). Late Tertiary uplift and erosion in the Skagerrak area; magnitude and consequences. Nor. Geol. Tidsskr. 72, 275– 279.

Jensen, L.N., Schmidt, B.J. (1993). Neogene uplift and erosion offshore South Norway: magnitude and consequences for hydrocarbon exploration in the Farsund Basin. In: Spencer, A.M. (Ed.), Generation, Accumulation and Production of Europe's Hydrocarbons III. Spec. Publ. Eur. Ass. Petr. Geosci., vol. 3, pp. 79– 88.

Johansen, S.E., Ostisty, B.K., Birkeland, Ø., Fedorovsky, Y.F., Martirosjan, V.N., Bruun Christensen, O., Cheredeev, S.I., Ignatenko, A.A. and Margulis, M. (1993). Hydrocarbon potential in the Barents Sea region: Play distribution and potential. In: Vorren, T.O. et al. (eds.), Arctic Geology and Petroleum Potential, NPF Special Publication 2. Elsevier, New York, NY, pp. 273–320.

Johnsen, J.R., Rutledal, H., Nilsen, D.E., 1995. Jurassic reservoirs; field examples from the Oseberg and Troll fields: Horda Platform area, in: Norwegian Petroleum Society Special Publications. Elsevier, pp. 199–234. https://doi.org/10.1016/S0928-8937(06)80043-3.

Jonassen, P. (2015). "Fault Analysis Based on 3D Seismic Data from the Northern Horda Platform." University of Oslo.

Jordt, H., Faleide, J. I., Bjørlykke, K., Ibrahim, M. (1995). Cenozoic sequence stratigraphy of the central and northern North Sea Basin: tectonic development, sediment distribution and provenance areas. Marine and Petroleum Geology, Vol. 12, No. 8, pp. 845-879.

Keary, P., and Brooks, M. (1991). An Introduction to Geophysical Exploration (Second Edition). Oxford: Blackwell Science.

Kjennerud, T., Faleide, J.I., Gabrielsen, R.H., Gillmore, G.K., Kyrkjebø, R., Lippard, S.J. and Løseth, H. (2001) Structural restoration of Cretaceous – Cenozoic palaeo-bathymetry in the northern North Sea. In: Sedimentary Environments offshore Norway – Palaeozoic to recent (Eds O.J. Martinsen and T. Dreyer) Norwegian Petroleum Society, 10, 347–364.

Knox, R.W.O. and Morton, A.C. (1988) The record of early-Tertiary N Atlantic volcanism in sediments of the North Sea Basin. In: Early Tertiary Volcanism and the Opening of the NE Atlantic (Eds A.C. Morton and L.M. Parson), Geol. Soc. London Spec. Publ., 39. 407–419.

Kolnes, J.F., (2019). Reconstruction of the Subsidence and Uplift History of a proposed CO_2 Storage Site in the Northern North Sea 97.

Koson, S., Chenrai, P., Choowong, M. (2014). Seismic Attributes and Their Applications in Seismic Geomorphology 6, 9.

Land, Carlon S. (1968). "Calculation of Imbibition Relative Permeability for Two- and Three-Phase Flow from Rock Properties." Society of Petroleum Engineers Journal 8 (02): 149–56. https://doi.org/10.2118/1942-PA.

Landrø, M. (2010) Anvendt geofysikk – Et innføringskurs i de vanligste geofysiske metodene som blir brukt for å kartlegge jordas bergarter.

Lauritsen, H., Kassold, S., Meneguolo, R., Furre, A. (2018). Assessing Potential Influence of Nearby Hydrocarbon Production on CO_2 Storage At Smeaheia. Presented at the Fifth CO_2 Geological Storage Workshop, Utrecht, Netherlands. https://doi.org/10.3997/2214-4609.201802970.

Leeder, M.R. (1983). Lithospheric stretching and the North Sea Jurassic sourcelands. Nature, 303:510-514.

Lidmar-Bergström, K., Ollier, C., and Sulebak, J. (2000). Landforms and uplift history of southern norway. Global and Planetary Change, 24(3-4):211–231.

Martini, E. (1971). Standard Tertiary and Quaternary calcareous nannoplankton zonation. In: Proceedings for the II Planktonic Conference, Rome, 1970 (Ed. A. Farinacci), Edizioni Tecno scienza No. 2, 739-785.

Martinsen, O.J., Boen, F., Charnock, M.A., Mangerut, G. and Nøttvedt, A. (1999) Cenozoic development of the Norwegian margin 60-64°N: sequences and sedimentary response to variable basin physiography and tectonic setting. In: Petroleum Geology of NW Europe, Proceedings of the 5th Conference (Ed. A.J. Fleet and S.A.R. Boldy). Geol. Soc. London, 293–304.

Martinsen, O.J., Dreyer, T. (2001). Sedimentary environments offshore Norway — Palaeozoic to recent: an introduction, in: Norwegian Petroleum Society Special Publications. Elsevier, pp. 1–5. https://doi.org/10.1016/S0928-8937(01)80005-9.

Martinsen, O.J., Boen, F., Charnock, M.A., Mangerut, G. and Nøttvedt, A. (1999) Cenozoic development of the Norwegian margin 60-64°N: sequences and sedimentary response to variable basin physiography and tectonic setting. In: Petroleum Geology of NW Europe, Proceedings of the 5th Conference (Ed. A.J. Fleet and S.A.R. Boldy). Geol. Soc. London, 293–304.

Michelsen, O. (1994) Stratigraphic correlation of the Danish onshore and offshore Tertiary successions based on sequence stratigraphy. Bull. Geol. Soc. Denmark, 41, 145–161.

Michelsen, O., Danielsen, M., Heilmann-Clausen, C., Jordt, H., Laursen, G. V. and Thomsen, E. (1995). Occurrence of major sequence stratigraphic boundaries in relation to basin development in Cenozoic deposits of the southeastern North Sea. In: Sequence Stratigraphy on the Northwest European Margin (Eds R. J. Steel, V. L. Velt, E. P. Johannesen and C. Mathieu) NPF Spec. Pub No. 5, 4:5-4:27.

Mitchum, R.M.J., Vail, P.R. and Thompson, S.I. (1977) Seismic stratigraphy and global changes in sea-level, part 2: the depositional sequence as the basic unit for stratigraphic analysis. In: Seismic Stratigraphy: Application to Hydrocarbon Exploration (Ed. C. Payton), AAPG Mem., 26, 53–62.

Molnar, P., England, P. (1990). Late Cenozoic uplift of mountain ranges and global climate change: chicken or egg? Nature 346, 29–34. https://doi.org/10.1038/346029a0.

Mondol, N.H., Fawad, M., Park, J. (2018). Petrophysical Analysis and Rock Physics Diagnostics Of Sognefjord Formation In The Smeaheia Area, Northern North Sea. Presented at the Fifth CO_2 Geological Storage Workshop, Utrecht, Netherlands. https://doi.org/10.3997/2214-4609.201802951.

Mörner, N.A. (1977). Past and present uplift in Sweden: glacial isotasy, tectonism and bedrock influence. Geol. fören. Stockh. Förh. 99, 48– 54.

Nielsen, O. B.; Sørensen, S., Thiede, J., Skarbo, O. (1986). Cenozoic differential subsidence of North Sea. Am. Assoc. Pet. Geol. Bull. 70, 276– 298.

Nguyen, D.N., (2003). “Carbon Dioxide Geological Sequestration: Technical and Economic Reviews,” 6.

Nordbotten, J.M., Celia, M.A., Bachu, S. (2005). Injection and Storage of CO_2 in Deep Saline Aquifers: Analytical Solution for CO_2 Plume Evolution During Injection. Transport in Porous Media 58, 339–360. https://doi.org/10.1007/s11242-004-0670-9.

NPD-Factmaps (2015). Norwegian Petroleum Directorate (Oljedirektoratet), URL: http://gis.npd.no, [last accessed: May 2019].

NPD-Factpages (2019). Norwegian Petroleum Directorate (Oljedirektoratet), URL: http://factpages.npd.no, [last accessed: May 2019].

Nøttvedt, A., Gabrielsen, R.H. and Steel, R.J. (1995). Tectonostratigraphy and sedimentary architecture of rift basins, with reference to the northern North Sea. Marine and Petroleum Geology, 12, 881-901. DOI: 10.1016/0264-8172(95)98853-W.

Oakman, C.D. and Partington, M.A. (1998). Cretaceous. In: K.W. Glennie (Editor), Petroleum Geology of the North Sea. Basic Concepts and Recent Advances. 4th edition, Blackwell Science Ltd., London, pp. 294-349.

Olaussen, S., Larsen, B.T. and Steel, R.J. (1994). The Upper Carboniferous-Permian Oslo Rift; basin fill in relation to tectonic development. In: Embry, A.F., Beauchamp, B. and Glass, D.J. (eds.), Pangea; Global Environments and Resources. Canadian Society of Petroleum Geologists, Calgary, Memoir 17, pp. 175–197.

Paasch, B., Ringrose, P., Furre, A.-K., Zweigel, P., Nazarian, B., Thorsen, R., Ivar, P. (2017). Industrial-scale CCS in Norway: experience gained and application to future projects 4.

Patruno, S., Hampson, G.J., Jackson, C.A.-L., Dreyer, T. (2015). Clinoform geometry, geomorphology, facies character and stratigraphic architecture of a sand-rich subaqueous delta: Jurassic Sognefjord Formation, offshore Norway. Sedimentology 62, 350–388. https://doi.org/10.1111/sed.12153.

Pirmez, C., Pratsen, L.F., Steckler, M.S. (1998). Clinoform development by advective diffusion of suspended sediment: modelling and comparison to natural systems: Jour. Geophysical Research, v.103, p.141-157.

Pruess, K. and Nordbotten, J. (2011). Numerical simulation studies of the long-term evolution of a CO_2 plume in a saline aquifer with a sloping caprock. Transport in Porous Media, 90, 135-151.

Riis, F. (1996) Quantification of Cenozoic vertical movements of Scandinavia by correlation of morphological surfaces with offshore data. Global Planet. Change, 12 , 331–357.

Riis, F. and Halland, E. (2014). CO_2 Storage Atlas of the Norwegian Continental Shelf: Methods Used to Evaluate Capacity and Maturity of the CO_2 Storage Potential. Energy Procedia, 63, 5258-5265.

Ringrose, P. S., Thorsen, R., Zweigel, P., Nazarian, B., Furre, A. K., Paasch, B., ... and Karstad, P. I. (2017). Ranking and Risking Alternative CO_2 Storage Sites Offshore Norway. In Fourth Sustainable Earth Sciences Conference, 3-7 September 2017, Malmö, Sweden.

Roberts, D.G., Thompson, M., Mitchener, J., Hossack, J., Carmichael, S. and Bjcrnseth, H.-M. (1999). Palaeozoic to Tertiary rift and basin dynamics: mid-Norway to the Bay of Biscay a new context for hydrocarbon prospectivity in the deep water frontier. In: A.J. Fleet and S.A.R. Boldy (Editors), Petroleum Geology of Northwest Europe: Proceedings of the 5th Conference. Geological Society, London, pp. 7-40.

Rohrman, M., Van der Beek, P., Andriessen, P., Cloetingh, S. (1995). Meso-Cenozoic morphotectonic evolution of southern Norway: Neogene domal uplift inferred from apatite fission track thermochronology. Tectonics 14, 700– 714.

Ryseth, A., Augustson, J.H., Charnock, M., Haugerud, O., Knutsen, S.-M., Midbøe, P.S., Opsal, J.G., Sundbø, G. (2003). Cenozoic stratigraphy and evolution of the Sørvestnaget Basin, southwestern Barents Sea. Norw. J. Geol. 83, 107-130.

SCM. (2011). Smoothing 2D Grids Petrel. Retrieved from http://www.scminc.com/website/tips-tricks/SCM_Smoothing_2D_Grids_Petrel_2010.pdf. [last accessed: May 2019].

Sejrup, H. P., Larsen, E., Landvik, J., King, E. L., Haflidason, H., Nesje, A. (2000). Quaternary glaciations in southern Fennoscandia: evidence from southwestern Norway and the northern North Sea region. Quaternary Science Reviews, 19, 667-685.

Shukla, R., Ranjith, P., Haque, A., and Choi, X. (2010). A review of studies on CO_2 sequestration and caprock integrity. Fuel, 89(10):2651–2664.

Skibeli, M, Barnes, K., Straume, T., Syvertsen, S. E. and Shanmugan, G. (1995). A sequence stratigraphic study of Lower Cretaceous depo- sits of the northernmost North Sea. In Steel, R. J. et al. (ed.): Sequence Stratigraphy on the Northwest European Margin. Norwe- gian Petroleum Society Special Publication 5, 389-400.

Skogseid, L., Pedersen, T., Larsen, V.B. (1992). Vøring Basin: subsidence and tectonic evolution. Nor. Pet. Soc. Spec. Publ. 1, 55– 82.

Steel, R.J., Olsen, T. (2002), Clinoforms, Clinoform Trajectories and Deepwater Sands. ResearchGate. Chapter: January 2002. DOI: 10.5724/gcs.02.22.036 7.

Stewart, I.J. (1987) A revised stratigraphic interpretation of the Early Palaeogene of the Central North Sea. In: Petroleum Geology of North West Europe (Eds J. Brooks and K.W. Glennie), London: Graham and Trotman, 557–576.

Stewart, D.J., M. Schwander, and L. Bolle. (1995). “Jurassic Depositional Systems of the Horda Platform, Norwegian North Sea: Practical Consequences of Applying Sequence Stratigraphic Models.” In Norwegian Petroleum Society Special Publications, 5:291–323. Elsevier. https://doi.org/10.1016/S0928-8937(06)80073-1.

Stuevold, L.M, Skogseid, J., Eldholm, O. (1992). Post-Cretaceous uplift events on the Vøring continental margin. Geology 20, 919– 922.

Stuevold, L.M. and Eldholm, O. (1996) Cenozoic Uplift of Fennoscandia inferred from a study of the mid- Norwegian Shelf. Global Planet. Change, 12, 359–386.

Sundal, A., Nystuen, J.P., Rørvik, K.-L., Dypvik, H., Aagaard, P. (2016). The Lower Jurassic Johansen Formation, northern North Sea – Depositional model and reservoir characterization for CO_2 storage. Mar. Pet. Geol. 77, 1376-1401. https://doi.org/10.1016/j.marpetgeo.2016.01.021.

Surlyk, F. (1990). Timing, style and sedimentary evolution of late Palaeozoic-Mesozoic extensional basins of East Greenland. In: R.EE Hardman and J. Brooks (Editors), Tectonic Events Responsible for Britain's Oil and Gas Reserves. Geol. Soc., London, Spec. Publ., 55: 107-125.

Sættem, J., Bugge, T., Fanavoll, S., Goll, R.M., Mørk, A., Mørk, M.B.E., Smelror, M., Verdenius, J.G. (1994). Cenozoic margin development and erosion of the Barents Sea: core evidence from southwest Bjørnøya. Mar. Geol. 118, 257– 28.

Underhill, J.R. (1998). Jurassic. In: K.W. Glennie (Editor), Petroleum Geology of the North Sea. Basic Concepts and Recent Advances. 4th ed., Blackwell Science Ltd., London, pp. 245-293.

Underhill, J.R. and Partington, M.A. (1993). Jurassic thermal doming and deflation in the North Sea: implications of the sequence strati- graphic evidence. In: J.R. Parker (Editor), Petroleum Geology of Northwest Europe: Proceedings of the 4th Conference. Geological Society, London, pp. 337-346.

Van der Beek, R. (1994). Mechanisms of post-rift margin uplift: the case of southern Norway. In: R van der Beek (Editor), Tec- tonic Evolution of Continental Rifts. Inferences from Numerical Modelling and Fission Track Thermochronology. Thesis, Free University, Amsterdam, pp. 107-140.

Van der Zwaan, C.J., Boulter, M.C. and Hubbard, R.N. (1985). Climatic change in the Lower Carboniferous in Euramerica, based on multivariate statistical analysis of palynological data. Palaeogeogr., Palaeoclimatol., Palaeoecol., 52: 1-20.

Vollset, J. and Doré, A.G. (1984). A revised Triassic and Jurassic lithostratigraphic nomenclature for the Norwegian North Sea. Norwegian Petroleum Directorate Bulletin, 3, The Norwegian Petroleum Directorate, Stavanger, 65 pp.

Vorren, T. O., Kristoffersen, Y., Andreassen, K. (1986). Geology of the inner shelf west of North Cape, Norway. Nor. Geol. Tidsskr. 66, 99– 105.

Walday, M., and Kroglund T. (2002). The North Sea – bottom trawling and oil/gas exploration. In N. Liamine (Ed.), Europe's biodiversity - biogeographical regions and seas. (pp. 31) European Environment Agency.

Whitaker, M.F. (1984) The usage of palynostratigraphy and palynofacies in definition of Troll Field geology, offshore Northern Seas: reduction of uncertainties by innovative reservoir geomodelling. In: Offshore Northern Seas Conference and Exhibition, 6, Paper G6, pp. 44. Norske Petroleumshorening, Stavanger.

Whiteman, A., Naylor, D., Pegrum, R. and Rees, G. (1975). North Sea troughs and plate tectonics. Tectonophysics, 26: 39-54.

Wien, S. T., and Kjennerud, T. (2005). 3D cretaceous to Cenozoic palaeobathymetry of the northern North Sea. In B. T. G. Wandås, J. P. Nystuen, E. A. Eide and F. M. Gradstein (Eds.), Norwegian Petroleum Society Special Publications (Vol. 12, p. 241-253). Elsevier.

Yielding, G., Badley, M.E. and Freeman, B. (1991). Seismic reflections from normal faults in the northern North Sea,in A. M. Roberts, G. Yielding and B. Freeman (eds), The Geometry of Normal Faults, Vol. 56 of Special Publication , Geological Society of London, pp. 79–89

Zanella, E., Coward, M. P., and McGrandle, A. (2003). Crustal structure. In D. Evans, C. Graham, A. Armour and P. Bathurst (Eds.), The Millennium Atlas: Petroleum geology of the central and northern North Sea. (p. 35-42) London: The Geological Society of London.

Zhang, D., Song, J., (2014). Mechanisms for Geological Carbon Sequestration. Procedia IUTAM 10, 319–327. https://doi.org/10.1016/j.piutam.2014.01.027.

Ziegler, P. (1981). Evolution of sedimentary basins in North-West Europe,in L. V. Illing and G. D. Hobson (eds),Petroleum Geology og the Continental Shelf of North West Europe , Vol. 2, heyden & Son, London, chapter 1, pp. 3–39.

Ziegler, P.A. (1982). Geological Atlas of Western and Central Europe. Shell International, The Hague.

Ziegler, RA., (1987). Evolution of the Arctic-North Atlantic borderlands. In: J. Brooks and K.W. Glennie (Editors), Petroleum Geology of North West Europe. Graham and Trotman, London, pp. 1201-1204.

Ziegler, P.A. (1992). North Sea rift system. Tectonophysics 208,55–75.

Øvrebø, L., Kjennerud, T., Lippard, S.J., Rivenæs, C., Hamborg, M. (2001). Forward depositional modelling of the Cretaceous post-rift deposits in the northern North Sea. Norsk Geologisk Tidsskrift Vol. 81, pp.169-178. Trondheim 200 l. ISSN 0029-196X.

UiO 2019

MASTER THESIS

SHARON NICOLE

HARRIS